DESIGNING AUTOMATED SYSTEMS FOR SAMPLE PREPARATION OF NUCLEIC ACIDS USING ISOTACHOPHORESIS

A DISSERTATION SUBMITTED TO THE
DEPARTMENT OF CHEMICAL ENGINEERING
AND
THE COMMITTEE ON GRADUATE STUDIES
OF
STANFORD UNIVERSITY
IN PARTIAL FULFILLMENT OF
THE REQUIREMENT FOR THE DEGREE OF
DOCTOR OF PHILOSOPHY

Lewis A. Marshall
August 26, 2013

I certify that I have read this dissertation and that, in my opinion, it is fully adequate in scope and quality as a dissertation for the degree of Doctor of Philosophy.

Gerald Fuller, Co-Adviser

I certify that I have read this dissertation and that, in my opinion, it is fully adequate in scope and quality as a dissertation for the degree of Doctor of Philosophy.

Juan Santiago, Co-Adviser

I certify that I have read this dissertation and that, in my opinion, it is fully adequate in scope and quality as a dissertation for the degree of Doctor of Philosophy.

Kenneth Goodson

I certify that I have read this dissertation and that, in my opinion, it is fully adequate in scope and quality as a dissertation for the degree of Doctor of Philosophy.

Eric Shaqfeh

Approved for the Stanford University Committee on Graduate Studies.

Patricia J. Gumport, Vice Provost for Graduate Education

This signature page was generated electronically upon submission of this dissertation in electronic format. An original signed hard copy of the signature page is on file in University Archives.

Abstract

Purified DNA serves as a template for a wide array of analysis techniques, ranging from sequencing to PCR and hybridization assays. DNA analysis can be used for clinical diagnosis, for forensic investigation, and for a range of research purposes. These analysis techniques improve each year, but they are all constrained by the availability of purified DNA. DNA is typically derived from raw biological samples that contain a host of other molecular species, including proteins, lipids and metal ions. These species can inhibit analysis of the DNA, so purification of DNA from complex sample matrices is a necessary precursor to analysis. Typically, DNA purification is performed using either liquid-liquid extraction or solid-phase extraction, both of which require manual labor, involve toxic chemicals, and are difficult to miniaturize.

Isotachophoresis (ITP) is an alternative method for DNA purification that does not rely on specialized surface chemistry or toxic chemical species. Instead, ITP uses electric fields to selectively pre-concentrate DNA from a raw sample, and simultaneously separate it from inhibiting species. ITP purification of DNA has been demonstrated from human serum, plasma, and whole blood, and the same technique has been used to purify RNA from bacteria in human blood and urine. Until recently, the parameters governing extraction efficiency, throughput, and separation quality in ITP purification were not well established. This thesis is focused on rational analysis for designing and optimizing ITP systems for rapid, high quality DNA purification.

Preface

The nitrogen in our DNA, the calcium in our teeth, the iron in our blood, the carbon in our apple pies, were made in the interiors of collapsing stars. We are made of starstuff.

-Carl Sagan, *Cosmos* (1980).

Acknowledgements

I am forever grateful for my years at Stanford University. They constitute some of the best years of my life, and will forever shape me.

I am fortunate to have had the continual guidance of Prof. Juan G. Santiago. He is a passionate scientist and a creative thinker who is dedicates a tremendous amount of time to his students and his research. I learned more than I ever thought I would in working with him.

I also benefitted from the encouragement and support of Prof. Gerald Fuller, who acted as my co-advisor. He has been gracious whenever I needed his help.

My days in lab was made ever better by the other members of the Stanford Microfluidics Laboratory. It was a joy to know all of them, especially those I worked closely with, including Anita Rogacs, Yatian Qu, Crystal Han, and Prof. Hirofumi Shintaku.

I am lucky to have the support and camaraderie of great friends I made here at Stanford. I am especially indebted to Joe Foley for his meticulous nature, love of figurecraft, and insight into biology, and to Armand Rundquist for his enthusiasm for physics and engineering. Thanks also to the wonderful people of Atheists, Humanists, and Agnostics (AHA!) at Stanford and of the Fellowship for Religious Encounter (FRE), all of whom were great friends and stimulating thinkers.

Finally, I am grateful to my family, especially my mother, who always believed that I could achieve great things.

Table of Contents

List of Tables

List of Illustrations

Chapter 1 Introduction

Some of the contents of this chapter are under preparation for publication in *Analytical Chemistry* by Lewis A. Marshall, Klint Rose, and Juan G. Santiago, or for publication by Lewis A. Marshall, Anita Rogacs, and Juan G. Santiago in the *Journal of Chromatography A*. They are reproduced here with minor modifications.

Nucleic Acid Purification Via Isotachophoresis

DNA Purification

Purified DNA serves as a template for a wide array of analysis techniques, ranging from sequencing[1] to PCR[2] and hybridization assays[3]. The central dogma of molecular biology places DNA as the permanent storage location of the blueprint of life.[4] While new forms of RNA continue to add complexity to this relatively simple central dogma,[5] the importance of DNA cannot be overstated, either from a perspective of biological systems or as a tool for research, medical diagnosis, and forensic analysis. For example, DNA from clinical samples can act as a biomarker in diagnosis of infectious diseases,[6] indicator of genetic abnormalities[7]and as a predictor of cancer risk.[8] However, analysis of this DNA is contingent upon the availability of pure samples of intact DNA from sources that often contain complex mixtures of molecular species.

Purification using Isotachophoresis

ITP is a well-established technique for ion separation and stacking.[9] In ITP, as in other forms of electrophoresis, molecules electromigrated and separated based on differences in their electrophoretic mobility (describing their observable velocity under an applied electric field). This relationship between electric field and migration velocity is typically expressed as a simple proportionality:

$$U_i = \mu_i E$$

where U_i is the velocity of species *i*, *E* is the electric field, and μ_i, the electrophoretic mobility of species *i*, is a proportionality constant that depends on the charge and drag on the species.

ITP is unique from other forms of electrophoresis in that the presence of a non-uniform electric field cans selectively focuses ions into a highly concentrated zone. The gradient in electric field is achieved by creating multiple electrolyte zones in the device, each with a different conductivity. The separation channel is initially filled with a high-conductivity leading electrolyte (LE), which contains a fast ion of the same charge sign as the analyte (a.k.a: co-ion). In series with the separation channel is a reservoir filled with a low-conductivity trailing electrolyte (TE), which contains a slower co-ion.. Both the LE and TE also contain a counter-ion species of opposite charge sign as the analyte, to maintain charge neutrality and to buffer the pH. When ITP is initiated, the current continuity across the interface of the LE and TE establishes an electric field gradient in microseconds.[10] The electric field in each zone can be calculated as follows:

$$E = \frac{I}{A\sigma}$$

Here, *I* is the applied current, *A*, is the local cross-sectional area of the channel, and σ is the local conductivity, defined as

$$\sigma = \sum_i c_i \lambda_i = \sum_i \left(c_i \sum_j f_i^j z_i^j \mu_i^j \right)$$

where, *ci* is the local concentration of species and λ_i is the molar conductivity of species *i*. The molar conductivity can be calculated as a summation of the conductivities of all of the charge states *j* of species *i*, where *f* is the fraction of species *i* in state *j*, *z* is the charge in state *j*, and μ is the mobility of state *j*. This coupling between concentration, electric field, and conductivity gives rise to the nonlinear effects observed in electrophoretic systems, including ITP.[11]

After initiating ITP, the trailing co-ion electromigrates into the channel, displacing the leading co-ion, and creating a zone with low conductivity and high electric field. The electric field and conductivity in this zone adjust so that the trailing ion has the same

velocity as the leading ion in the leading zone. The adjusted concentrations of trailing co-ions and associated counter ions at this interface can be predicted from the Kohlrausch, Alberty, and Jovin conservation equations.[12]

The name, isotachophoresis, comes from this adjustment of electric field and ion velocity. The Greek roots of the word isotachophoresis are “isos”, meaning equal, and “takhos” meaning speed.[13] At steady state, conductivity and electric field adjust so that each co-ion moves at an equal speed. The interface between the leading ions and the trailing ions is known as the ITP zone. When an analyte such as DNA, with electrophoretic mobility between the leading and trailing ion, is introduced anywhere into the system, it has a net mobility toward the ITP zone. In the leading electrolyte, the DNA experiences a low electric field, and moves slower than the ITP zone, while in the trailing electrolyte zone, the DNA experiences a high electric field, and catches up to the ITP zone. Thus, the electric field gradient causes accumulation of DNA at the interface between the leading and trailing ions as this interface propagates through the system.

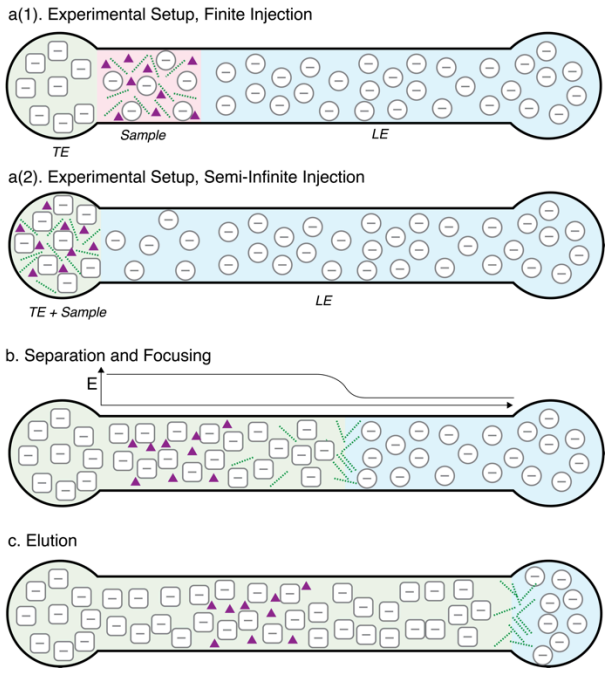

Figure 1-1. Schematic of ITP purification of nucleic acids. The separation can be initiated with the sample in either the finite injection or semi-infinite injection condition. In finite injection (a1), the sample is injected into the channel, between the TE and the LE. In semi-infinite injection (a2), the sample is mixed into the TE reservoir. When electric field is applied, (b) ions propagate down the channel, and an electric field gradient forms at the interface between the LE and the TE. DNA begins to focus to this interface and separate from contaminants. DNA eventually elutes (c) into the leading electrolyte reservoir, where it can be collected and pipetted off-chip for storage and analysis. In this schematic, only anionic species are illustrated. Cationic species are present everywhere, but not shown.

Anion and Cationic ITP: Isotachophoresis can be categorized based on the charge state of analyte species being focused and separated. In this paper, we focuse on anionic ITP, since nucleic acids are negatively charged at pHs above ~3, due to the phosphate group on the nucleic acid backbone, which has a pKa of approximately 1.5.[14] We note, however, that the concept we discuss equally applicable to cationic ITP, which we typically use for protein focusing and separation. In anionic ITP, the leading and trailing co-ions are strong or weak acids, while the counter-ion is typically a buffering weak base.

Peak versus Plateau Mode: A second way of categorizing ITP systems is whether analytes migrate in peak mode or plateau mode. In peak mode, an analyte focuses into a near-Gaussian peak between two adjacent co-ion zones, is not the dominant charge-

carrying species.[15] This is the typical mode for DNA/RNA migration during ITP. In plateau mode ITP, the analyte forms a wide zone with uniform concentration that is typically not shared by any other co-ion species, and is therefore the majority charge carrier in its own zone. a Bocek used this feature in analytical ITP systems, in which the ions are read off by the conductivity of their zone.[16] It is possible for a single ITP experiment to contain some analytes in peak mode and others in plateau mode. In a 100 μm x 100 μm channel, it takes on the order 10 picomoles of a species to form a plateau mode ITP zone.

Finite and Semi-Infinite Injection: ITP systems can also be classified by how the sample is introduced into the system. Finite injection mode, the sample begins in the separation channel, bounded by leading electrolyte on one side and trailing electrolyte on the other side. In semi-infinite injection mode, the sample begins in the buffering reservoir in which electrolysis is performed.[13] The difference between these modes is illustrated in Figure 1.

There is an inherent limit imposed on extraction efficiency when using semi-infinite injection. We can analyze this limit by tracking the flux of ions in and out of the trailing electrolyte reservoir. Neglecting diffusion, the anions (the trailing ion and DNA) exit the trailing electrolyte reservoir at a rate proportional to their mobility and their concentration.

$$\left(\frac{\Delta N_{DNA}}{\Delta N_T}\right)_{TER} = \left(\frac{\mu_{DNA}[DNA]}{\mu_T[T]}\right)_{TER}$$

At the same time, counter-ions are entering the reservoir from the channel. The same relationship between flux, concentration, and mobility is true for the counter-ion and the trailing ion. However, this time, the mobility and concentrations are from the adjusted TE in the reservoir.

$$\left[\frac{\Delta N_C}{\Delta N_T}\right]_{TER} = \left[\frac{\mu_C c_C}{\mu_T c_T}\right]_{ATE}$$

We can simplify these equations by assuming that all of the mobilities are of roughly the same magnitude. In addition, can assume that the ratio of the counter-ion and the trailing ion don't change between the TE and the adjusted TE. In this case, there is a simple relation between the change in concentrations of species in the TE reservoir over the course of the experiment.

$$\frac{\Delta[C]}{[C]^o} = -\frac{\Delta[T]}{[T]^o} = -\frac{\Delta[DNA]}{[DNA]^o}$$

Hence, to extract half of the DNA molecules, 50% of the trailing co-ion concentration must be extracted and an additional 50% must be added to the counter-ion. The change in pH induced by this exchange of ions can be estimated using the Henderson Hasselbach equation. Assume that the pH of the trailing reservoir is buffered at the pKa of the counterion, and that the trailing ion is fully ionized.

$$pH = pKa + \log_{10}\left(\frac{[CH^+]}{[C]}\right) \approx pKa + \log_{10}\left(\frac{[T]_a}{[C]_a - [T_a]}\right)$$

If we restrain the pH to within 0.3 units of the pKa of the counterion, then the maximum achievable extraction efficiency is 14%.. Importantly, the relationship between pH and extraction efficiency is highly non-linear, and the pH change accelerates as more trailing ion is removed.

Constant Voltage versus Constant Current Separation: Once the buffer system for ITP has been set up, the separation can be performed in either constant voltage or constant current modes. In constant voltage mode, the current decreases over the course of the experiment, as the high-conductivity LE is displaced by low-conductivity TE. As a

consequence, the velocity of the ITP zone decreases over the course of the experiment. Conversely, in constant current mode, the velocity of the ITP zone stays the same over the course of the experiment, but the voltage increases. This constant velocity often makes constant-current ITP easier to analyze, but the highest sample throughput is achieved by using the maximum voltage that can be supplied by the power supply. The maximum applied current is limited by Joule heating in the channel, because increasing temperature can change buffer conditions[17], and eventually cause outgassing. Typical voltages for separation are 100-3000 V, while typical currents can range from less than a microamp for etched glass microchannels to a few milliamps for large cross-section channels.

Counterflow and Gradient Elution: Various process control methods have been implemented to improve ITP. Some methods focus on inducing bulk liquid flow to extend the focusing time before the ITP zone exits the channel. This allows a short separation channel and a low separation voltage to be used to achieve higher throughput separations. Bulk flow can be induced by electro-osmotic flow (EOF) in so-called counterflow ITP, or by a pressure gradient, as in gradient elution ITP (GE-ITP). In GE-ITP, pressure-driven flow is also leveraged to selectively control which species are able to elute from the separation channel.[18]

Another process control improvement leverages electric fields applied perpendicular to a pressure driven flow, in so-called free-flow ITP. In this type of setup, ITP performs separation continuously rather than via batch processing.[19] Free-flow versions of ITP are often more difficult to control, but the throughput advantages of the continuous process are significant.

Overview on Designing ITP Systems

ITP-based nucleic acid purification requires knowledge of the concentration and electrophoretic properties of analyte and the interfering species present in raw samples. Designing a separation chemistry for ITP purification of nucleic acids is a complex task that involves choosing at least three ions (the leading, trailing, and counter-ions) and their initial concentrations in their respective zones. Additional complexity arises from the

evolving nature of ion concentrations, as new zones are formed by electromigration and dispersion during the separation process.

In this paper, we will review the work that has been done in selecting optimal separation chemistry for extraction and ITP-based purification of DNA and RNA from a range of complex samples. To manage the large number of variables in the system, it's helpful to break the design of ITP separation chemistry into a few component decisions.

DNA/RNA Mobilities: The free solution mobility of DNA increases monotonically with molecular weight, plateauing at 3.57 x 10^4 $cm^2/V/s$ for DNA equal or longer than 400 bp. This value was determined in Tris-acetate buffer at 27.5°C and is independent of DNA concentration, sample size, electric field strength, and capillary coating. There are several methods to achieve size-dependent changes in free solution mobility including entropic trapping (ref), use of microfabricated obstacles (ref) or end-labeling of nucleic acid with uncharged, monodisperse, polymeric "drag-tags" [20]. However, the most widely adopted method for inducing size- and secondary structure-based mobility shift is to use a sieving matrix such as agarose or polyacrylamide gels, or entangled linear polymers. (refs: Barron?)

The influence of sieving on DNA mobility depends on three key factors: (1) the relative size of the molecule with respect to the effective pore size of the matrix, (2) the effect of the electric field on the matrix, and (3) the specific interactions of molecule with the matrix during electrophoresis.[21] In our group, we have demonstrated the integration of ITP with sieving induced size-based separation using entangled linear polymers[22], [23], [24], themoreversible hydrogel [25], and cross-linked polyacrylamide.[13] In general, sieving effects on the electrophoretic mobility of DNA and RNA are ad hoc and difficult to predict. Detailed discussion and models for these sieving methods can be found in the literature. (refs)

Electrophoresis of Known PCR Inhibitors: There are a wide range of known PCR inhibitors reported in literature.[26] A well-designed ITP electrolyte system will extract nucleic acids from the sample matrix and prevent all inhibiting species native to that sample from reaching the extraction reservoir.

The easiest contaminants to separate from DNA are small cations such as magnesium, sodium, potassium, calcium, and iron. Each of these species can inhibit PCR, but they are easily separated from DNA during isotachophoresis because they countermigrate with respect to the anionic DNA. In semi-infinite injection mode, these species do not enter the separation channel.

Anionic species are harder to separate from the nucleic acid via ITP. Proteins can have a range of mobilities that vary greatly with pH. The pKas of individual amino acids range from 3.5 and 10.6. The isoelectric point distribution of serum proteins varies over a similar range with the highest frequency at 5.5, and the minimum at 7.5, near biological pH.[27] Based on the sequence of the amino acid, the mobility of short peptide sequences can be estimated by computing its net charge and drag on the molecule. [28] For large proteins this method is insufficient, and we recommend direct measurement of their electrophoretic mobility.

We believe that humic acids pose a great challenge for purification of NA. They have a range of structures and are strongly negatively charged at biological pH.[32]

A summary of PCR inhibitors, their source, inhibiting concentrations and charge properties is shown in Table 1. Highly acidic species (low pKa) and species with low isoelectric points are likely to be the most challenging to separate from DNA, and should be carefully monitored during the design the separation chemistry.

Table 1-1. PCR inhibitors, their typical sources, inhibiting concentrations, and charge characteristics. Table adapted from Bessetti et al.[26] Charge characteristics are reported through either the acidity (pKa) constant, or through the isoelectric point (pI), depending on the species.

Inhibitor	Source (Typical concentration)	Inhibiting Concentration	pKa, pKb, or pI
Bile Salts	Feces		pKa, 1-4 [29]
Complex Polysaccharaides	Feces, plant material		
Collagen	Tissues	~25 ng/µL [30]	pI 7.8[31]
Heme and Hematin	Blood	2 µM[30]	
Humic Acids	Soil, plant material	~1 ng/µL[30]	pKa 4, 10[32]
Melanin and eumelanin	Hair, skin	2 ng/µL [30]	pKa ~3.1[33]
Myoglobin	Muscle tissue		pI 6.9[34]
Proteinases	Milk		
Calcium	Milk (30 mM), bone	~100 nM [30]	pKa 13.6, 12.6 [35]
Urea	Urine (330 mM)	50 mM [36]	Cation pKa 0.2 [37]
hemoglobin	Blood (2.32 mM)	52 µg/mL	pI 6.6-7.3[38]
lactoferrin	Blood (0.25 ng/ul)	1 µg/mL	pI 8.7[39]
Immunoglobin	Blood (10 ug/uL)	3.2 µg/mL	pI 5.2-9.4[40]
Indigo dye	Denim	<100 µM (dye quenching?)[30]	pKa 8.0 and 12.7[41]
iron	Blood and Serum (1 mM)	10 µM	Cation pKa 8.3, 9.3 [35]
magnesium	Blood (1.2 mM)	5 mM	Cation pKa 11.4, 12.2[35]
Potassium	Blood (4.5 mM)	20 mM	Cation pKa 13[35]
Sodium	Blood (140 mM)	40 mM	Cation pKa 13.7[35]

pH (Counterion in Anionic ITP): The first step in designing separation chemistry for ITP purification of nucleic acids is to choose the operating pH. The simplest way setting the system pH is to choose a counter-ion that buffers in that pH range. The pH in the leading zone can be adjusted by titrating the counterion with the leading ion. During ITP, the counterion will migrate to titrate the sample and the TE zones, stabilizing the pH throughout the experiment.

At pH 4, NA is still negatively charged, but ions with higher pKa are neutral or positively charged, making their separation from the NA fairly straightforward. When purifying NA from sample matrices of low protein content, we thus recommend choosing a low pKa weak base for the counterion (e.g.: Bis-Tris, histidine, E-aminocaproic acid). However, this pH range corresponds to the range of isoelectric point of the abundant proteins.[27] When pH~pI, the proteins become netural, and their solubility is reduced, leading to protein aggregation and precipitation in samples containing protein-rich matrices.. Many researchers have therefore chosen to perform ITP purification of nucleic acids near biological pH, despite the associated increase in the mobility of some contaminating species.

For purification of DNA using ITP, Tris is the common counter-ion among published research. Tris has a pKa of 8.2, and buffers between pH=7.7 and 8.7, in the range of biological pH. For RNA purification, 6-aminocaproic acid (pKa 4.1), and bis-Tris (pKa 6.8), as well as Tris, have been used as buffering counter-ions.

The choice of pH and ionic strength can also affect the EOF mobility of the system. For glass, and other channel surfaces with acidic surface groups, electro-osmotic flow will always be in the direction opposite to NA migration. While this can expand the effective separation volume of the channel, it also causes dispersion of the sample zone. Choosing a lower pH and a higher ionic strength can reduce EOF mobility.

Leading Ion: In the ITP purification studies reviewed here, chloride was chosen as the leading electrolyte. Chloride is biologically compatible, and typically present in biological samples. Hydrochloric acid is readily available as a reagent to adjust the chloride content of a buffer. In addition, chloride is strongly ionizing, allowing it to titrate bases with a wide range of pKas. The possible disadvantage of using chloride is that it's

high mobility allows a wide range of fast ions to focus into the ITP zone. This includes, for example, carbonic acid, which has a high mobility compared to DNA, but is much slower than chloride.

Very few systems for ITP purification have taken into account species that overspeed the ITP zone (as EDTA would). Typically these species elute into the extraction reservoir ahead of the DNA, contaminating the outlet reservoir. An exception to this is are the assays developed by Kondratova, which involved the excision of a narrow band of DNA from the separation gel, excluding species both ahead and behind the focused DNA.

Trailing Ion: The trailing ion is the species that has the most variation among published research for ITP purification, and there are clear trade-offs between using faster and slower trailing ions. Choosing a relatively fast trailing ion, such as MES, reduces the range of species capable of focusing between the LE and TE ion. This is critical to avoid focusing anionic contaminants. However, when the sample is mixed with the trailing ion, as in semi-infinite injection, using a fast trailing ion reduces the rate at which nucleic acids focus to the interface.

Zone Concentrations: The choice of the leading electrolyte and trailing electrolyte zone concentrations is another factor when selecting sample chemistry. This choice mainly depends on the ionic strength of the sample being used.

For finite injection mode ITP, there is a minimum total charge required to separate the nucleic acid from inhibitors. The amount of charge, called the separation parameter Q_s, was first derived by Bocek.[42] To a first approximation, Q_s depends on the concentration of ions in the sample to be separated. Therefore the minimum concentration of the LE zone is set by the electrolyte concentration in the sample. In a typical system, it is possible to separate the nucleic acid from a biological sample by using a separation channel with the same volume and ion concentration as the sample. This approximate configuration is used by both Kondratova[43] and Marshall[44] in their high extraction efficiency setups.

If the separation is being performed in finite injection mode, it is generally beneficial to use the highest buffer concentrations in the reservoirs possible. This choice maximizes

the buffering capacity of the reservoirs. These concentrations are limited by the solubility of the species. In addition, the concentration in the leading electrolyte reservoir is limited if it is being used as the elution location for the nucleic acids. A high electrolyte concentration here will carry over into downstream applications, and can change the buffer properties in, for example, PCR. This problem can be resolved by using separate reservoirs for elution and buffering, as in Marshall et al.[44]

For semi-infinite injection mode ITP, the focusing rate of nucleic acids from reservoir to the interface is maximized when the LE concentration is set highest and the TE concentration is set to the lowest applicable values.(ref: Tharun)

Adjusting Sample Chemistry: When performing ITP purification of a biological sample with finite injection, users face a difficult choice. Is it better to inject a raw biological sample, with its native pH and ionic strength, into a separation channel, or to try to add additional buffering ions to the sample to achieve better control? Adding ions can allow the user to adjust the pH and adjust the ionic strength reliably, but these additional ions increase the separation time. To date, no study has addressed this question in detail. Kondratova circumvented this problem by dialyzing the sample to reduce the concentrations of ionic species, while the Santiago group has tended to add buffering ions to their samples prior to lysis.

Numerical Simulation for Optimization: Analytical solutions to pH and effective mobility can provide some insight into the expected properties of an ITP purification system. However, because of the high degree of nonlinearity of ITP systems, and the adjustment of zones based on the Alberty and Jovin functions to new ion concentrations, we recommend numerical simulations of the ITP system to gain further insight into its behavior. There are number of tools are available to perform these simulations, including SPRESSO, an open source, MATLAB-based code from Stanford University.

Literature Review: DNA Purification using Isotachophoresis

Valentina N. Kondratova is the first researcher that we know of to apply ITP to the purification of nucleic acids from biological samples. She published four papers on this subject, starting in 2004.[43,45,46] Through the course of these papers, she developed ITP purification of DNA from human serum or plasma samples, with a focus on sample processing volume and DNA quality.

Kondratova performed very thorough sample pretreatment to simplify the ITP pufification process. To degrade proteins in the serum or plasma, she always subjected them to proteinase K treatment for 16 hours. In her first two works, this was in a solution of 0.5% sodium dodecyl sulfate (SDS). In the two later works, this proteinase K treatment took place in 0.5% sarcosyl, 10 mM Tris–HCl, pH 8, and 5 mM EDTA. In these later works, samples were also subjected to phenol-chloroform to remove proteins. The samples were also dialyzed to remove the high ionic strength salts native to the serum. These prepared serum and plasma samples were then subjected to ITP to purify the DNA from the other serum contents.

Kondratova used the same system of ions in each of these papers, but adjusted their concentration as she developed the technique. She always used Tris as the counterion, chloride as the leading ion, and β-alanine as the trailing ion. The choice of β-alanine as the trailing ion in this system caused her to focus species over a wide range of mobilities, due to the extremely low mobility of β-alanine in the pH range buffered by Tris. In her first two papers, she used a LE pH of 7.6, while the later two papers had a LE pH of 6.7.

Kondratova used several different apparatuses for ITP separation. In her first two papers,[46] she used a standard gel box (Figure 2a) containing an agarose gel to perform counterflow ITP. This choice is attractive because gel boxes are commonly available in most experimental biology labs. However, this setup posed problems. Non-uniform electric field across the ITP interface made the agarose gel prone to warping. Despite this, Kondratova was able to purify DNA from serum samples and use the resulting sample to perform PCR. She emphasized applications for purification of extracellular nucleic acids from serum and plasma as a cancer diagnostic method.

In her third report on the isolation of DNA using ITP,[45] Kondratova, used significantly different experimental setup. She performed ITP through 18 quartz glass

tubes filled with agarose gel (figure 2b). Each of these tubes was 5 mm in diameter and 12.5 cm long, resulting in total volumes of about 2 mL. Each rod was used to separate between 0.5 and 1.5 mL of serum or plasma sample. This experimental setup is perhaps the largest,to date, employed to purify DNA using ITP. The large cross-sections enabled the purification to complete in 30-40 min. However, Kondratova did not directly address purification efficiency in her work, so we cannot know definitively how effective this large device was.

In her last paper in this field,[43] Kondratova again focused on updating the apparatus used to perform this extraction. She substituted plastic rods for glass rods in order to simplify excising the gel (figure 2b). She also estimated the total efficiency of the isolation process at 93%. In this last work, Kondratova emphasized the importance of dialysis when working with large blood and plasma samples: "ITP of 0.5–1.0 ml of nondialyzed blood plasma takes too much time and very long tube length (in our hands several hours were not enough)". She also addressed the purpose of deproteinization, saying that if protein digestion and removal is incomplete, DNA may complex with the remaining proteins species. These complexes may not focus under ITP, and will lead to lost DNA extraction efficiency.

While the overnight protein digestion, phenol deproteinization, and dialysis addresses these inherent challenges, they also make Kondratova's process take a long time compared to other DNA sample preparation methods. Solid-phase extraction and liquid-liquid extraction techniques take on the order of an hour, and Trizol extraction does not suffer the size selectivity problems that Kondratova cites for solid phase extraction. Lastly, given the removal or degradation of inhibiting proteins during Kondratova's sample manipulation prior to ITP, it's possible that these unpurified samples would also function as PCR templates.

Aside from the sheer novelty of her work, Kondratova set a high bar for sample processing capacity by using large tube gel devices for purification. Her quartz tube devices could process 1 mL dialyzed plasma solution in 30-40 minutes, using a 200 V power source.

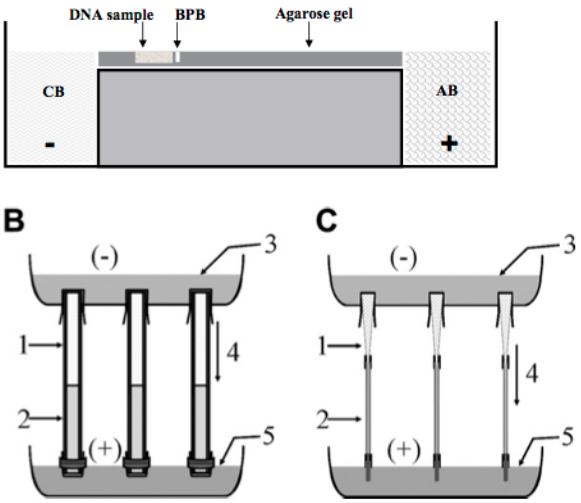

Figure 1-2. Experimental setups used by VN Kondratova. a. The counterflow ITP setup used in Kondratova's 2004 and 2005 papers. A DNA sample is injected into a pocket in an agarose gel. The gel is in an electrophoresis bath with reservoirs buffering reservoirs for the anode and cathode electrodes. Bromophenol blue (BPB) is injected ahead of the DNA to track the ITP zone. b. In her 2009 paper, Kondratova used a set of 18 quartz tubes filled with gel to perform ITP. This system had extremely high volume processing capability. c. In her 2011 paper, Kondratova replaced the quartz rods with plastic tubes to simplify the equipment needed.

The Santiago group has published numerous papers on the purification of DNA using ITP. Their first work in this field was published in 2009.[47] That paper was first demonstration of ITP purification of nucleic acids from whole human blood, rather than plasma or serum.

This work provided some insight into the problem of histone binding when purifying genomic DNA from prokaryotes. Without application of proteinase K, nucleic acids did not focus into the ITP zone. When samples were digested using proteinase K, the nucleic acids could focus. The group theorized that this was caused by histones and other binding proteins altering the electrophoretic mobility of DNA, and preventing it from being focused.

The major downfall of this work was the size of the device used. The authors used an etched glass microfluidic chip (Caliper) with a total finite injection sample volume of 25 nl. Because of this, the total nucleic acid content of their extracted sample was low, estimated as 45 pg, equivalent to only 2.5 cells worth of DNA. This extremely low throughput made sequence-specific analysis by any method other than PCR unworkable.

The Santiago group continued its work on DNA purification with two papers on the purification of DNA from malaria-infected whole blood samples.[48,49] In the first of these papers,[48] the group used a device that allowed semi-infinite injection of cell lysate into a capillary device in an attempt to increase sample throughput. They also applied counterflow using a hydrodynamic pressure setup to extend the focusing time of the nucleic acids.

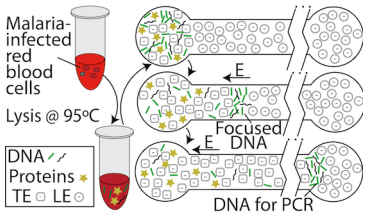

Figure 1-3. The workflow for purification of DNA from malaria-infected blood samples. In this case, blood lysate was injected into the trailing electrolyte reservoir, and nucleic acids were focused under semi-infinite injection.

In another paper analyzing malaria-infected whole blood,[49] the group implemented the same ITP-based purification assay on an integrated nucleic acid purification device developed by the Bachman group at UC Irvine. This device is based on printed circuit board (PCB) heaters and temperature sensors integrated with a microfluidic layer defined by soft lithography. With this device, the group could pipette a whole-blood sample directly onto the chip. The sample was lysed and mixed with trailing electrolyte by the integrated heater and induced convective mixing. The sample was then separated using ITP through the integrated microfluidic channel. A major advantage of this combination of platform and separation technique was the full electrical actuation of both the lysis and separation steps. In addition, the insensitivity of ITP to surface properties allowed inexpensive plastic components to be used to manufacture the device.

In both of these pieces, throughput continued to be an issue. The techniques used to increase throughput only increased the total yield of DNA by about 10-fold over the group's previous work with human blood. The increased channel cross-sectional areas

used in these experiments increased the total yield of nucleic acids collected, but they also resulted in higher sensitivity to pressure-driven flow during the experiments.

A new application of ITP purification is the simultaneous processing of nucleic acids and proteins from the same sample. This has been demonstrated in a preliminary fashion by Charles C. Young in a 2010 patent application, and by the Santiago group in a 2013 conference publication.

Young suggests that nucleic acids and proteins from a sample be simultaneously purified and eluted into a single elution volume using ITP. He shows preliminary gel electrophoresis data demonstrating this method from a *Bacillus atrophaeus* spore sample.

The Santiago group has demonstrated purification of nucleic acids and proteins from a single serum sample into separate elution volumes using two counter-migrating ITP zones. The group constructed a custom PDMS microfluidic device for this work. They operated at a low pH to positively charge the proteins and negatively charge the DNA. The DNA was then purified into one channel using anionic ITP, while proteins were simultaneously purified into a separate channel using cationic ITP.[50]

Literature Review: Design for Isotachophoresis

How big does a device need to be to fully separate a sample under isotachophoresis (ITP)? The term "big" is, of course, ambiguous. For capillary zone electrophoresis (CZE) the relevant figure of merit is the channel length. Species separate into peaks and move down the channel. The distance between peaks grows linearly with the length of the separation channel. The peak width also grows due to diffusion.

The situation in ITP is much different. As species move down the channel, they separate, but they are always in a set of adjacent zones. The diffusion of the species affects the boundary width between zones, but this width stays relatively constant throughout the experiment. The relevant parameter is not the length of the channel, but rather a function of the volume and the ionic strength of the leading ions. This term, the separation capacity (as coined by Petr Bocek in his 1978 paper) is one of the key design parameters for ITP systems, as important as channel length in CZE. Despite this, the values are rarely reported, even approximately, in modern papers on ITP devices.

The foundations of device size and separation capacity for ITP were mainly explored by Petr Bocek and Takeshi Hirokawa, although certain other papers are relevant. Below are the papers most important to the field, listed chronologically, alnong with descriptions of their contributions.

Brouwer and Postema (1970), "Theory of the Separation in Displacement Electrophoresis"

Brouwer and Postema provide the first theoretical explanation for how zones form in ITP (although they always use the term "displacement electrophoresis"). They use a moving-boundary model to predict the interface locations during finite injection ITP. They neglect diffusion, and assume that a single counter-ion species is present. They also assume that all species are fully ionized, and use the Kohlrausch regulating function (KRF) to determine zone concentrations. This paper contains only theoretical work, and no actual experiments.

Importantly, this paper introduces the use of spaciotemporal plots to display the positions of boundaries in isotachophoresis. The primary example is shown in figure 1. The zone locations are plotted in the frame of reference of the leading ion (A) zone. A mixed zone (BCDEF) separates into distinct, single-species zones over time, and the

trailing zone (X) follows. Two concentration boundaries, stationary in space, are shown moving in the frame of reference of the leading ion.

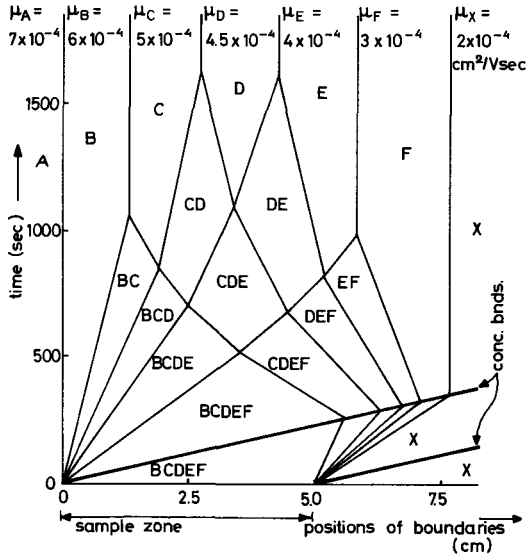

Fig. 3. Development of the various zones in the case of a five-component sample. In this arithmetical example: $C_A = 10^{-5}$ gEq. cm^{-3}, $C_B = C_C = C_D = C_E = C_F = 2.5 \times 10^{-6}$ g-equiv. cm^{-3} in the original sample zone, and $E_A = 30$ V cm^{-1}.

Figure 1-4. Spaciotemporal plot from Brouwer and Postema showing zone formation from a finite injection zone under ITP. This style of figure is seen repeatedly in later years, especially in the works of Bocek and Hirokawa.

Everaerts and Routs (1971), "Calculation and Measurement of Concentrations in Isotachophresis"

Everaerts and Routs provide both theoretical and experimental analysis of zone composition in this paper. Their theoretical analysis is similar to that of Brouwer and Postema, in that they use moving boundary equations to determine relationships between zones under ITP. However, Everaerts and Routs allow for weak ions in their analysis, and so cannot use the KRF to calculate zone concentrations. They use a function that they call an extended form of the KRF, but in reality, it does not provide an invariant along the channel. Instead, it is a current conservation function is used in conjunction with mass balance functions to calculate the ion concentrations in each zone. They use this method to calculate the theoretical pH and conductivity of a number of trailing zones, and compare these to experimental measurements. These measurements generally show good agreement.

Bocek, Deml, Kaplanova and Janak (1978), "Analytical Isotachophoresis: The Concept of the Separation Capacity"

This is the foundational paper on device size and ITP separation. Here, Bocek directly lays out a method for calculating the separation capacity of a device and the separation parameter of a sample. Most importantly, Bocek introduces the idea that when we think about ITP, one should think primarily not about electric field, nor even about current, but about total charge transferred through the system. This idea is expounded in Bocek's 1991 paper on charge-based models.

This analysis is limited to a sample containing two fully ionized species that will separate and focus under ITP, with a single fully ionized counter-ion. The model is based on calculating the flux of ions out of the mixed zone as a function of the charge transferred through the column.

The paper contains experimental validation of the model based on measuring the size of the mixed zone that remains from a sample after separation on columns with differing separation capacities. The results are within 10% of the predictions.

Thormann (1984), "Review: Principles of Isotachophoresis and Dynamics of the Isotachophoretic Separation of Two Components"

In 1984, there is already a review on the subject of separation dynamics in ITP, despite the fact that the years 1985-1991 will be some of the most productive in terms of theoretical understanding of the subject. Thormann's article covers much of the same ground as the preceding papers, but the presentation is tractable and well-written. Thorman simplifies the analysis by combining quantities that appear repeatedly in the analysis, such as the transference number. This strategy makes the theoretical explanation much easier to read. Thormann discusses some methods of manipulating the separation capacity and detection sensitivity of the column, including leading electrolyte cascade, as introduced by Bocek in 1978, and channel constriction.

Gebauer and Bocek (1985), "Optimization in Isotachophoresis: The Concept of Selectivity and Separation Speed"

In 1985, Bocek expanded on the concepts laid forth in the 1978 paper to propose a design method for ITP separation systems. He focused narrowly on systems with only

two separable components, but these components are not restricted to fully ionized species. The analysis method is still based on moving boundaries equations.

In this work, Bocek introduces a new parameter, the selectivity of the separands.

$$p = \frac{\mu_{B,BC}}{\mu_{C,BC}} - 1$$

This represents the relative speeds of the two ions in the mixed zone, and it determines how long the zone will take to separate. Importantly, this parameter may be a function of pH. It is also related to the two figures of merit that are proposed in the paper for optimality of separation: the separation volume and the separation time. These values are plotted relative to the pH of the leading zone to optimize the separation.

This paper considers the constraints of voltage, current, and heat dissipation in setting the time of the separation. It provides a useful diagram of the separation space, ash shown in figure 2.

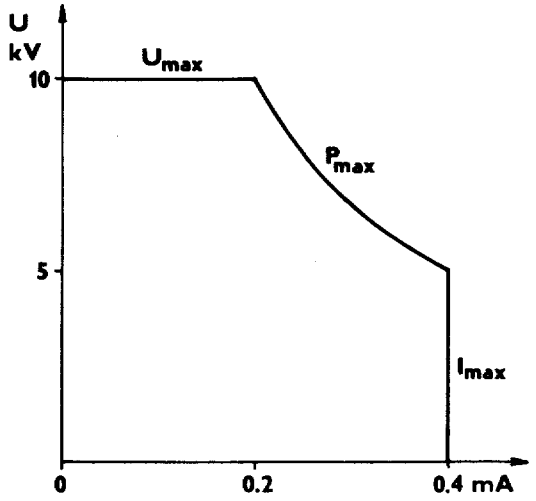

Figure 1-5. Operating space for current and voltage, as constrained by heat dissipation. Original caption reads, "Working diagram (voltage U vs. current I) of a model device with maximum parameters from Table I.

This paper focuses on optimizing chemistry for a fixed device geometry. It is complimentary to the next paper, which focuses on optimizing device geometry for a fixed chemistry.

Dolnik, Deml, and Bocek (1985), "Large Sample Volume Preseparation for Trace Analysis in Isotachophoresis"

In Bocek's second 1985 paper, he uses the theory he laid out in 1978 to construct an analytical device for detecting trace components in samples using ITP. The paper reasons that to detect a component, under ITP, a certain number of molecules are required. As the concentration of the species of interest goes down, the volume of sample that needs to be processed increases. To detect species at 1 μM, the device needs to process 1 mL of sample. As far as I know, this is the first example of someone explicitly using theoretical considerations about the physics of ITP to design a device to analyze large samples.

The device itself is complicated, and contains multiple buffering reservoirs and electrodes. This design reduces the voltage required to drive current through particular parts of the device, and increases buffering capacity, but it makes the device complicated to operate The separation channel has a high aspect-ratio, rectangular cross section to improve heat dissipation. The detection channel is narrow, to improve sensitivity.

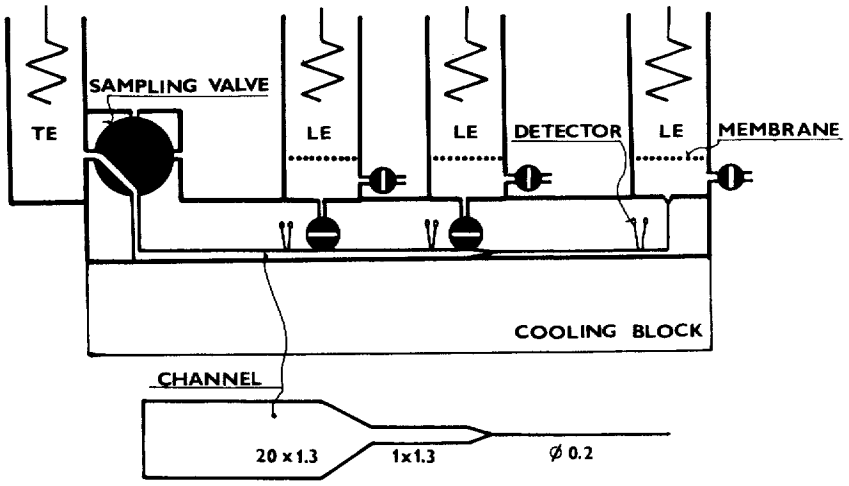

Fig. 4. Diagram of migration unit. TE = Terminating elecrolyte; LE = leading electrolyte.

Figure 1-6. Bocek's device for trace analysis in ITP.

Mosset, Gareil, Desbarres, and Rosset (1987), "Simple Approximate Relationships and Accurate Computer Simulation as Complementary Means for Optimizing Separation Conditions in Isotachophoresis"

This paper is a more rigorous attempt to create a computer-aided model of ITP using moving boundary analysis. It includes weak acids and bases, ionic strength

corrections and activity corrections, and shows the relative importance of each. They derive an equation for separation capacity that is much more general than the equation derived by Bocek. They use this analysis to optimize their separation to prevent trace analytes from disappearing in mixed zones. The electropherograms produced by the model compares favorably with experimental results from ITP of a sample with 6 distinct analytes, although this comparison is made for fully resolved zones. There are experiments that contain mixed zones, but these are compared to theory only based on resolved zone length, not full electropherograms.

Hirokawa, Nakahara, and Kiso (1989), "The Separation Process in Isotachophoresis: I. A 32-Channel Ultraviolet-Photometric Zone Detector"

This article has relatively little to contribute to the theory of separation capacity in ITP, but it is tremendously important to Hirokawa's later work in visualizing ITP separation. Hirokawa et al. construct a device to collect UV electropherograms at 32 points along a separation capillary during ITP experiments. They then overlay these electropherograms in such a way that they can reconstruct 3-dimensional wireframe plots of ITP separation in real time. Thus, this paper contains the first 3D (time, space, UV absorption) visualization of ITP zones separating.

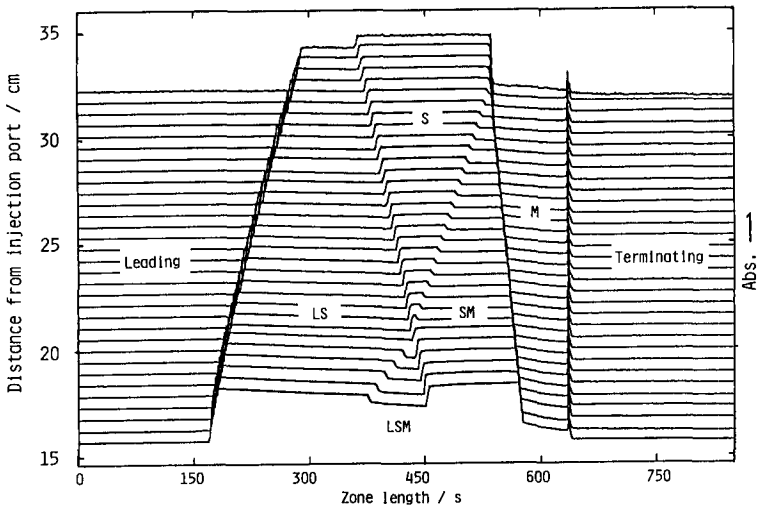

Fig. 4. Transient isotachopherogram of SPADNS and monochloroacetic acid observed by the use of the 32-channel UV-photometric detector. The injected sample zone was pushed toward the terminating electrolyte compartment. The position of baselines of the UV absorption shows the distance of the photocell from the sample injection port. The observed boundaries between the terminating and the preceding MCA zones were rearranged at the same abscissa position. Samples: 5 m*M* SPADNS(S); 5 m*M* monochloroacetic acid (M), 10 μl. LS, LSM and SM denote the mixed zones formed among the leading ions(L), SPADNS(S) and monochloroacetate ions(M). The leading electrolyte was 1 m*M* hydrochloric acid and the pH was adjusted to 3.6 (buffer β-alanine). The terminating electrolyte was 10 m*M* caproic acid. The migration current was 98.4 μA. The I.D. of the separation tube was 0.51 mm.

Figure 1-7. The first reported visualization of ITP zone separation occurring 3 dimensions. The images are difficult to understand initially, but they are conceptually similar to the plots created by Brouwer and Postema (see figure 1.) The main difference is that these are the history of the zones moving past a set of stationary detectors, rather than complete zones in space at a single time.

Hirokawa, Nakahara, and Kiso (1989), "The Separation Process in Isotachophoresis: II. Binary Mixtures and Transient State Models"

Hirokawa immediately used the new 32-channel detector to begin testing models for the separation process in ITP. In this paper, we see more of the 3 dimensional visualizations of zone formation. This paper contains the most complete comparison between theory and experiment regarding zone formation in ITP

This paper goes into substantial detail about constructing a moving boundary simulation, although the theoretical method is similar to the ones shown in previous papers. The paper compares two different models, which it calls SPR and non-SPR, (SPR standing for "sample property reflecting"). The separation in the non-SPR model depends only on the conditions in the leading electrolyte, while the SPR model also takes into account the pH of the sample. The non-SPR model is an acceptable approximation for fully ionized monovalent ions with no ionic strength effects. The experiments are

compared to these different modeling regimes in two different analyte systems. Again there are detailed visualizations of the separation process. Concentration ratios, separation times, zone pHs, and other important parameters are pulled from the data and compared to the predictions.

Dolnik, Deml, Gebauer, and Bocek (1991), "Optimization of Isotachophoretic Analysis: Use of the Charge-Based Transient-State Model"

In this paper, Bocek more fully addresses using a model based on charge to analyze ITP systems. He considers pH as a variable for optimization, similar to the work by Bocek in 1985 and by Rosset in 1987. Here, he creates an algorithm to optimize the pH of the leading electrolyte through iteration reduce separation time.

Perhaps the most interesting portion of the paper is the introduction of a graphical method for determining the minimum separation capacity of a column required to fully separate a set of species using ITP. Components are plotted on an unrestrained spaciotemporal plot, with both axes scaled by charge. The spatial dimension is scaled by the separation capacity of the column up to that point, while the temporal axis is scaled by the charge transferred through the system to that point. The sample separates as it travels up and to the right on the plot. Zone boundaries disapper. The rightmost boundary to disappear is the boundary that sets the separation parameter.

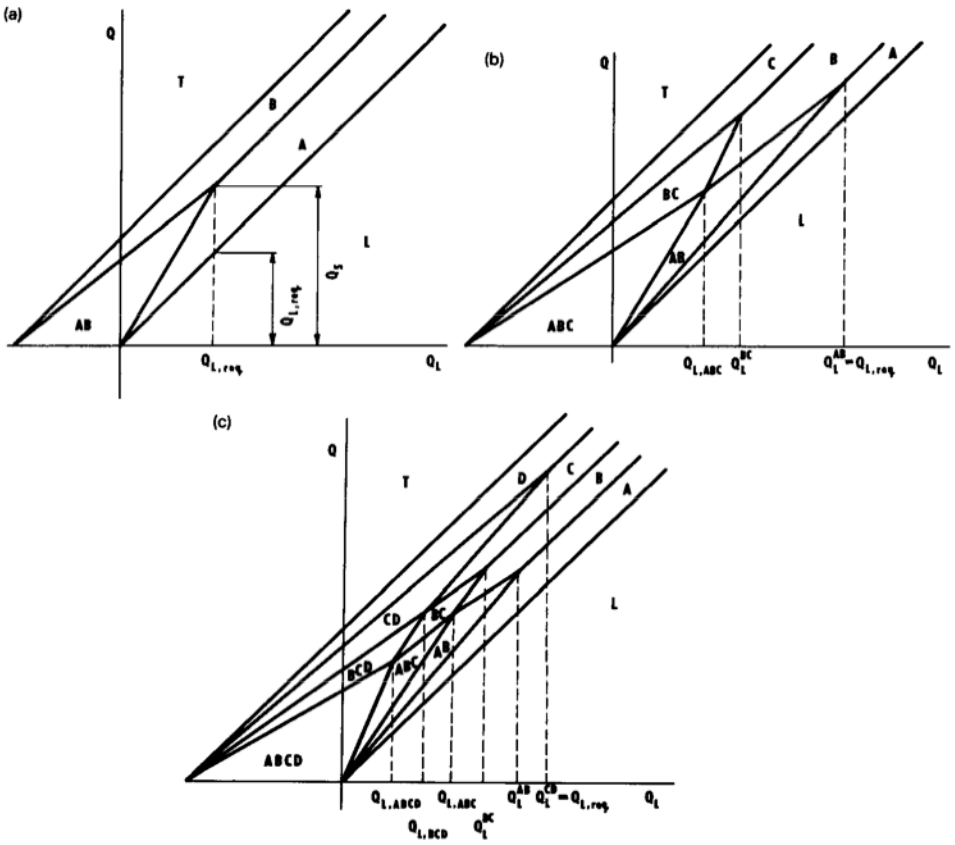

Fig. 1. Scheme of isotachophoretic separation of multi-component sample containing (a) two components A and B, (b) three components A, B and C and (c) four components A, B, C and D.

Figure 1-8. Graphical representation of required separation capacity of a column to separate complex samples.

Hirokawa, Yokota, and Kiso (1991), "Effects of Sample Composition on the Separation Efficiency of Isotachophoresis"

Prior to this paper, most analysis assumed that the sample composition was set, and designed the buffering chemistry of the leading and trailing electrolytes to suit the sample. This paper addresses whether adding species to the sample itself can improve separation.

The short conclusion is that addition of a third component to a sample increases the separation time of the other two components, especially when the third component has a mobility near the other two. Importantly, this analysis again devolves to the case of fully ionized species. It also omits analysis of the situation in which the additional species has a mobility between the two species to be separated. Lastly, it takes its efficiency in terms of the charge of separation, but does not address whether the total separation

capacity of the column will be favorably affected. This is possible if, for example, a component is added that overruns the sample.

The theoretical results are again compared to experimental results from Hirokawa's multi-channel UV setup, and they match reasonably well.

This paper creates a reasonable theoretical approach to the problem of additional species in ITP, but it doesn't substantially address the reasons one might want to add additional species; namely, to change the pH of the sample and alter the mobility of the analytes in the sample zone.

Hirokawa, Omori, Yokota, Hu, and Kiso (1991), "Isotachophoretic Separation of Minor Components from a Matrix Component in the Case of Strong Electrolytes"

Here, Hirokawa treads some of the same ground initially walked by Rosset in assessing the presence of minor sample components in ITP systems. This paper is similar in many ways to the other 1991 paper in that it addresses the separation time for multi-species samples. However, while the first 1991 paper primarily kept the sample equimolar, this one varies the concentration ratios in a sample with a fixed number of components.

Problems not addressed in the literature

Multiple Countermigrating Ions

Countermigrating ions do affect the separation parameter of the sample, but they are not addressed in the literature. It is usually assumed that there is a single countermigrating species, and this is the same species that is present in the leading electrolyte. Particularly in blood, the sample initially contains a high concentration of sodium, and lower concentrations of potassium and magnesium, that is displaced by the counterion of the LE. This displacement affects the conductivity of the sample zones.

Non-focusing Co-ions

The literature assumes that all coions present in a given sample will focus. This is not the intention of our extraction experiments, where we design ITP conditions to separate undesired co-ions. These non-focusing contaminant are in essence under CZE conditions, and the distance between the focused zone and the unfocused contaminant is an important figure of merit. The issue is treated extensively in chapter 2.

When is it desirable to add species to the sample?

Hirokawa addresses the effect of additional species on separation parameter in his 1991 paper, but he doesn't really address the reason that one would want to add a species: to change the pH. The desire to change the pH of the sample, and to add a buffer, is the primary reason we would alter the chemistry. Buffering problems can develop when, for example, ITP of blood lysate creates a temporary zone that contains only sodium and chloride. An interesting question is, what are the minimal additions that can be made to provide buffering, and how will they affect the separation parameter?

Unmet Needs in Nucleic Acid Purification

We ran a survey of contemporary practices in nucleic acid purification to assess the unmet needs in this field. We conducted the survey through an online webform (Google Docs), and advertised the form to life science researchers through email requests and online advertisements. We collected responses between 5/17/2012 and 5-20-2013.

Survey Text

The survey text is included below. For brevity, the answers for multiple choice questions are excluded. Questions with asterisks (*) were mandatory.

Sample preparation is often the most manually intensive work in a laboratory. Our group is working to develop new sample prep methods with the hope of furthering the technology and addressing unmet needs. We are conducting this survey to understand current practices and needs for sample preparation of nucleic acids. We will publish the results of this survey as a set of statistical summaries. We will not attribute responses to individuals, specific labs, or specific companies. We thank you for your information.

You may include your email address at the end of this form to enter a drawing for a $500 Amazon gift card. One entry per person. Your email address will not be used for any other purpose. You may enter this drawing without completing the survey by sending a message containing your email address to sampleprep [at] stanford [dot] edu.

Juan G. Santiago
Lewis A. Marshall
May 11, 2012
microfluidics.stanford.edu

Institution

*Which of the following best describes your institution? **

*Which of the following best describes the type of organism(s) with which you work? **

Starting Material

We here ask about the types of samples with which you work. If you work with multiple sample types, you can either describe the samples you use most often or you can select all that apply.

*What type of starting samples are you analyzing? *Please check all that apply.*

*What is your ideal starting sample volume? *Please select the best option.*

How much total nucleic acid content do you expect in a typical starting sample?

Targets

*What type(s) of target are you trying to extract and purify? **

Current Sample Prep Method

What extraction technique(s) do you currently use?

If you use a commercial kit, which commercial kit do you most commonly use?

Lysis

Does your sample require lysis?

Which methods do you use to lyse?

What lysis efficiency do you absolutely need?

Workload

*How long does each sample extraction currently take? **

Roughly how many samples do you process per week?

Quantitation and Validation

*How much is your ideal output volume? **

How much yield (i.e., extraction efficiency) do you require, as a percentage? ?

Do you quantify target immediately after extraction?

How do you quantify your target molecule (after extraction but before performing other assays)?

How would you describe the accuracy you require for quantitation, after extraction and before performing other assays?

After sample preparation, what assays and/or processes do you perform?

Conclusion

What is your biggest challenge in preparing nucleic acids?

Would you like to be entered into a drawing for $500 Amazon gift card? If so, please include your email address below. Your email address will not be used for any other purpose

Thank you for your time. If you have any comments, please leave them below. If you have questions and would like a response, please email sampleprep [at] stanford [dot] edu.

Results

We collected responses from a total of 157 respondents. Of these respondents, the 91% (143) were from academic research institutions. The remainder was split between governmental research institutions (7), commercial research institutions (5) and other (2).

The respondents worked with a wide range of organisms. The largest fraction, 43% (67) worked with bacteria. They also worked with a range of sample types, with the most prevent being cultured cells (100) and tissues (87). The most common targets for extraction were genomic DNA (108), plasmid DNA (72) and messenger RNA (29).

Table 1-2. Responses to the question, "Which of the following best describes the type of organism(s) with which you work?" Respondents may have selected more than one checkbox, so percentages add up to more than 100%.

Organism	Number	Percentage
Humans	49	31%
Non-human mammals	51	32%
Non-mammalian vertebrates	11	7%
Invertebrate animals	25	16%
Plants	12	8%
Bacteria	67	43%
Immortalized cell lines	41	26%
Viruses	20	13%
Other	9	6%

a. b.

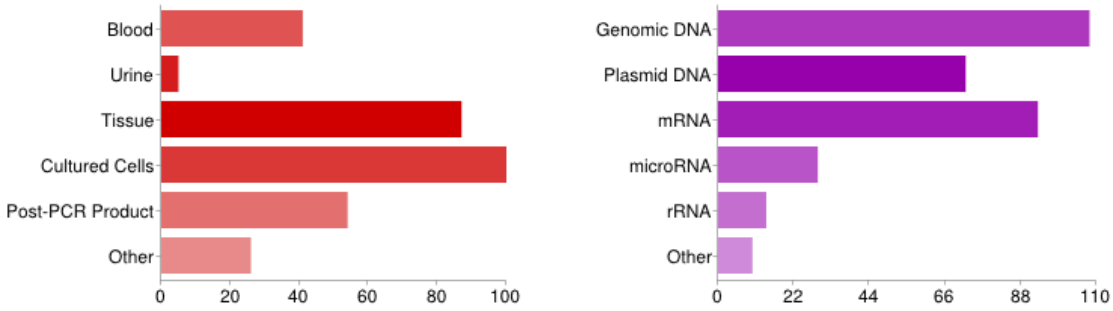

Figure 1-9. ***a.*** *Responses to the question, "What types of samples are you analyzing?* ***b.*** *Responses to the question, "What type(s) of target are you trying to extract and purify?" For both questions, respondents may have given more than one answer.*

We asked respondents which extraction techniques they currently use for nucleic acid purification. The majority of respondents used one or both of solid phase extraction (76) and phenol chloroform extraction (94).

Table 1-3. Responses to the question, "What extraction technique(s) do you currently use?" Respondents may have selected more than one checkbox, so percentages add up to more than 100%.

Technique	Number	Percentage
Solid phase extraction	76	50%
Phenol/chloroform extraction	94	62%
Bead Capture	45	30%
Other	19	13%

Critically the results of this survey reveal an unmet need in the preparation of nucleic acids from small sample volumes, with small total nucleic acid content. While many respondants respondents typically deal with samples larger than 500 µL (46), there are significant fractions of researchers dealing with sample volumes less than 50 µL (66). It is challenging to work with samples in this volume range with convential SPE and liquid-liquid extraction. In addition, a significant fraction of respondents (45) reported dealing with nucleic acid masses of less than 100 ng. In this range, solid phase extraction kits can have low operation efficiency due to nucleic acids retained on the column.

These observations were supplemented by anecdotal responses from the question, "What is your biggest challenge in preparing nucleic acids?" Some representative responses were:

- "Sorting out specific cells. Getting good mRNA from single cells or <10 cells."
- "Few good methods for extracting mRNA from very few cells (~10)."
- "Getting consistently pure preps."
- "Getting enough mRNA from a small, precious sample to do sequencing…"
- "Getting high yield from low cell numbers."
- "Getting sufficient concentrations of RNA from small amounts of tissue. Small elution volumes could be helpful."
- "Speed."

Research in sample preparation of nucleic acids using new techniques, particularly microfluidic techniques, should be focused on solving problems that cannot be solved using current techniques. ITP has the potential to deal with small samples at high efficiency and high speed, allowing it to address many of the currently unmet needs in sample preparation. However, addressing these problems requires a better understanding of the design of systems for ITP purification.

Chapter 2 Design for Purification using Isotachophoresis

Some of the contents of this chapter are under preparation as an article in Analytical Chemistry by Lewis A. Marshall and Juan G. Santiago. They are reproduced here with minor modifications.

2.1. Introduction

Isotachophoresis (ITP) is a well-established electrophoretic technique for ion separation, purification, and pre-concentration via focusing.[1,2] In ITP, sample ions are focused by an electric field gradient between a high conductivity leading electrolyte (LE) and a low-conductivity trailing electrolyte (TE). This focusing leads to self-sharpening ion concentration waves that steepen and propagate under application of an electric field.[1] If the total number of sample ions is low, the process results in so-called peak mode ITP where multiple sample ion species focus into a common peak. Given sufficient amount of sample, focusing time, and sample ion solubility, sample species concentrations can reach a maximum and self-sort into contiguous plateau regions ordered by effective electrophoretic mobility.[1,3]

ITP has long been used as an analytical technique to stack ionic species in adjoining zones, and to increase the concentration of dilute ions prior to detection. Analytical ITP can be coupled with a variety of detection modalities including potential gradient,[4] UV absorbance,[5] and fluorescence.[6] The same features that make ITP a powerful analytical technique make it a valuable purification tool for collecting dilute ions from complex samples. Recently, ITP has been used to purify a nucleic acids from a variety of sample matrices including serum and plasma (after a buffer exchange step),[7] cultured kidney cell lysate,[8] blood lysate[9-10] and urine lysate[11] and to selectively concentrate proteins from serum.[12]

The design and optimization of ITP systems has been studied for several decades,[5,13,14] but the specific problems and challenges associated with ITP purification of a target species has not been addressed. Namely, the issue of rapidly and efficiently extracting desired species from undesired impurities. Also lacking are analyses applicable to the scaling and design features of on-chip systems. We here describe major design

principles associated with constructing and designing on-chip ITP protocols specifically for the purification of target ions from complex samples containing multiple impurities. This design process involves a different set of considerations and demands new and different figures of merit. These figures of merit include processed volume capacity, extraction efficiency, and the separation between focused analytes and unfocused impurities. We focus on the case of a high mobility analyte in the presence of lower mobility impurities, which is common to extracting nucleic acids from complex samples. We present an experimental validation of the model and experiments demonstrating an idealized purification process using a simple, well-characterized fluorophore as a model analyte.

2.2. Theory

2.2.1 Scope

We limited the scope of our problem to focus on the key issues and to make the analysis more tractable. We assume we are collecting under conditions (e.g., pH) in which we are extracting a dilute analyte ion with a relatively high electrophoretic mobility from a sample containing lower mobility impurities. For simplicity, we assume we suspend the sample ion mixture in either the TE or the LE (but not both). We also limit our scope to a batch separation processes (e.g., in contrast to continuous flow processes such as free-flow ITP[15]). With a view toward maximizing extraction efficiency, we assume that the sample is injected directly into a separation channel that is bounded by pure LE and pure TE (e.g., versus a sample mixture dispensed into and then extracted directly from an end-channel reservoir). We also assume that the analyte ions will focus into peak mode[16] ITP (rather than focusing in plateau mode) as this is the case most consistent with extraction of nucleic acids from complex matrices.

Lastly, we make some assumptions regarding the flow regimes of interest. We assume electroosmmotic flow is well suppressed so that deterministic transport through the chip is well described by electromigration. We also neglect dispersion,[17] including molecular diffusion, in our analyses. The latter assumption is consistent with operation with sufficiently large electrophoretic Peclet number.[18] For our purposes, this applies to

LE-to-TE interfaces (and ITP zones) with axial dimensions much smaller than the macroscopic species zones and channel lengths of interest. We use this assumption because we are interested in determining separation lengths required to fully extract target species, and separations distances between target species and impurities. The characteristic dimensions of ITP focused zones[17] and local concentration values at ITP zone peaks are much less interesting in the current analysis.

2.2.2 Recommended Separation Geometry

Channel geometry is perhaps the most important component of an ITP-based purification system design. Geometry is key to achieving high extraction efficiency and obtaining a good separation between the purified analyte and impurities.

As a model system, we will consider a system with five ionic species: the analyte (species to be purified), the highest mobility contaminant of interest (the "most problematic" species to be excluded from collection), the high mobility ITP leading ion, the low mobility ITP trailing ion, and a counter ion common to both the LE and TE. We will assume that the analyte and contaminant species are of sufficiently low concentration so they do not contribute to local zone conductivity or pH. The pH and conductivity of all zones in the system are then dominated by the properties of the leading ion, trailing ion, and counter ions in the system.

In the derivations below, we assume that the sample is suspended in the TE. As mentioned above, it is also possible to suspend the sample in the LE. For both cases (sample in TE or LE), the resulting figures of merit are presented in Table 1.

We further consider that the system can be operated in either cationic or anionic mode. In anionic mode, all ions except the counter-ion are negatively charged, and migrate together toward the anode. In cationic mode, all ions except the counter-ion are positively charged, and migrate together toward the cathode. The common case of extracting NA from complex samples is an example of the former case.

We have explored various geometries and schemes for batch ITP-based purification protocols. Figure 1 shows our proposed minimum set of design features required to achieve highly efficient purification of a sample using ITP. The device consists of a sample channel, a separation channel, and three reservoirs. We introduce two reservoirs dedicated to buffering the electrolysis process, one for LE and one for TE.

These reservoirs contain high concentration buffer solutions (order 300 mM and higher) to provide the buffering capacity required to extract from relatively large volumes at high extraction efficiency. In addition to these buffering reservoirs, there is an extraction reservoir filled with relatively low concentration LE (10 to 50 mM) from which the purified sample will be extracted.

Our design also incorporates a fourth port to aid in channel loading. This is shown as the air outlet port in Figure 1. The purpose of this port is to draw a vacuum on the chip while the chip is being loaded and to control the location of the initial TE-to-LE interface. As shown in Figure 1, four key parameters in the system are respectively the length and cross-sectional area of the sample channel, L_s and A_s, and the length and cross-sectional area of the separation channel, L_{ch} and A_{ch}. These determine a critical parameter: the sample-to-separation channel volume ratio, $R_{vol}=(L_{ch}A_{ch})/(L_sA_s)$.

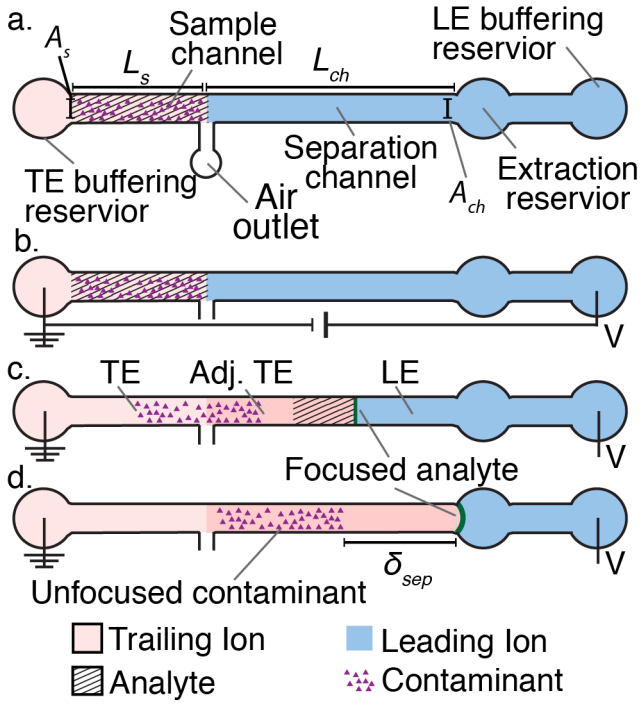

Figure 2-1. Schematic for purification process using a well-buffered ITP system. We show here sample mixed into the TE buffer as an example. ***a.*** *The device is initially filled with sample and separation buffers by applying vacuum to an air outlet port. On the left end is a buffering reservoir containing the high concentration buffering TE mixture (free of sample). On the right side are an extraction reservoir and a high concentration LE buffering reservoir. A weak electrolyte counter-ion is common to the entire system* ***b.*** *Electrodes are placed at the two buffering reservoirs, and current is applied.* ***c.*** *Anions, including sample, migrate toward the LE buffering reservoir. The adjusted TE zone is formed as trailing ions displace leading ions. The sample species focus at the ITP zone between the LE and TE co-ions. The contaminant ions have a mobility lower than the TE co-ion and so fall behind the ITP zone instead of focusing.* ***d.*** *Experiment ends shortly after the ITP zone enters the sample extraction reservoir. We define separation distance, δ_{sep}, as the distance between the ITP zone to be extracted and the fastest contaminant.*

2.2.3 Recovery Efficiency

We here describe the dependence of recovery efficiency on key system parameters. We generally follow the analysis approach of Bocek et al.[13] for separation capacity and a separation parameter, but we here generalize it to describe weakly ionized species. We can express the current carried through the channel, *I*, in terms of the total flux of trailing ions in the adjusted ITP zone as:

$$I = \frac{dQ}{dt} = A_{ch} j = A_{ch} \frac{j_T}{T_T} = A_{ch} U_{ITP} \left(\frac{\lambda_t c_T}{\mu_t T_T} \right)_{ATE} \qquad (1)$$

Here, Q is the charge transferred, t is time, A is the cross-sectional area of the channel, j is the current density, U_{ITP} is the velocity of the ITP zone. j_T is the current density carried by the trailing ion, while T_T is the transference number of the trailing ion (that is, the fraction of current carried by the trailing ion).[19] Finally, c_T is the concentration of the trailing ion, λ_T is the molar conductivity of the trailing ion, and μ_T is the effective mobility of the trailing ion. The subscript ATE indicates that the variable(s) are evaluated in the adjusted trailing electrolyte (ATE) zone. This ATE is defined as the TE zone in regions formerly occupied by the LE (and therefore subject to the appropriate regulating functions).[20]

The molar conductivity and the effective mobility can be calculated using Equations 2 and 3 based on the fraction of the species in each charge state z. We here follow the notation of Bercovici et al. for weak electrolytes as follows:[20]

$$\mu_i = \sum_z \mu_{i,z} g_{i,z} \tag{2}$$

$$\lambda_i = \sum_z g_{i,z} \mu_{i,z} F z \tag{3}$$

Here, $\mu_{i,z}$ is the absolute mobility of ion i in charge state z, and $g_{i,z}$ is the fraction of species i in charge state z. F is the Faraday constant.

Next, we can express the rate of analyte focusing in terms of the channel cross-section, analyte concentration in the adjusted TE, and local values of the analyte ion drift velocity, U_A, as follows:

$$\left(\frac{dN_A}{dt}\right)_{focused} = A_{ch}\left[c_A\left(U_A - U_{ITP}\right)\right]_{ATE} = A_{ch}\left[c_A\left(\mu_A - \mu_T\right)E\right]_{ATE} = A_{ch}U_{ITP}\left[c_A\frac{\mu_A - \mu_T}{\mu_T}\right]_{ATE} \tag{4}$$

Here, N_A is the number of focused analyte molecules, and μ_A is the local effective mobility[21] of the analyte. We note that this expression is proportional to the so-called separability, p_{ij}, between the TE and the analyte defined as[22]

$$p_{ij} = \left| \frac{\mu_i - \mu_j}{\mu_j} \right|. \tag{5}$$

Here μ_i and μ_j are the effective mobilities of two species of interest i and j. p is a non-dimensional expression describing the degree of difference in mobility between these ions.

We can combine Equations 1 through 4 to derive an expression for the number of analyte molecules focused per unit applied charge:

$$\frac{dN_A}{dQ} = \left[\frac{c_A}{c_T} \frac{\lambda_T p_{AT} T_T}{\mu_T} \right]_{ATE} \tag{6}$$

We integrate this and solve for the amount of applied electric charge, Q_s, required to drive some number of analyte molecules, N_A, to the interface. Further, setting N_A equal to the total analyte content of the sample, we derive an expression for the so-called separation parameter, Q_s:

$$Q_s = \left[N_A \right]_S \left[\frac{c_T}{c_A} \frac{\lambda_T}{\mu_T p_{AT} T_T} \right]_{ATE} \tag{7}$$

Here, the subscript S denotes parameters measured within the initial the sample volume. Q_s can be interpreted as the electric charge required to extract all of the analyte from the sample mixture.

We are here interested in well-buffered ITP systems wherein the local pH of all zones is approximately the same. In the common case of anionic ITP, this pH value is typically near the pK_a of the common counter-ion (a weak base). This lets us further

assume that the analyte and impurities ions have approximately the same effective mobilities in all zones. Accordingly, we here assume the analyte and impurity ions have the same effective mobility in both the (original) sample zone and the adjusted TE zone. Under this assumption, the concentration ratio c_T/c_A will remain constant between the sample and the adjusted TE zones.[23] This approximation is very useful to our system design analysis as it lets us express Q_s in terms of the number of trailing ions in the original sample zone, $\left[N_T\right]_S$, as follows:

$$Q_s = \left[N_T\right]_S \left[\frac{\lambda_T}{\mu_T p_{AT} T_T}\right]_{ATE} \tag{8}$$

Interestingly, Q_s depends only on the number of the ions in the sample, and the properties of the adjusted TE zone. In turn, the latter is typically dominated by the choice of buffers and initial concentration of the LE.

The experiment ends shortly after the ITP zone elutes into the extraction reservoir. The arrival of the ITP zone to the extraction reservoir occurs after a known amount of charge, Q_L, is transferred by the LE zone. Q_L has been called the separation capacity of the separation channel[13]and can be expressed as follows:

$$Q_L = \left[\frac{N_L \lambda_L}{\mu_L T_L}\right]_{LE} \tag{9}$$

Equations 8 and 9 show that the separation parameter and the separation capacity are directly proportional to the number of ions sample and separation channels, respectively.

Finally, we can express the recovery efficiency of the analyte, η, as follows:

$$\eta = \frac{Q_L}{Q_s} = \frac{[N_L]_{LE}}{[N_T]_S} \frac{\left[\frac{\lambda_L}{\mu_L T_L}\right]_{LE}}{\left[\frac{\lambda_T}{\mu_T p_{AT} T_T}\right]_{ATE}} = \frac{A_{ch} L_{ch}}{A_s L_s} \frac{[c_L]_{LE}}{[c_T]_S} \frac{\left[\frac{\lambda_L}{\mu_L T_L}\right]_{LE}}{\left[\frac{\lambda_T}{\mu_T p_{AT} T_T}\right]_{ATE}}.$$

(10)

η describes the fraction of analyte ions that reach the ITP zone before the ITP zone reaches the end of the separation channel. In the second and third equalities of Eq. (10), we show how the collection efficiency is directly proportional to the volume ratio we discussed earlier, $R_{vol}=(L_{ch}A_{ch})/(L_sA_s)$. Note that $[c_L]_{LE}$ is the concentration of leading ions in the leading electrolyte zone, while $[c_T]_S$ is the concentration of trailing ions in the sample. Clearly, the volumes and initial ion concentrations of the sample and separation channels have an immense influence on our ability to process samples with high recovery efficiency.

2.2.4 Separation From Contaminants

As we process the sample, co-ion contaminants in the sample zone electromigrate toward extraction reservoir at a velocity less than U_{ITP}. As mentioned above, we assume that these unwanted contaminants are present at a concentration significantly less than the local buffer ions and so do not contribute to current. A contaminant for removal with a local effective mobility μ_R will have an effective electromigraiton velocity U_R expressed as:

$$U_R = [\mu_R E]_{ATE} = \left[\frac{\mu_R}{\mu_T}\right]_{ATE} U_{ITP}$$

(11)

The distance between the ITP zone and the contaminant at the end of the experiment, δ_{sep}, is then simply.

$$\delta_{sep} = \int_{t_o=0}^{t_{sep}} (U_{ITP} - U_R)dt = \int_{t_o=0}^{t_{sep}} \left[E(\mu_T - \mu_R)\right]_{ATE} dt = \int_{t_o=0}^{t_{sep}} U_{ITP}\left[\frac{\mu_T - \mu_R}{\mu_T}\right]_{ATE} dt = [p_{RT}]_{ATE} L_{ch}$$

(12)

t_{sep} is the time to complete the separation. If the sample is diluted in the TE, δ_{sep} is only a function of the channel length and the separability between the trailing ion and the contaminant, p_{RT}.

The designer of an ITP-based extraction system is also interested in the additional amount of electric charge that can be applied after the ITP zone reaches the extraction reservoir, but before the contaminant first arrives at the extraction reservoir. This parameter, which we here call Q_{ex}, can be constructed using an approach similar to that of Eq. 12 (see also SI) and expressed as follows:

$$Q_{ex} = \left[\frac{\mu_T - \mu_R}{\mu_R} \right]_{ATE} Q_L = \left[p_{TR} \right]_{ATE} Q_L \tag{13}$$

The subscript "ex" refers to "extra" charge that can be applied to the system after the ITP zone reaches the sample reservoir, but before the first contaminant arrives. After the sample reaches the extraction reservoir, the system may apply an additional charge up to (but never exceeding) Q_{ex} to help position the sample zone inside the extraction reservoir.

2.2.5 Purification Time

Lastly, at constant applied current, the purification time can be written simply as the separation capacity divided by the current.

$$t_{sep} = \frac{Q_L}{I} = \frac{A_{ch} L_{ch}}{I} \left[\frac{c_L \lambda_L}{\mu_L T_L} \right]_{LE} \tag{14}$$

We use the second equality to show how separation time depends linearly on leading electrolyte concentration and separation channel volume. For a fixed sample volume and LE buffer concentration, we see that we can reduce the separation time by applying higher current. In practice, however, the maximum current is limited by considerations of Joule heating and/or buffering capacity. We discuss the operational constraints of buffering and Joule heating below.

2.2.6 Dilution Factor

The last factor to consider for purification is the dilution factor, F_{dil}. We define F_{dil} as the ratio between the concentration of analyte in the original sample and the concentration of the analyte in the extracted liquid. This ratio depends on the efficiency of extraction and the volume ratio of the input sample and extracted product as follows.

$$F_{dil} = \frac{V_{extract}}{\eta A_s L_s}$$

(15)

We believe the smallest usable value of $V_{extract}$ is a complex function of the method by which liquids are extracted off of the chip and the fabricated geometry of the extraction port. We hope to explore the minimum value of $V_{extract}$ in future work.

2.2.7 Figures Of Merit

Table 1 below summarizes the figures of merit we have so far identified in the design of an ITP-based sample extraction system. These figures of merit should be considered vis-à-vis operational constraints which are associated with running the system and which we explore in the following sections.

Table 2-1. Expressions of the figures of merit applicable to purification of high mobility target analytes via ITP. Separate equations are given for the cases where sample is suspended in the TE or in the LE.

Parameter	Symbol	Sample Diluted in TE	Sample Diluted in LE
Separation Parameter	Q_s	$[N_T]_S\left[\frac{\lambda_T}{\mu_T p_{AT} T_T}\right]_{ATE}$	$[N_L]_S\left[\frac{\lambda_L}{\mu_L p_{AL} T_L}\right]_{LE}$
Separation Capacity	Q_L	$\left[\frac{N_L \lambda_L}{\mu_L T_L}\right]_{LE}$	$\left([N_L]_{LE}+[N_L]_S\right)\left[\frac{\lambda_L}{\mu_L T_L}\right]_{LE}$
Separation Distance	δ_{sep}	$[p_{RT}]_{ATE} L_{Channel}$	$[p_{RT}]_{ATE}\left(1-\frac{[N_L]_S}{[p_{LR}N_L]_{LE}}\right)L_{Channel}$
Separation Charge	Q_{sep}	$[p_{TR}]_{ATE} Q_L$	$[p_{TR}]_{ATE}\left(1-\frac{[N_L]_S}{[p_{LR}N_L]_{LE}}\right)Q_L$
Recovery Efficiency	η	Q_L / Q_S	
Extraction Time	t	Q_L / I	
Dilution Factor	$F_{Dilution}$	$V_{extract} / A_s L_s$	

2.2.8 Operation Constraints

We here consider three primary constraints that limit the operation of our microfluidic device. The extraction time is controlled primarily by the maximum current, which is limited by two constraints: the maximum allowable temperature rise in the system due to Joule heating and/or the maximum allowable electrolysis gas generation rate at the electrodes. The third constraint is one on the total charge transferable charge through the device, which is limited by the buffering capacity of the electrolyte buffering reservoirs. We will address each of these constraints in turn.

2.2.9 Joule Heating

Joule heating is well studied in electrophoretic systems, and known to limit and/or disrupt separation.[24] The temperature rise an electrophoretic and/or ITP channel is a function of the channel geometry, the thermal and ionic conductivities of the electrolyte, the applied current, and the thermal coupling of the channel to the environment.

To achieve high sample throughput in our system, we have chosen to use high-aspect-ratio, rectangular-cross-section channels. The heat dissipation characteristics of channels of this type have been described by Cifuentes et al.[25] Cifuentes considered the common case where the advection of heat in the channel (e.g., due to residual electroosmotic flow) is negligible compared to the conduction flux in the channel cross-section (i.e., a low thermal Peclet number case). For large aspect ratio rectangular channels (treated as an infinitely wide channel), the temperature rise in the center of the channel relative to the temperature of the exterior walls can be estimated as,

$$\Delta T = \left(T_{cent} - T_{ext}\right) = \frac{j^2}{\sigma}\left[\frac{h^2}{8k_L} + \frac{hd_{wall}}{2k_{wall}}\right]$$

(16)

Where T_{cent} is the temperature at the center of the channel, T_{ext} is the temperature of the exterior wall of the substrate, h is the channel depth, d_{wall} is the thickness of the channel walls, k_l is the thermal conductivity of the liquid, and k_{wall} is the thermal conductivity of the channel wall.

Temperature changes due to Joule heating can have strong effects on the electrolyte properties, including viscosity, pH, ionic strength, and conductivity.[26] To preserve the design characteristics of the electrolytes we choose for our separation, we here limit our analysis to some maximum allowable temperature rise, $\Delta T_{max} = (T_{cent} - T_{ex})_{\max}$, which will have negligible effect on buffer properties In practice, we recommend ΔT_{max} of about 5°C or less. For this simple case, we can treat buffer parameters in Equation 16 as approximate constants and rearrange to find the maximum applicable current as follows:

$$I_{\max} = A_{\min}\sqrt{\frac{\Delta T_{\max}\sigma_{\min}}{\left[\frac{h^2}{8k_L} + \frac{hd_{wall}}{2k_{wall}}\right]}}$$

(17)

The "min" subscripts consider a case such as that depicted in Figure 1 where h and d_{wall} are uniform. A_{min} is the smallest cross-sectional area in the channel system carrying current I. For the system of Figure 1, A_{min} is then associated with the region of the sample or separation channels with the smallest width. σ_{min} is the minimum conductivity experienced by this minimum channel area, typically either the conductivity of the sample or the adjusted TE.

Variations in the width of the channel may be advantageous in, for example, aiding in loading of the device or to reduce electrophoretic dispersion around corners caused by varying path lengths and electric field intensities.[27] Figure 2 shows an example of a channel constriction intended to reduce electrophoretic dispersion. We also show visualizations of the temperature field obtained using calibrated infrared imaging of the channel under applied current conditions. Such images confirm our design approach of basing our temperature constraint on the smallest channel cross-section in the system (as per Eq. 17). See Section 2.3.2 for further description of these visualizations.

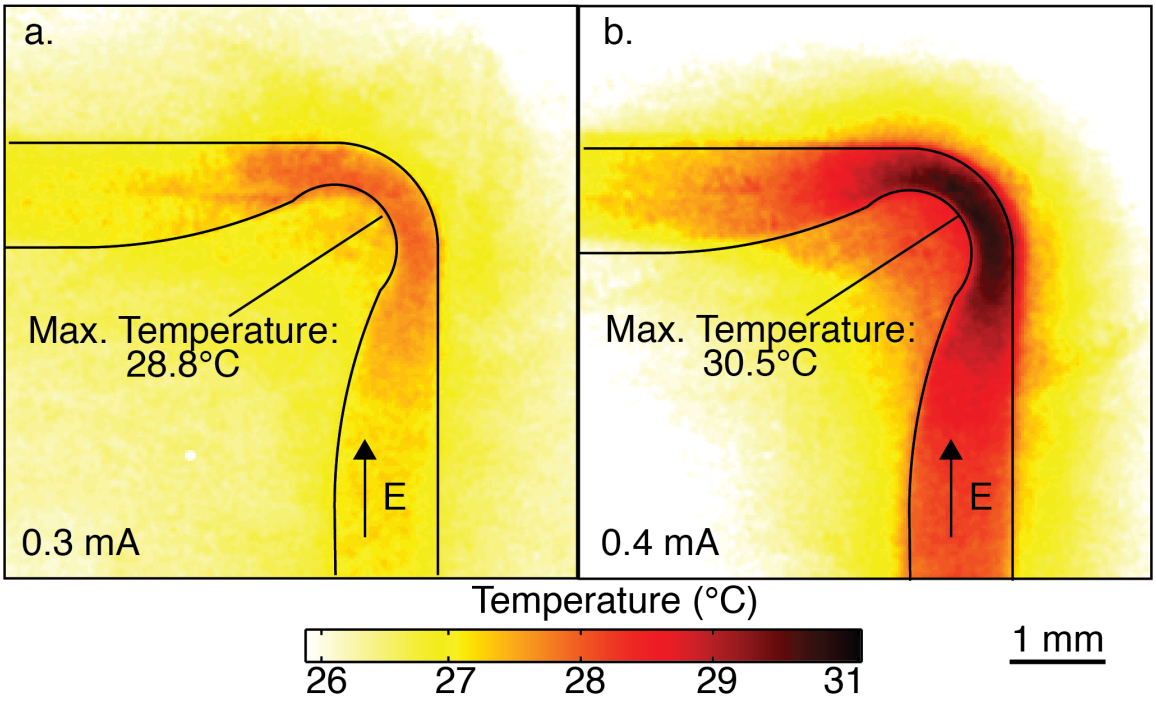

Figure 2-2. Infrared visualization experiment of local heating at a constriction in a microchannel. A polydimethylsiloxane (PDMS) channel bonded to a glass coverslip was filled with buffer 200 mM Tris and 100 mM HCl buffer. The chip was inverted and imaged with an infrared camera to measure temperature. Current was applied to the chip at (a) 0.3 mA and (b) 0.4 mA, causing the temperature to rise. A maximum temperature of 30.5 °C was observed in the channel. The highest temperature occurs at the channel constriction, the location of highest current density. In this case the maximum current density was 8.9 mA mm^{-2}

2.2.10 Buffering

The total charge that we can transfer through the channel is limited by the buffering capacity of the reservoirs. As electrolysis proceeds, H^+ and OH^- ions generated at the positive and negative electrodes introduce acid and base distributions to the pH. This effect has been discussed and analyzed by Persat et al.[21] Eventually, charge transfer leads to significant pH changes in the electrolysis reservoir as the local buffering capacity is exceeded, causing the pH to change. For changes in pH that are significantly less than one pH unit, we can estimate the change as a function of applied charge using the buffering capacity, β, [21] as follows:

$$\Delta pH = \frac{Q}{F\beta V_{buff}},$$

(18)

where V_{buff} is the volume of the buffering reservoir.

The mobility of weak acids and bases is highly sensitive to pH. Thus, maintaining a stable pH in the separation channel is critical to effective ITP separation. We can define some small allowable pH change, ΔpH_{max}, that the buffer system can tolerate. We then use this to estimate the maximum applied charge as

$$Q_{\max} \approx \Delta \mathrm{pH}_{\max} F \beta V_{buff}$$

(19)

We note that Equation 19 is a linear approximation valid for small changes in pH.[21] We use it here as we are interested in preserving the pH stability of buffering reservoirs within a small tolerance. We recommend values of ΔpH_{max} of typically 0.1 to 0.3 pH units.

As an example, consider the common case of a buffer composed of two moles of weak base for each mole of strong acid. We can estimate the buffering capacity as $\beta = 0.56 c_B$, where c_b is the concentration of the weak base.[28] Thus, we can improve the maximum applied charge by introducing dedicated buffering reservoirs with very high buffer concentrations, on the order of 1M.

2.2.11 Gas Generation

Electrolysis of water causes gas generation at electrodes.[21] The largest volume of gas will be generated at the cathode, where 2 moles of H_2 are being produced for each mole of O_2 at the anode. This phenomena was analyzed in detail by Gabrielli et al.[29] At low current, bubbles nucleate, but remain small as dissolved gas diffuses away from the electrodes. At high current, bubbles nucleate on grow on electrode surfaces. These bubbles reduce the surface area of the electrodes in contact with the electrolyte, resulting

in increased electrical resistance. Eventually bubbles grow large enough to detach and float to the top of the reservoir. For the experiments described in this paper (and other experiments involving relatively large cross-section channels and applied currents), we have observed that this nucleation, growth, detachment, and transport processes can cause significant disturbances to the system. This includes pressure fluctuations in reservoirs which can propagate into channels, visibly disturbing the ITP zone (even for channel locations 2 to 3 cm from the electrolysis reservoirs). Further, at constant applied currents above 0.25 mA, we observed saw-tooth voltage traces similar to those described by Gabrielli as being indicative of bubble disturbances.[29] For applied currents below 0.25 mA, these disturbances to the ITP zone and voltage traces were negligible, and thus we choose to apply currents below 0.25 mA to achieve stable operation.

These and similar observations led us to incorporate a design constraint in our analysis based on the maximum allowable volume flow rate of the electrolysis gases in our system. To simplify the current presentation, we propose here an empirically determined estimate for this constraint (0.25 mA for our system). We hope to explore this constraint further in the future.

2.3. Materials And Methods

2.3.1 Separation Visualization

For visualization experiments, we fabricated polydimethylsiloxane (PDMS) devices. Each device contains channels with a height of 150 μm and a width of 1 mm ($\underline{A_s}=A_{ch}=$0.15 mm^2). The length of the sample channel, L_s, is 1 cm, while the length of the separation channel, L_{ch}, is 2 cm. The devices also contain an air outlet channel for loading.

We visualized Alexa Fluor 488 (AF) (Life Technologies, Carlsbad, CA) and fluorescein (FL) (sodium derivative, Baker, Center Valley, PA). We adjusted the AF and FL concentrations between 10 nM and 1 μM to achieve high contrast. For the separation of AF and FL, we used two buffering chemistries. When diluting sample in the TE, we used ascorbic acid as a trailing ion, and Bis-tris as a counter-ion. When diluting the

sample in the LE, we used citric acid as the trailing ion and 6-aminocaproic acid as the counter-ion. In both cases we used hydrochloric acid for the leading anion.

To capture images of separation in the channel, we used using a 12-bit, 1300 × 1030 pixel array CCD camera (Micromax1300, Princeton Instruments, Trenton, NJ) mounted on a stereoscope (SZ40, Olympus). The camera was triggered by a pulse generator (DG535 Stanford Research, Stanford, CA). The stereoscope incorporated an emission filter (Semrock, FF01-550/32-25). Two borlow lenses, 0.3x and 1.5x (110 ALK0.3x and 100AL1.5x, Olympus) were used simultaneously to adjust the magnification of the stereoscope. The stereoscope was used at 0.63x internal magnification, leading to a total magnification of 0.28x. Illumination was provided by an off-axis collimated blue LED (M470L2-C1 Thor labs). Images were processed using custom Matlab script.

We applied constant current to the device through platinum electrodes using a high voltage power supply (Keithley 2410, Keithley Instruments, Cleveland, Ohio). We applied currents of 20-100 μA, and recorded the voltage using a computer running custom Matlab software.

2.3.2 Thermal Imaging

For thermal imaging, we used a custom PDMS chip adhered to a number 1.5 glass coverslip. This PDMS chip contained constricted 90° turn optimized to reduce electrokinetic dispersion.[27] We filled the chip with a buffer containing 200 mM Tris and 100 mM HCl, and inserted 1 cm platinum wire elctrodes into the reservoirs. We sealed the reservoirs with PCR tape (Microseal B Adhesive Sealers, Bio-Rad) and inverted the chip to image through the glass coverslip.

We used an infrared microscope (Quantum Focus Instruments) to map the channel temperature. First, we generated an emissivity map to calibrate each pixel within the field of view by imposing isothermal conditions on the surface (~35^{o}C) and recording the corresponding radiance. After calibration, we applied 0.3 and 0.4 mA across the

platinum electrodes using the Keithley high voltage power supply. We observed the chip until the temperature reached steady state (~30 s). We then obtained 100 images, and calculated the mean of these images to determine the final temperature inside the channel.

2.4. Results And Discussion

2.4.1 Design Proceedure

Systems for purification using ITP are influenced by a range of geometric and chemical factors. As summarized in Table 1, we can make the problem of designing these systems more tractable by analyzing the variables that influence recovery efficiency, separation quality, and processing time. The challenge is then to achieve all of the desired separation properties simultaneously. We recommend design of systems be performed in the following steps:

Choose device geometry: This decision is primarily tied to the desired volume of the input sample, and is relatively independent of the sample chemistry used.

Set buffer chemistry: LE and TE buffer chemistries depend on the mobilities of the analyte and contaminant molecules to be separated.

Adjust concentration of LE in the separation channel to achieve the desired separation parameter, and adjust applied current to minimize processing time within the constraint set by Joule heating: The LE concentration and applied current are parameters that can be adjusted experiment-to-experiment to deal with, for example, some variation in input sample properties.

The design procedure for each of these steps is outlined in the sections below.

2.4.2 Design Of Geometry

We treat the volume of the sample channel as an input parameter set by the application. Typically, the sample input volume depends on the mass of analyte in the extracted product and the concentration of the analyte in the sample.

As discussed by Dolnik et al.,[4] high-aspect ratio rectangular channels have better heat-dissipation characteristics than circular channels. We here therefore assume channels with rectangular geometries. To specify the basic geometry of Figure 1, we then set four parameters: A_s, A_{ch}, L_s, and L_{ch}. As per Equation 17, increasing the cross sectional area of the channel, increases current and sample throughput. However, cross-sectional area is also limited by several factors discussed below.

First, large cross-sectional areas can lead to overly large pressure driven flow velocities (due to small differences in height of liquid in reservoirs). For simple aqueous solutions at room temperature, we recommend limiting the channel height to approximately 200 μm for ease of handling fluids. For pressure drops of order 10 Pa (order 1 mm differences in hydrostatic heights), wide aspect ratio channels of this depth and order 10 cm lengths yield bulk velocities of order 400 μm/s.[30]

The channel width is relatively unconstrained by the physics of the separation, but it may be constrained by the channel material and fabrication method. For example, PDMS typically enables a maximum channel aspect ratio of about 10:1 to avoid channel deformation.

Within these approximate constraints, we choose the largest practical cross-sectional area for the channel. Once the cross-sectional area is maximized, we can adjust channel lengths to achieve the appropriate volumes in both the sample channel and the separation channel.

As per Equation 10, the recovery efficiency of the process is a function of the volume ratio between the sample channel and the separation channel. We recommend that these two volumes be on the same order, and for the separation channel volume to be somewhat larger than the sample channel volume. For particularly difficult separations (i.e., values of p_{AC} of 0.3 or less) a substantially larger separation-to-sample volume ratio volume may be required.

2.4.3 Choosing Separation Chemsitry

Choosing the chemistry for an ITP separation can be complex and involves choosing the operating pH, choosing a target TE mobility, and then finding convenient buffer ions (e.g., Goods type buffers[31]) that approximately represent these ideal conditions. Rather than analyze this problem in detail, were here make several recommendations.

First, we recommend a high mobility, fully ionized leading ion. This will ensure focusing of a fast analyte (e.g., DNA), and promotes formation of a sharp ITP zone.[17] Chloride is a good choice for anionic ITP, and sodium is a common choice for cationic ITP. Next, we choose to suspend sample in either the LE or TE buffer. We recommend dilution in the LE when the sample chemistry itself contains a high concentration of the LE ion (e.g., blood or urine samples in anionic ITP with chloride as a leading ion). For relatively simple sample matrices (e.g., diluted cell culture), we typically opt to dilute in the TE. In all cases, the figures of merit in Table 1 should be explored both for suspending the sample in the LE or TE.

As an example design problem, we here chose to analyze a model system composed of the two fluorophores, AF and FL. We treat AF as the analyte and FL as the contaminant. In real situations, contaminants may vary widely across sample types and desired downstream assay. In fact, contaminants may not be well characterized or even identified, but we offer the current discussion as illustrative of the key issues in selecting buffer chemistry. We start our idealized process of designing the chemistry by plotting the mobilities of the analyte and the contaminant as a function of pH, as shown in Figure 3a. For these estimates, we neglect ionic strength effects,[32] and base the effective mobilities only on pH, pKa, and fully ionized mobility.[20]

On this same figure, we plot two sets of suggested mobilities of the trailing ion. When diluting the sample in the TE, we are driven to choose a low mobility TE to maximize the separability between the analyte and the TE. However, the mobility of the trailing ion must remain above that of the contaminant. For this case, we recommend

using a trailing ion with a mobility of about 110% that of the contaminant ion. As per Equation 12, this will lead to a separation distance of about 9% of L_{ch}.

When diluting the sample in the LE, we should use a high value of the trailing ion mobility. Here, the separability between the analyte and trailing ion is no longer important, as the analyte is never mixed with the trailing ion. Using a higher trialing ion mobility increases the conductivity of the TE, and this reduces Joule heating, as per Equation 16. To focus the analyte, we need a trailing ion with a mobility lower than that of the analyte. Here, we recommend a trailing ion with a mobility of 90% that of the analyte. These target trailing ion mobilities are also shown in Figure 3a. A trailing ion mobility closer to that of the analyte is not advisable as this results in tailing of the ITP zone.[17]

Once we have set the target trailing ion mobility, we can estimate the separability of the analyte as a function of pH. These values are plotted in Figure 3b. For suspension in the TE, we plot p_{AT}; and for dilution in the LE, we plot p_{AL} for the case of anionic ITP with chloride as the leading ion. The separation parameter of the sample, Q_s, scales with these two separabilities, as shown in Table 1.

We use these separabilities to estimate the minimum separation time. In Table 2 below, we combine Equations 14 and 17, and express the conductivity and transference numbers in terms of the component molar conductivities, to explicitly show the minimum separation times as a function of pH. These times are plotted in Figure 3c.

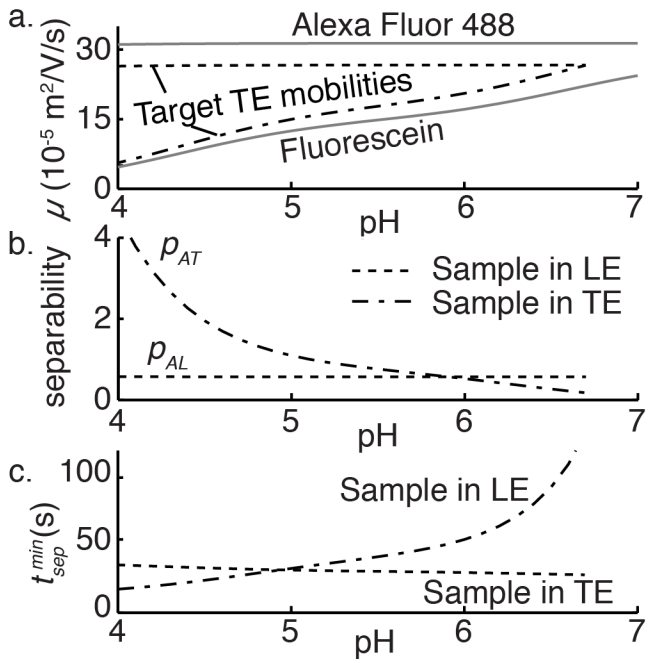

Figure 2-3. Example case of selection of a buffer chemistry for purification of samples using ITP. a. The mobilities of ions in a model system where FL is the contaminant, and AF is the analyte. Suggested target TE mobilities for separations with the sample diluted in the LE and the TE are shown as dashed curves. b. The separability of the analyte from the trailing ion (sample in TE), or the leading ion (sample in LE). c. The minimum processing time for 1 μL of sample in 10 mM buffer, based on the equations in Table 2. We can select the lowest separation time as our operating point.

Table 2-2. Equations for minimum separation time to completely focus the analyte molecule. Here, $k=c_T/c_L$ is the ratio of trailing ion concentration in the adjusted TE to leading ion concentration in the LE. These constants can be calculated numerically using the SPRESSO simulation tool.[20] The ratio $\chi_T=c_C/c_T$ represents the counter-to-trailing-ion concentration ratio in the adjusted trailing electrolyte zone, while $\chi_L=c_C/c_L$ is the co-ion-to-leading-ion concentration ratio.

$t_{sep}^{\min}$ for Dilution in TE	$t_{sep}^{\min}$ for Dilution in LE
$t_{sep}^{\min} = A_s L_s A_{\min} \sqrt{\left[\frac{h^2}{8k_L} + \frac{hd_{wall}}{2k_{wall}}\right]\Delta T_{\max}} \frac{\sqrt{\lambda_T + \chi_T \lambda}}{p_{AT}\lvert\mu_T\rvert}$	$t_{sep}^{\min} = A_s L_s A_{\min} \sqrt{\left[\frac{h^2}{8k_L} + \frac{hd_{wall}}{2k_{wall}}\right]\Delta T_{\max}} \frac{\lambda_L + \chi_L \lambda_C}{\sqrt{\lambda_T + \chi_T \lambda_C}} \frac{1}{p_{AL}\lvert$

The minimum separation times from the expressions in Table 2 are plotted as a function of pH in Figure 3c for the AF and FL case discussed above. In this case, the fastest separation is available at pH < 5, with the sample suspended in the LE. However, we note that we might choose suboptimal separation times for practical considerations (e.g. solubility).

Once a target pH range and trailing ion mobility are chosen, finding suitable ions to achieve these conditions can still be a challenge. Typically, we may first choose a counter-ion which acts as a buffer at the desired pH. We then choose a trailing ion for its mobility characteristics near this pH. As a final confirmation, the properties of the system can be verified using a numerical simulation tool such as SPRESSO.[20]

2.4.4 Sample Processing Efficiency

We validated our model of the dynamics that govern sample processing efficiency by visualizing our model system in which we focus AF. The top row of Figure 4 shows spatiotemporal diagrams. Plotted are analyte concentration as a function of distance along the channel and applied electric charge. For reference, we also thin and dark solid lines to indicate the trailing edge of the analyte zone and the position of the ITP zone, respectively. The bottom row shows the corresponding spatiotemporal plots determined from our experimental visualizations (no lines are superposed on the experimental plots). We predicted and visualized the case of focusing and purifying AF with three different LE concentrations. As per Equation 9, separation capacity, and thus recovery efficiency, are governed by LE concentration. Low LE concentration (first two columns) is associated with low separation capacity, and the ITP zone leaves the separation channel before the analyte can fully focus into the ITP interface (labeled “ITP zone”). High LE (last column) is associated with high separation capacity and a complete focusing of the analyte. In the latter case, the trailing edge of the analyte zone merges with ITP zone. As per Equation 8, we see that the applied charge required to fully focus the analyte is relatively independent of LE concentration. For the case of Figure 4, the required applied charge is approximately 4.5 mC for all cases (as per an extrapolation to the point where the trailing edge and ITP zone merge for each figure).

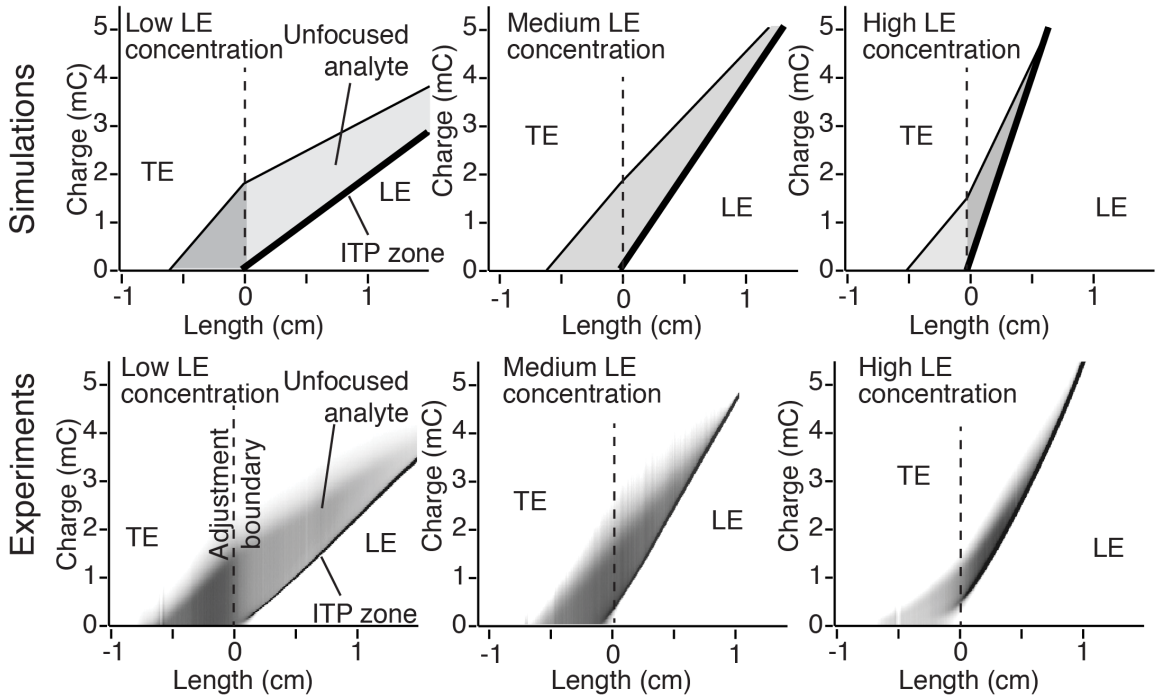

Figure 2-4. Spaciotemporal plot of focusing of AF at three LE concentrations. The top row shows results of simulations using the equations in Section 2.2.3. The bottom row contains experimental realizations constructed using visualization setup described in Section 2.3.1. AF concentration is plotted as a function of length along the channel and total applied electric charge. The three columns correspond to LE concentrations of 10, 20, and 40 mM. These correspond to separation capacities of 2.5, 5, and 10 mC. In all cases, the initial analyte zone is an approximately 0.5 cm long region of AF dye mixed into the TE. The left edge of the initial LE zone is shown as an "adjustment line" (which will mark the left edge of the ATE region). The separation parameter of the sample, Q_s, is approximately 4.5 mC.

2.4.5 Separation Distance

We used a second model chemistry system to validate our analysis of the separation distances between unfocused contaminants and a focused analyte. We performed ITP purification of a sample containing both AF and FL. These dyes fluoresce in approximately the same wavelength, 520 nm, when illuminated by blue light, allowing us image them simultaneously. Their distinct, well-characterized electrophoretic mobilities at pH<7,[33] allows us to identify them and quantify their motion. Predictions and associated experimental validations are shown in Figure 5.

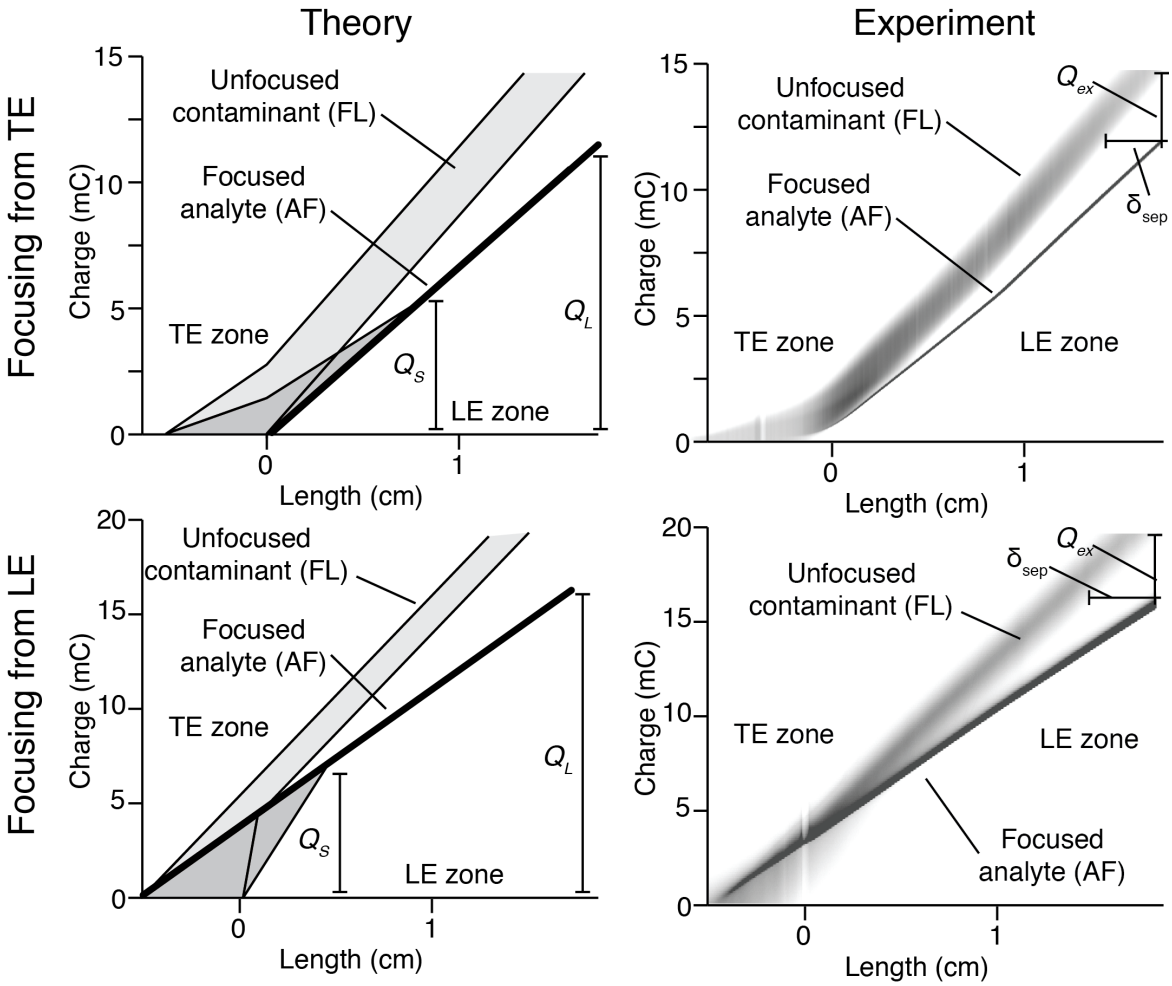

Figure 2-5. Separation of AF from FL using ITP. The left column shows predictions from equations of Sections 2.2.3 and 2.2.4. The right column shows results of visualization experiments. We show cases where the analyte is mixed with the TE and LE in the top and bottom rows, respectively. Plotted are analyte concentrations as a function of channel length and applied electric charge. For the simulations, we highlight the trailing edge of the analyte zones using thin, solid lines and highlight the ITP zone with a thick line. No lines are superposed on the experimental data. The separation distance, δ sep, is the channel length between the focused analyte and the contaminant when the ITP zone reaches the end of the channel. The separation charge, Qex,is the amount of charge that must be transferred after the ITP zone exits the channel but before the contaminant exits the channel.

2.4.6 Operational Regime Plot

As a design aid, we have developed what we term an operational regime plot for ITP purification experiments. In this plot, we show the effects of varying LE ion concentration and applied current for a fixed device geometry and buffer chemistry. Two example operational regime plots are shown in Figure 6. For each point in the space,

there is a fixed time to complete the purification process, equal to Q_T/I as defined in Equation 14.

The constraints on buffering, Joule heating, and electrolysis rate are plotted on the operational regime plot. The maximum separation parameter is limited by the buffering at the reservoirs, as described by Equation 19. The current is limited by Joule heating, as described by Equation 17. Note that the heat generation depends on the conductivity of the buffer, and thus on the concentration of the leading ions. In addition, there is a limit imposed by bubble generation at the electrodes, as described in Section 2.2.10. We grey out all regions which violate the operational constraints. In the workable region of the plot, we plot solutions for various values of the separation time.

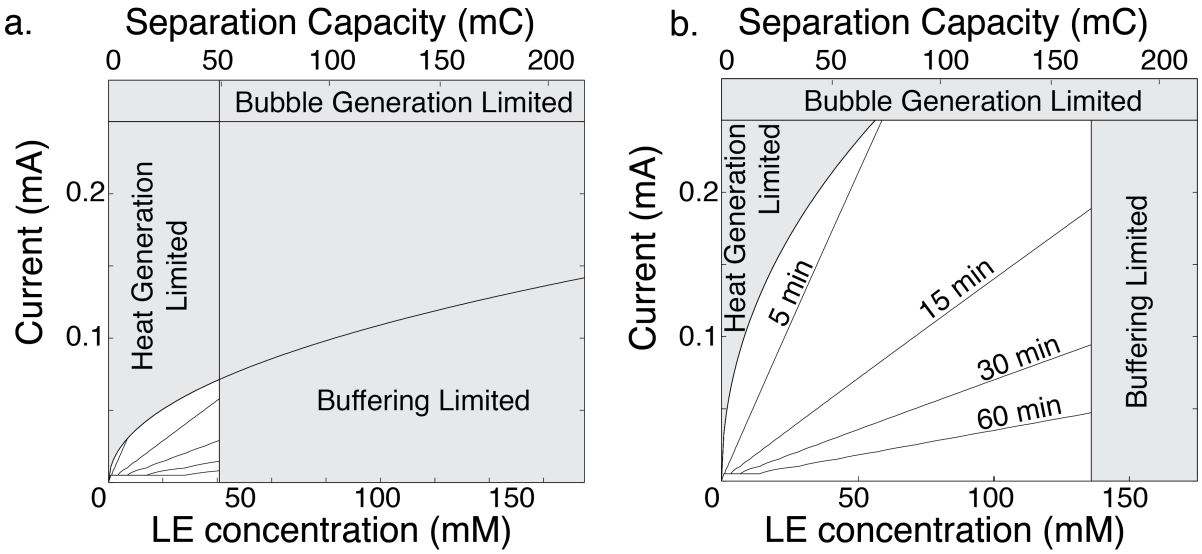

Figure 2-6. Operational regime plots for a single microfluidic device designed for ITP purification of 10 µL samples. The buffers are composed of a leading electrolyte of Tris HCl (pH 8.2) and a trailing electrolyte of Tris HEPES (pH 7.9), with the sample diluted in the TE. Operating outside of the white area will lead to a violation of one of the operational constraints. a. A poorly designed purification device designed with 3 µL buffering reservoirs and a relatively small channel cross section 50 x 100 µm. Here low buffering capacity limits the separation capacity to 50 mC, and small cross sectional area lead to excessive Joule heating for currents above 80 µA. b. A well-designed purification device with 10 µL buffering reservoirs and a channel cross-section of 100 x 300 µm. Here, higher buffering capacity and channel cross-sections enable applications of higher current and separation capacity without excessive Joule heating.

Table 2-3. Constraint relations for the operating space in shown in Figure 6. The maximum separation parameter is controlled by the buffering capacities at the reservoirs. The maximum current is controlled by Joule heating in the channel. In addition to these constraints, we also impose an empirical limit of 250 μA maximum current at the electrodes to avoid gas bubble detachment, as discussed in Section 2.10.

$Q_s^{\max}$	$\Delta \mathrm{pH}_{\max} F \beta V_{buff}$
$I^{\max}$	$A_{\min} \sqrt{\frac{\Delta T_{\max} \sigma_{\min}}{\left[\frac{h^2}{8k_L} + \frac{hd_{wall}}{2k_{wall}}\right]}}$

2.5. Summary

Purification using ITP is a complex process in which operating parameters are set by a combination of chemistry and device geometry. Here, we analyze for the first time in detail the factors driving analyte recovery efficiency, separation quality, and processing time. We address recovery efficiency by examining the separation capacity of system in comparison to the separation parameter of the input sample. To address separation quality, we examine the distance between the ITP zone and the contaminating species at the end of the experiment, which is driven primarily by the mobility of the trailing ion. Finally, to minimize processing time, we examine the maximum applicable current within the constraints imposed by Joule heating and electrolysis gas generation.

With the design principles outlined here, we can begin to design microfluidic devices for highly efficient purification of nucleic acids and other biomolecules using ITP with short separation times. These devices have the potential to make ITP purification a viable alternative to existing methods such as gel electrophoresis, solid phase extraction, and liquid-liquid extraction techniques.

Our analysis was significantly simplified by considering the case where the analyte possessed a higher electrophoretic mobility than contaminating species. Future work on purification using ITP should address the more complex problem of purifying target species in the presence of impurities with both higher and lower effective mobilities. The latter may be important for purification and fractionation of, say, proteins from complex samples such as plasma or serum.

2.5.1 Funding Sources

We gratefully acknowledge funding from Defense Advanced Research Projects Agency (DARPA) under contract no. HR0011-12-C-0080, program manager Daniel J. Wattendorf, and from the DARPA MF3 Center (UC Irvine), under contract no. N66001-10-1-4003.

2.5.2 Acknowledgment

We gratefully acknowledge help from Michael Barako in collecting the thermal images used in Figure 2.

Chapter 3 An Optimized Chip for Purification via Isotachophoresis

Some of the contents of this chapter are under preparation as an article in *The Analyst* by Lewis A. Marshall, Anita Rogacs, Carl Meinhart, and Juan G. Santiago. They are reproduced here with minor modifications.

Introduction

Isotachophoresis (ITP) for nucleic acid purification from biological samples is a sample preparation technique with a growing portfolio of applications. There have been a range of publications describing the theory and practice of using ITP for nucleic acid purification including host and pathogen DNA from human blood,[1-3] serum, and plasma,[4,5] as well as RNA purification from kidney cells[6] and from bacteria in urine[7] and blood.[8]

Important early work in ITP purification was performed by V.N. Kondratova and co-workers who concentrated and isolated extracellular DNA from blood plasma and urine by agarose gel ITP. Their devices were capable of delivering highly efficient extraction in limited time.[4,5] However, their isolation procedure used centrifugation and buffer exchanges as crucial steps in removing all cells (and potentially PCR inhibitors) prior to ITP. Also, their ITP isolation procedure yielded DNA within an agarose gel slab, which required further purification steps prior to analysis. Further their use of slab gels and tube gel devices makes their approach difficult to automate and miniaturize. Glass[3] and plastic[2] microfluidic chips have been used as platforms for ITP purification, but to date these devices have been unable to provide high nucleic acid yield compared to the total nucleic acid load delivered to the chip. The record of these microfluidic ITP purification chips and their extraction efficiencies is summarized in Table 1. Typically, less than 1% of nucleic acids loaded onto a chip have been extracted.

Table 3-1. Previous device capacity in microchip ITP. Here, efficiency is defined as the percentage recovery of nucleic acids dispensed onto the device.

Sample (dilution factor)	Extraction target	Lysate volume (dispensed)	Lysate volume (processed)	Efficiency	Author (year)
Human blood (10x)	gDNA	1	0.025	0.25	Persat (2009)
Human blood (50x)	Total RNA	10	0.02	0.2	Rogacs (2012)
Kindey culture (10x)	microRNA	5	0.02	0.04	Schoch (2009)
Urine (10x)	rRNA (16s)	2	0.02	0.1	Bercovici (2011)
P. falciparum in blood (10x)	gDNA	15-50	0.5-1.5	3	Marshall (2011, 2012)

In this paper, we demonstrate an injection-molded plastic microfluidic chip for ITP purification of nucleic acids that achieves high extraction efficiencies and is capable of processing 25 μL of blood lysate in a single experiment. We describe the design features of this chip, and analyze its performance using fluorescence quantification and quantitative PCR (qPCR).

The low extraction efficiencies so far demonstrated by microfluidic chips are the result of primarily two factors: the small volume of the separation channels, and the insufficient pH-buffering capacity of the electrode reservoirs. Here, we directly address each of those issues. We achieve high volume separation channel with a 2 x 0.15 mm channel cross section which maintains sufficient heat rejection to minimize effects of Joule heating. We placed the electrodes in dedicated buffering reservoirs that do not contain sample and do contain locally high buffer concentration. These reservoirs are effective in preventing pH changes due to electrolysis even while processing large volumes. The design draws on scaling analyses for ITP purification as presented in detail in Marshall et al.[9]

Materials and Methods

Device Design and Features

We generated the geometry of our custom microchip using commercial computer aided drawing (CAD) software (AutoCAD, AutoDesk, San Rafael, CA). The design has a nominal channel depth of 150 µm, a nominal width of 2 mm, and a total channel length of 20 cm. The channel is divided into a sample channel, with a total volume of 25 µL, and a separation channel, with a total volume of 30 µL. The design includes four reservoirs with access to the fluidic channel, and each reservoir can hold a total volume of 70 µL. In addition, each reservoir is designed to be compatible with Leur lock connectors.

Our microfluidic device design was fabricated by a commercial microfluidic foundry (Microfluidic Chipshop Gmbh, Jena, Germany). The devices were fabricated by injection molding the fluidic layer and reservoirs. These devices were manufactured both in poly-methyl methacrylate (PMMA) and Topas, a cyclic olefin copolymer (COC). The devices were sealed with plastic films with thickness of 140 µm (COC) or 175 µm (PMMA).

The polymers here were chosen for their different surface properties. Topas has a reported equilibrium water contact angle of around 97°, while the PMMA is more hydrophilic, with a reported water contact angle of 60°.[10] The finished device is shown in Figure 1.

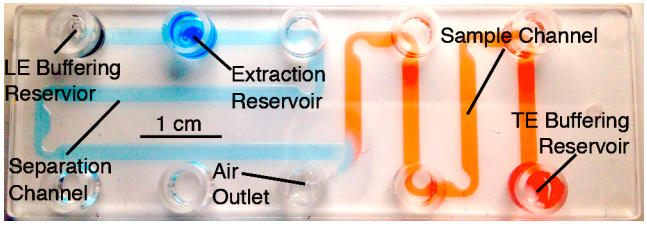

Figure 3-1. Image of the finished device, with channels loaded with water dyed with blue and red food coloring. The sample channel (on the right half of the 25.5 by 75.5 mm chip) is red, while the separation channel is blue. A more detailed view of the junction between these two channels and the structure of the connected air outlet channel is shown Figure 2. The device was manufactured using injection molding of COC and PMMA.

Each channel corner in the device is an optimized 90° turn designed by Molho et al. to minimize electrokinetic dispersion due non-uniform electric fields in the turn.[11]

These turns have a constriction ratio of 0.5 and a recovery ratio of 1.0, as defined by Molho.

The reservoirs in the device are arranged so that the electrode-containing reservoirs can be configured for extremely high buffering capacity without affecting the chemistry of either the sample or the extracted nucleic acids.[12] To achieve this, the sample is loaded directly into the sample channel section, and not into the trailing electrolyte (TE) buffering reservoir. Further, the leading electrolyte (LE) buffering reservoir is separate from the sample extraction reservoir, and connected to the latter by a short channel. See loading process below for more details.

We designed and introduced specialized loading structures at the junction between the sample and separation channels to allow creation of a sharp interface between the sample and the leading electrolyte solutions. These structures also enable loading of the sample into the device without wasting liquid into the vacuum port. These structures operate in a principle similar to the phaseguide described by Vulto et al.,[13] or more commonly applied microfluidic capillary valve structures.[14] We use ramps and a sudden expansion in channel height to achieve what we term capillary barriers. The ramps reduce the height of the channel from 150 μm to 75 μm over a distance of about 2 mm along the channel. This ramp rises from the bottom wall of the channel and terminates in a sharp step in channel height back to 150 μm. Liquid wicking up to this structure faces an energetic barrier associated with expanding past the ramp (as additional liquid surface area is required for the liquid to advance). These valve structures are oriented so that the liquid stopped by the capillary barrier can be wetted by liquid from an adjacent channel, creating a bubble-free liquid-to-liquid interface. We used two capillary barriers: one at the sample-to-separation buffer interface, and a second inside the connected vacuum outlet channel (labeled “Final fluid stop” in Figure 2). The filling and liquid-to-liquid mating operation enabled of these structures is summarized in Figure 2.

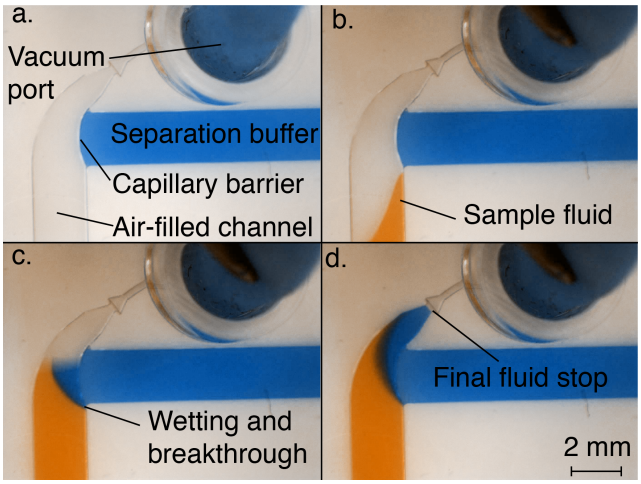

Figure 3-2. Stages in capillary-barrier-aided loading visualized using food coloring in water. ***a.*** *The blue liquid, simulating separation buffer, is initially loaded into the separation channel. -0.1 psig vacuum is applied at the vacuum port, and the separation buffer flows to the capillary barrier, where it stops at the precise edge of the expansion downstream of the ram.* ***b.*** *The red liquid, simulating the sample solution, enters through the sample channel.* ***c.*** *The sample solution forms a liquid-to-liquid interface (repeatedly free of bubbles) with the separation buffer. The two liquids volumes then flow in parallel toward the air outlet.* ***d.*** *The volume near the liquid-to-liquid interface is run up against and stopped by the second capillary barrier inside the vacuum port. This avoids wasting either liquid into the vacuum. A sharp interface is preserved between the two liquid zones and the ITP process is ready to begin.*

Visualization

We monitored ITP by fluorescence imaging using either an epifluorescence microscope or a stereoscope and adsorption filters. The upright epifluorescent microscope (BX40, Olympus) was equipped with a 2x objective (PlanApo NA=0.08, Olympus), and a collimated blue LED (M470L2 Thor Labs). We filtered the fluorescent signal using a filter cube designed for FITC (excitation/emission of 485/535 nm, Omega, VT). The images were collected through a 0.63x demagnification lens (model RD060-CMT, Diagnostic Instruments, MI).

The stereoscope (Olympus SZ40) with adjustable magnification was used for imaging, and was optionally fitted with 0.3x or a 1.5x Barlow lenses to adjust the magnification. This resulted in a total magnification as low as 0.19x, which allowed the stereoscope to include the entire custom chip in the field of view. For fluorescence visualization in the stereoscope, the chip was illuminated by the collimated blue LED, and the light was filtered using a single emission filter (Semrock, 550/32 BrightLine®

Bandpass Filter, 25 mm) placed in the camera light path. For color imaging, ambient light was used for illumination, and no filter was used, and for Figure 2 the Barlow lens was removed. The images were captured on a color CCD camera (CoolSnap cf, Photometrics, Tuscon, AZ). In both microscope setups, we acquired images with a CCD camera (MicroMax, Roper Scientific).

Experimental Chemistry

To perform fluorescence quantification of extraction efficiency on these devices, we used an idealized chemistry with samples composed of salmon sperm DNA diluted in buffer. To create the calibration curves, we diluted the sodium salt of salmon sperm DNA (Sigma Aldrich, St. Louis, MO) in an aqueous buffer composed of 20 mM Tris, 10 mM Hepes, with 1x SYBR Green I (Invitrogen, CA), pH = 8.2. We used DNA concentrations ranging from 100 pg/μL to 10 ng/μL. To perform ITP with these same samples, we prepared a LE composed of 100 mM Tris, 50 mM hydrochloric acid (HCl), and 1x SYBR Green I, pH = 8.2. We used a buffering leading electrolyte (BLE) with 500 mM Tris, 250 mM HCl, and 25% w/v Pluronic F-127. The buffering trailing electrolyte (BTE) was composed of 500 mM Tris, 250 mM HEPES, and 25% w/v Pluronic F-127.

To perform ITP purification of blood with these devices, we used an LE composed of 90 mM Tris and 60 mM HCl (pH=7.9). The BLE and BTE solutions are the same as used for fluorescence quantification. We prepared blood lysate by mixing 10 μL of whole blood anticoagulated with acid-citrate-dextrose (ACD) with 190 μL lysis buffer, composed of 25 mM Tris, 17 mM HCl, and 1% Triton x-100, and proteinase K, 1x SYBR Green, 0.1% PVP, and 40 mM dithiothreitol (DTT). (We note this whole blood was purchased from the Stanford Blood Center and stored frozen at -20C prior to use.) This sample was then held at 65°C for 10 min. The blood lysate was then placed on ice until it was pipetted onto the chip as the sample.

We also performed experiments in which we separated fluorescent dyes in the device. We separated fluorescein (FL) and Alexa Fluor 488 (AF488), which emit fluoresce in the same wavelength region (excitation at 495 nm, emission at 519 nm), but have different mobilities at pH below 7.[15] For these experiments, we used an LE composed of 70 mM ε-aminocaproic acid and 35 mM HCl with 0.1% w/v PVP (pH=4.6). The sample was composed of 30 mM ε-aminocaproic acid and 15 mm ascorbic acid,

0.1% w/v PVP, 5 μM AF488, and 100 μM fluorescein (pH = 4.6). The BLE was composed of 200 mM ε-aminocaproic acid, 100 mM HCl, and 20% Pluronic F-127. The BTE was composed of 200 mM ε-aminocaproic acid, 100 mM Ascorbic acid, and 20% Pluronic F-127.

Lastly, we used commercial food coloring for preliminary visualizations of the channels in the device, as shown in Figures 1 and 2. In these cases, we mixed Super Red and Super Blue food coloring (Ateco, Sea Cliff, NY) with deionized water until the desired color saturation was achieved.

Loading Process

Microchips were received dry from manufacturer and kept dry until use. In each experiment, the liquids were loaded in the same order. First, we pipetted 50 μL LE into the extraction reservoir. Vacuum (-0.1 psig) was applied at the buffering LE reservoir until the channel adjacent to it was filled, then 25 μL BLE solution was added to the buffering LE reservoir. We then applied vacuum (-0.1 psig) at the air outlet until the LE filled the entire separation channel. Then, we added the 25 μL sample to the buffering TE reservoir. Vacuum was again applied at the air outlet until the sample wetted the LE interface. Finally, BTE solution was immediately pipetted into the buffering TE reservoir to arrest pressure driven flow. This loaded chip was then used for ITP.

ITP Purification

We performed purification by placing 2 cm platinum wire electrodes in the LE buffering reservoir and the TE buffering reservoir. We applied a constant current of 100-250 μA between these two reservoirs using a Kiethley 2410 sourcemeter (Keithley Instruments, Cleveland, OH). The current was deactivated when the nucleic acid zone reached the extraction reservoir.

Off-Chip PCR

We monitored the DNA zone in the channel during ITP by fluorescently imaging the SYBR-labeled DNA using a fluorescence microscope. When the ITP interface fully eluted into the extraction reservoir, we gently mixed the liquid in the reservoir (~25 μL) by pipetting, then collected it into an Eppendorf tube using the same pipettor.

For each collected sample, we ran triplicate PCR reactions. To set up each PCR reaction, we pipetted 2 μL ITP-purified DNA into a PCR tube containing 10 μL of 2x Fast SYBR Green I master mix (Applied Biosystems, CA), and 200 nM primers (Invitrogen, CA). The primers were designed to amplify a 201 bp segment of the human BRAC2 gene.[3] We used DNAse free water to adjust the volume of each reaction to 20 μL. We then performed off-chip quantitative PCR (qPCR) using a miniOpticon qPCR thermocycler (Bio-Rad, Hercules, CA). We performed the reaction with the following thermal profile: 20 s initial hold at 95 °C and 40 cycles composed of 3 s denaturation at 95 °C and 30 s annealing and extension at 60 °C. We then obtained post-amplification melting curves between 55 and 85°C using the same instrument. In addition to using ITP-purified DNA as template, we ran positive control reactions using DNA purified from whole blood with a commercial solid phase extraction kit (Qiagen, Valencia, CA). We also ran negative control reactions using the LE and nuclease-free water.

Results and Discussion

Device operation map

For our chip design, we took advantage of the design process described by Marshall et al.[9] for the design and operation of high throughput and fast ITP purification. Marshall performed a study that considered maximum sample throughput for ITP purification, while considering the constraints of Joule heating, buffering capacity, and gas generation at electrodes. They used this to plot purification time and separation capacity[16] as a function of leading ion concentration and applied current. Finally, they then imposed design constraints on this plot, which they termed an operational regime map. These constraints are associated with the maximum allowable temperature rise due to Joule heating, the maximum allowable pH change in electrode reservoirs due to electrolysis, and the maximum current the electrodes can supply without creating bubbles that disrupt the separation process. We followed this design process for our custom chips using the following parameters: 150 um channel height, 1 mm minimum channel width, and buffers composed of Tris HCl at pH 8.2. We also applied the following constraints: a maximum allowable temperature rise of 1 °C, a maximum allowable pH change of 0.2 pH units, and a maximum current of 250 μA.

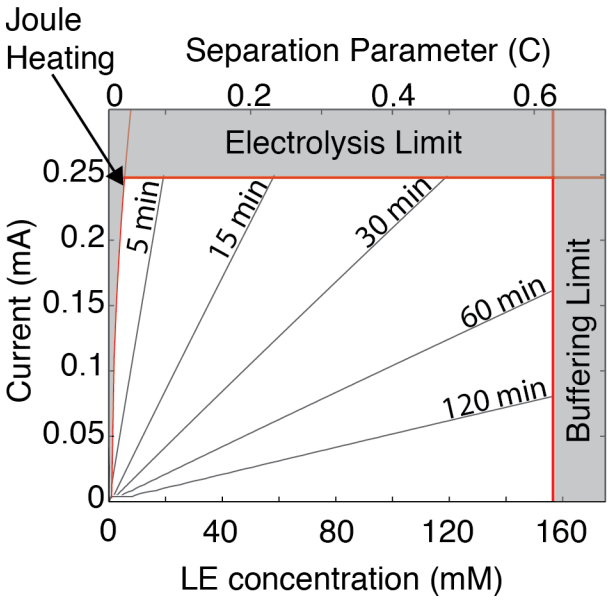

Figure 3-3. Operation regime map for ITP purification process using with the current plastic chip design. Plotted is required LE concentration and current for achievable values of extraction time (and separation parameter, in Coulombs). Areas in gray are precluded by design constraints and lead to unstable chip operation. At low concentrations, low LE conductivity causes high Joule heating. At high current, large bubbles form on the electrodes, causing poor electrical connection. At high separation capacity, electrolysis changes the pH in the electrode reservoirs. Operation inside the white area is stable, and the ITP is completed in a time determined by the LE concentration and the current.

Separation Demonstration

We demonstrated separation in the device using a model system composed of two dyes, AF488 and FL. We separated them at pH 4.4, where fluorescein has a mobility of 12 x 10^{-9} $m^2V^{-1}s^{-1}$, while AF488 has a mobility of 36 x 10^{-9} $m^2V^{-1}s^{-1}$. We recorded the separation of this system using a stereoscope. Figure 4 shows this system near the end of the separation process. The AF488 is focused to the ITP interface. The FL remains unfocused, in a wide zone behind the ITP zone. There is a dye-free zone, approximately 3.5 cm long, between the AF488 peak and the leading edge of the FL. This is the separation distance that allows collection of the AF488 peak without contamination by FL. This model system is illustrative of the separation that takes place to purify nucleic acids from contaminating species like proteins.

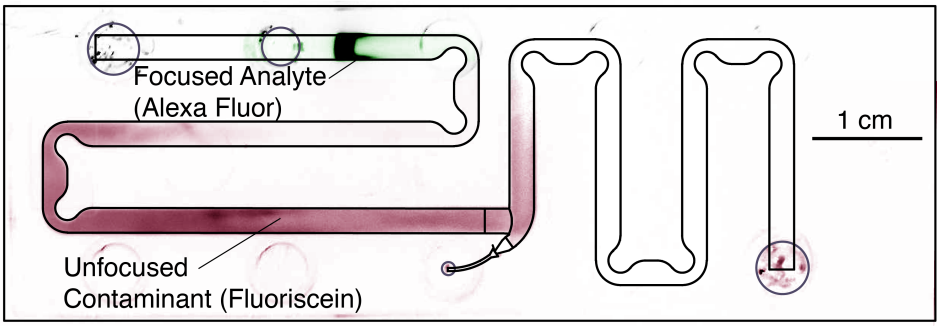

Figure 3-4. Demonstration experiment showing separation between FL and AF488 on the chip. The FL (red) is electromigrating in a long zone well behind the ITP interface. The AF488 (dark green) has collected to the ITP interface. The AF488 is about to elute into the extraction reservoir, allowing it to be selectively collected, while the FL remains in the chip.

In this system, the LE has a separation capacity of approximately 173 mC, and the sample has a separation parameter of 24 mC.[9,16] The separation capacity is greater than the separation parameter, and so AF488 can be collected at the ITP interface with high efficiency (prior to its arrival at the extraction well). The separation was performed at 100 μA, and took approximately 30 min to complete.

Quantification Demonstration

We measured the recovery of salmon sperm DNA with the chip using fluorescence quantification. First, we filled the channel with known concentrations of salmon sperm DNA suspended in LE, and established a calibration curve relating the fluorescent signal collected by the CCD camera to DNA concentration (Figure 5). We then performed ITP from samples of salmon sperm DNA of known concentrations suspended in LE. We used a device configuration in which the sample had a separation parameter of 55 mC, and the device had a separation capacity of 159 mC, so that the processing efficiency is not limited by the flux of nucleic acid to the ITP interface. A set of 10 images of the ITP zone were taken near the extraction reservoir, and the average integrated fluorescence signal of the zone in these images was used to quantify total DNA amount. The DNA recovery was computed using the DNA calibration curve. The calculated recovery efficiencies over three orders of magnitude are shown in table 1. As

shown, recovery efficiency is consistently 76-86%, for the entire 250 pg to 250 ng of DNA range explored.

Table 3-2. Fluorescence quantification results. Known masses of DNA, ranging from 250 pg to 250 ng, were injected into the chip. Recovery was estimated by integrating the fluorescence of the ITP zone near the extraction reservoir. An average of 81% ± 4% of the DNA, as measured by fluorescence quantification, was recovered from the chip.

Injected DNA Mass	Calculated Recovery Mass	Recovery Efficiency
250 ng	209 ng	84%
25.0 ng	20.1 ng	80%
2.50 ng	1.91 ng	76%
0.250 ng	0.215 ng	86%

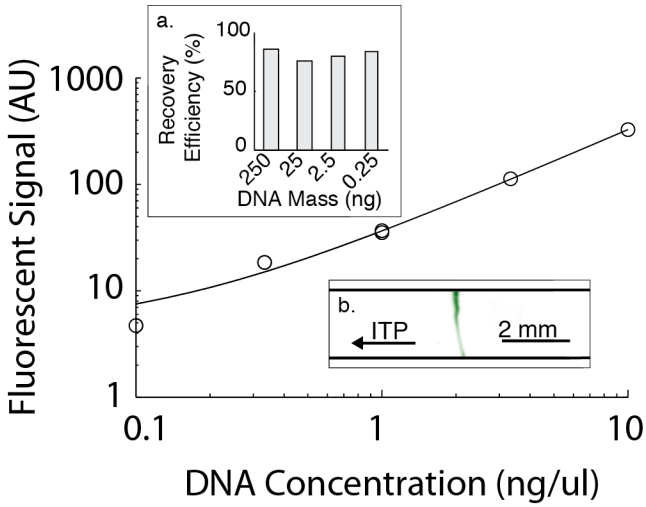

Figure 3-5. Fluorescence quantification of DNA. The fluorescence calibration curve of DNA dyed with SYBR Green I, measured by fluorescent signal from the CCD camera. The data points were fit with a linear curve over 2 orders of magnitude with a regression value of R^2=0.9997. ***Inset a.*** *The estimated recovery efficiency of known concentrations of salmon sperm DNA spiked onto the chip. The efficiency estimate is based on fluorescence quantification, computed from the calibration curve.* ***Inset b****. A representative image of DNA focused to the ITP interface and electromigrating through the device. This DNA band is approximately 8 mm from the extraction reservoir.*

DNA purification from Whole Blood

Finally, we purified DNA from whole human blood samples using this device. While nucleic acid purification from blood samples has been demonstrated,[1-3,5,8] the results have always been complicated by the dilution factor of the extracted sample into the qPCR reaction. For example, typical previous ITP extraction studies have diluted

blood samples 10^3 to 10^4-fold as the liquid is dispensed into the PCR reaction. The latter dilution also dilutes inhibitors, and so it becomes interesting to test less aggressive dilutions of the extracted DNA.

In this demonstration, blood was diluted 10x when preparing the blood lysate. DNA from the 25 µL blood lysate sample was then extracted via ITP and eluted into the 25 µL volume of our chip's extraction reservoir. Therefore, both the chip and extraction processes contribute to no change of volume (no dilution). After extraction, the DNA sample was diluted 10x into the PCR master mix. The total dilution factor of the entire process (the lysing, extraction, and PCR solution preparation) was 100x, more directly showing the power of ITP as a purification method.

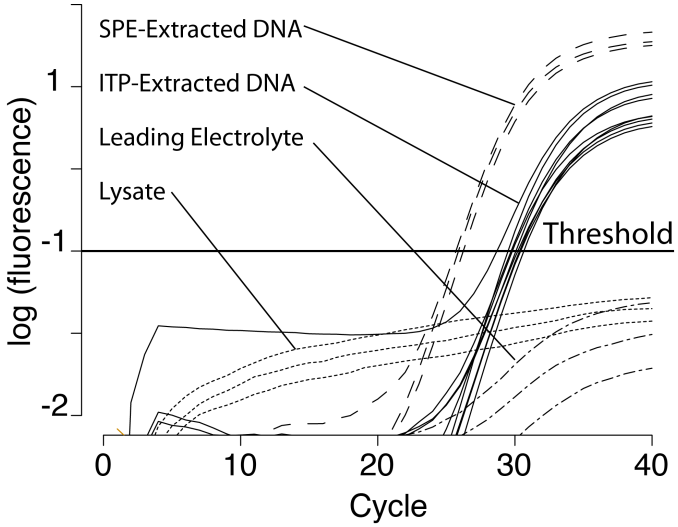

Figure 3-6. qPCR analysis of DNA purified from whole human blood using ITP on the new microfluidic device. DNA extracted using ITP, and control samples were amplified in the presence of a primer for the human gene BRAC2. The log of fluorescence signal versus cycle number is plotted. The negative control samples, (template-free LE buffer and unprocessed blood lysate) have fluorescent signals that remain below the threshold, indicating negligible PCR amplification. DNA extracted from blood using ITP, and the positive control sample (DNA extracted from blood using a commercial solid phase extraction kit) both amplify, leading to fluorescence well above threshold. The melting temperature of the amplicon (not shown) from all amplified samples was 74°C. This temperature matches theoretical predictions from the Promega amplicon melting tool.[17]

Summary

We have demonstrated for the first time a microfluidic chip capable of achieving highly efficient ITP purification of nucleic acids from 25 μL blood samples. We designed this chip by taking into account principles of ITP separation capacity, throughput, pH buffering capacity, and dispersion minimization. The chip incorporates high aspect-ratio channels to improve heat dissipation, and optimized turn geometries to reduce dispersion around corners. The chip uses separate buffering reservoirs to decouple the buffering capacity of the device form the sample and extraction reservoir chemistry. The chip incorporates a capillary barrier structure to allow sequential loading of the fluids without loss of fluid into the vacuum port. These structures provide robust, repeatable loading using easily achievable vacuum levels. Lastly, the chip was designed for and fabricated in common COC and PMMA using injection molding, which shows the possibility for simple and scalable fabrication of these devices. This chip design can act as a platform for future studies of ITP purification by allowing practical sample volumes to be processed in less than an hour, without wasting precious sample volume.

Chapter 4 ITP Purification from Realistic Samples

Some of the contents of this chapter have been printed as an article in *Analytical Chemistry* by Lewis A. Marshall, Crystal M. Han, and Juan G. Santiago. They are adapted here with permission from Marshall, Han, Santiago (2011) Extraction of DNA from Malaria-Infected Erythrocytes using Isotachophoresis, *Analytical Chemistry 83*, 9715-9718. Copyright 2011 American Chemical Society.

Introduction

Microfluidic platforms are an attractive alternative to benchtop solutions for diagnostic medical testing because they consume low sample and reagent volumes, and offer the potential of integrating multiple assay steps. However, sample preparation in microfluidic devices is a continuing challenge because of the complexity and variety of biological samples and the low concentrations of target molecules.[1]

Blood is an attractive sample for microfluidic analysis because it is collected routinely, and contains information about the entire body.[2] However, blood contains a complex mixture of cells, proteins, and electrolytes, which can interfere with diagnostic tests. Extraction of DNA from erythrocytes for downstream polymerase chain reaction (PCR) is a particular challenge because of the abundance of hemoglobin, a PCR inhibitor.[3]

Microfluidic systems exist for preparation of nucleic acids from blood and other biological fluids.[4,5] These systems typically seek to adapt benchtop-scale methods like solid phase extraction or magnetic bead purification.[4] Such methods rely on specific channel geometries, porous structures, and/or surface chemistries, and may require pumping and valves to implement wash steps. Some systems require external manipulations of magnets.

Isotachophoresis (ITP) offers an alternative to surface-based purification methods for nucleic extraction and purification. ITP-based DNA purification does not require surface chemistry-dependent DNA adsorption, rinses during extraction, or pumping of fluid streams. ITP purification is also weakly dependent on surface chemistry as it can be performed under conditions of strongly suppressed electroosmotic flow (which aids in reproducibility). ITP is a robust sample preparation method,[6,7] can be highly selective,[8,9]

and can provide up to one million-fold preconcentration.[10] We have used ITP for extraction of small RNA from cell cultures,[11] micro-RNA from total RNA,[8,9] genomic DNA (gDNA) from whole blood,[12] and ribosomal RNA from bacteria in urine.[7] With ITP, analytes are extracted and pre-concentrated at the interface between a leading (LE) and trailing electrolytes (TE) of a two-buffer system. Selectivity is based on electrophoretic mobility. The strong electric field gradient at the TE-to-LE interface stabilizes and sharpens the focusing zone. Nucleic acids can be preferentially separated and pre-concentrated, while excluding proteins and PCR-inhibiting molecules.

As mentioned above, we demonstrated extraction of human gDNA from whole blood.[12] That method was developed to lyse and extract nucleic acids from host cells, used a relatively gentle lysis process, was performed in a small channel volume, and used pressure-driven finite injection. Here we demonstrate an ITP-based technique to extract pathogenic DNA from human red blood cells infected with the malaria-causing parasite *Plasmodium*. This work differs from our previous work on ITP-based extraction of host gDNA from blood,[12] as we here offer a new lysing and ITP chemistry which achieves more aggressive chemical and thermal lysing applicable to the malaria parasite. Our current method also uses larger channel volumes, semi-infinite injection,[10] and pressure-driven counter flow to increase sensitivity. We start by showing that higher lysis temperatures are required to lyse malaria parasite cells. We show that ITP-based DNA preparation can extract DNA from pathogenic cells as well as host cells. The work suggests that ITP can be integrated into blood diagnostic systems for a wide range of pathogenic diseases.

Experimental Methods

A schematic of our extraction process is shown in **Figure 1a.** We used heat and chemical treatment to lyse malaria parasites infecting erythrocytes. We then mixed the resulting lysate with a TE buffer, and pipetted the mixture onto a simple capillary setup. We applied an electric field to perform ITP. The nucleic acids were separated via electric field, and traveled from the TE sample well to an LE well. The purified nucleic acids were pipetted from the LE well for off-chip PCR.

Plasmodium Falciparum Samples

We received *P. falciparum* W2 cells cultured in human erythrocytes from the Stanford Blood Center (Stanford, CA). The cells were cultured using the method described by Trager and Jensen.[13] Culture samples were taken with culture parasitemia of 3.5% and 9%. These samples were stored at -20 °C for later use.

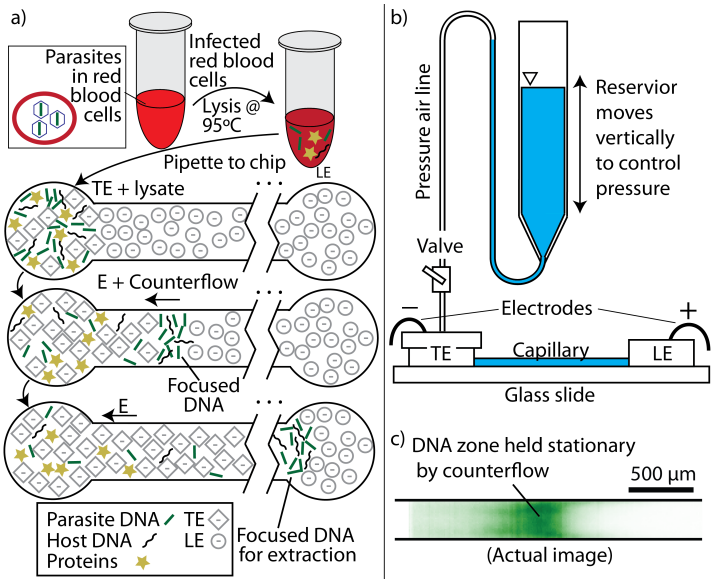

Figure 4-1. a) DNA extraction process. A culture sample containing P. falciparum parasites infecting (within) red blood cells was diluted, mixed with proteinase K, and lysed at 95 °C. During lysis, parasite cells released their DNA into the cell lysate. The cell lysate was pipetted directly into the microfluidic well containing the TE. An electric field was applied, and the DNA was pulled into a capillary, where it focused at the ITP interface. In this process, PCR inhibitors (including proteins) remain unfocused in or near the TE well. The focused ITP zone containing purified nucleic acids eventually reached the LE well, where it was extracted for off-chip PCR. b) Experimental setup. TE and LE wells are connected by a 300 x 30 µm x 2.5 cm rectangular cross-section capillary. Pressure in the TE well is controlled using an elevated water chamber connected to an air-filled pressure line. c) CCD camera image of extracted DNA focused at the ITP interface. DNA is visualized using SYBR Gold fluorescent dye.

Capillary Preparation

We used a free-standing, rectangular-cross-section, borosilicate capillary (not a microfluidic chip) for these experiments. We glued a 2.5 cm long, 30 x 300 µm (inner dimensions) capillary (Vitrocom Inc., Mountain Lakes, NJ) to a 2.5 cm x 7.5 cm glass slide (VWR, West Chester, PA) using UV-cure optical adhesive (Norland, Cranbury, NJ). The capillary axis was aligned with the 7.5 cm axis of the slide, and the 300 µm by 2.5

cm face of the capillary laid flat against the glass slide with the 30 μm dimension parallel to the optical axis. We cut the threaded rings from two plastic screw-top 1.5 mL microcentrifuge tubes (Applied Scientific, South San Francisco, CA) and adhered these over the capillary ends as wells (using the same adhesive). We taped a 2 x 2 cm piece of aluminum foil (Reynolds Wrap, Richmond, VA) over the capillary to improve heat dissipation. An image of the capillary setup is shown in **Figure S-1.** This simple, free-standing capillary offers an inexpensive, easy-to-reproduce channel geometry with large cross section relative to most etched microchannels. Large cross section increases the sample volume from which we extract DNA.

We used the commercial silanizing agent, Sigmacote (Sigma-Aldrich, St. Louis, MO), to reduce electroosmotic flow and chemical adsorption to the glass channel walls.[12]

Prior to the first use, and between runs to avoid cross-contamination, we rinsed the capillary with 50 uL 10% bleach followed by 200 μL deionized water, and dried with vacuum for 2 min. Immediately before each experiment, we filled and rinsed with 50 μL LE.

We controlled pressure-driven counterflow using a water column attached to the TE well. A schematic of this setup is shown in **Figure 1b**. Briefly, we used a three-port Luer connector to connect a 1 m long tube to the TE well. This tube acted as a hydrostatic water column open to atmosphere. It was held in place with small magnet and a ring stand. This let us apply vacuum to the capillary by lowering the water column.

LYSIS: We diluted infected culture samples with uninfected erythrocytes and deionized water. This provided samples containing 9%, 1%, 0.1%, 0.01% and 0% parasitemia and 50% hematocrit to simulate infected human blood samples while also providing well-controlled dilutions of parasite loading. We further diluted 30 μL of each sample with 185 μL deionized water and added 17 μL of proteinase K (Invitrogen, Carlsbad, CA). We mixed each sample by pipetting and incubated at 65 °C for 1 min, then 95 °C for 9 min using a PCR thermocycler (Techne, Burlingon, NJ).

We performed manual cell counts to examine the efficiency of our lysis process as a function of temperature. We prepared lysis mixtures containing 10 μL erythrocyte sample with 0.9% nominal parasitemia, 10 μL proteinase K, 5x SYBR Gold (Invitrogen, Carlsbad, CA), and nuclease-free water to bring the mixture to 100 μL. We divided the

samples into lysed and unlysed groups. We counted the cells in the unlysed samples immediately. We incubated the lysed samples at elevated temperature for 10 min in a benchtop thermocycler. As a comparison case, we incubated one lysed sample for 10 min at 56 °C, in the same manner as Persat *et al*.[12] We held all other samples for 1 min at 65 °C for proteinase K digestion, then an additional 9 min at elevated temperatures ranging between 65 °C and 95 °C.

We counted the cells using disposable hemocytometers (Cell-Vu, New York, NY). Malaria cells were visualized with SYBR Gold fluorescent dye, which fluoresces strongly when bound to nucleic acids. We prepared the hemocytometer for counting as described in the Cell-Vu operation manual.

Extraction

We prepared aqueous LE and 2x TE buffers prior to each experiment. The LE contained 0.1% Triton X-100 (Sigma-Aldrich, St. Louis, MO) and 1x SYBR Gold (Invitrogen, Carlsbad, CA) in 100 mM Tris and 60 mM hydrochloric acid at pH 7.9. The 2x TE contained 2x SYBR Gold in 40 mM Tris and 40 mM HEPES (pH 7.9). To prepare the TE, we mixed the cell lysate 1:1 with 2x TE, for a final buffer concentration of 20 mM Tris and 20 mM HEPES.

At the start of each experiment, we filled the capillary with LE, and emptied the wells with vacuum. We pipetted 50 μL LE into one well and 50 μL of TE into the other well. We placed platinum wire electrodes into each well (and connected to high voltage leads). We applied +600 V to the LE well, grounded the TE well, and recorded applied current over time using the Keithley voltage source and a computer running custom Matlab code. Current traces for experiments under counterflow are shown in **Figure S-2**.

We monitored the ITP zone using epifluorescent microscopy (see below). For experiments requiring extended focusing time, we induced counterflow by applying vacuum to the TE well with our water-column system. We held the interface in the channel for 10 min, then approximately eliminated pressure-driven flow by returning the water column to its original height. When the ITP interface entered the LE well, we turned off the electric field and pipetted 4 μL of the LE from the region near the capillary exit into a 200 μL PCR tube for analysis. We note visual inspection and measured

current traces each provide feedback which can be used to hold the ITP zone stationary (see SI).

Imaging System

We performed on-chip visualizations using an inverted epifluorescence microscope (Nikon, Tokyo, Japan) equipped with a 4x objective (Plan, NA 0.10, Nikon, Tokyo, Japan). A blue LED light source (Thor Labs, Newton, NJ) was used for excitation. We used a filter cube optimized for detection of FITC (FITC-A-Basic, Semrock, Rochester, NY) and a 0.63x demagnification lens (Diagnostic Instruments, Sterling Heights, MI). We captured images using an intensified CCD camera (PI-MAX: 512, Princeton Instruments, Trenton, NJ). The DNA fluorescent dye was SYBR Gold included in the lysis buffer as described above.

PCR

We used off-chip quantitative PCR to validate our ITP extraction method. We added 4 μL of DNA extract from ITP to a PCR tube containing 10μL 2x Fast SYBR Green PCR master mix (Applied Biosystems, Carlsbad, CA), 6μL DNAse free water, and 150nM primers targeting the PFCS. Validated primers[15] for the circumsporozite protein gene in *P. falciparum* were used to verify the presence of *P. falciparum* DNA. The primers were PFCS79, 5'-GGAAGTCGTCAAACACAAG-3', and PFCS233, 5'-CCATCATCATTTTCTCCAAG-3'.

We performed off-chip quantitative PCR using a real-time PCR thermocycler (7500 Fast, Applied Biosystems, Carlsbad, CA) with the following thermal profile: 20 s initial hold at 95 °C and 40 cycles composed of 3 s denaturation at 95 °C and 30 s annealing and extension at 60 °C. We obtained post-PCR dissociation curves using the same instrument.

Results And Discussion

Lysis

We used heat and chemistry to lyse the malaria parasites. Proteinase K aids in lysis, and may assist in removal of nucleic acids from packing proteins.[12] We chose this method to avoid adding high-concentration ions, which may interfere with ITP

separation. For example, high concentrations of chaotropic salts are often used for lysis and denaturation during nucleic acid extraction.[16] However, high ionic strengths (e.g. >500 mM) can be challenging to integrate with ITP and/or require significant dilution steps.

Visualizations of malaria with SYBR dyes have been used to detect malaria infection in blood.[17] DNA-specific dyes provide a high-contrast way of visualizing the DNA-containing malaria parasite inside red blood cells (which contain no DNA). We used SYBR Gold to visualize intact parasite cells to determine lysing efficiency (*c.f.* **Figure S-3**).

Meausured cell lysis efficiencies are shown in **Figure 2**. We defined cell lysis efficiency as:

$$\text{Efficiency} = 1 - \frac{\text{Lysed Cell Count}}{\text{Unlysed Cell Count}}$$

We did not observe significant cell lysis at temperatures below 85 °C. To estimate the uncertainty in lysis efficiency, we propagated the 90% confidence intervals from Student-t distributions of the lysed and unlysed cell count using the equation above assuming that these cell counts were uncorrelated.[18] Lysing efficiency is ideally a positive quantity. However, the slight negative values in our measured estimate of lysing efficiency (for data at 56 °C) is an expected result of experimental uncertainties in the lysed vs. unlysed cell estimates. The lysing data shows a monotonic increase in lysing efficiency with increasing temperature from 56 °C to 95 °C. We therefore chose 95 °C for the second, higher-temperature incubation step of our assay.

Visualization

We visualized total DNA extracted from infected erythrocyte samples during the ITP process by observing the scalar fluorescence of SYBR Gold dye. Example images of this fluorescence are shown in **Figures 1c** and **S-4**. DNA visibly accumulates during the counterflow period, when the ITP zone is stationary in the channel.

PCR

Figure 3 shows measured PCR threshold cycles for circumsporozite protein gene primers of DNA extracted from human erythrocytes with ITP. We explored parasite

densities ranging 4 orders of magnitude from 0.5 to 500 ¢/nL. We show example raw data from PCR runs in **Figures S-5** and **S-6**. Counterflow extends focusing time and enables a decrease in the limit of detection by an order of magnitude. We did not observe amplification during 40 thermal cycles in negative control PCR reactions in which we analyzed unlysed malaria-infected erythrocytes and nuclease-free water as templates.

Dissociation curves of the PCR product are shown in **Figure S-7**. Amplified sequences dissociated at 69.5 °C. This matched the dissociated temperature measured for PCR product of *P. falciparum* DNA as extracted from cell cultures using a commercial solid phase extraction kit (Qiagen, Valencia, CA) (a value of 69.5 °C). As a second comparison, we calculated a theoretical dissociation temperature of 69.7 °C for this target sequence[15] using numerical DNA thermodynamic tools (mFold, RNA Institute, University of Albany, Albany, NY).

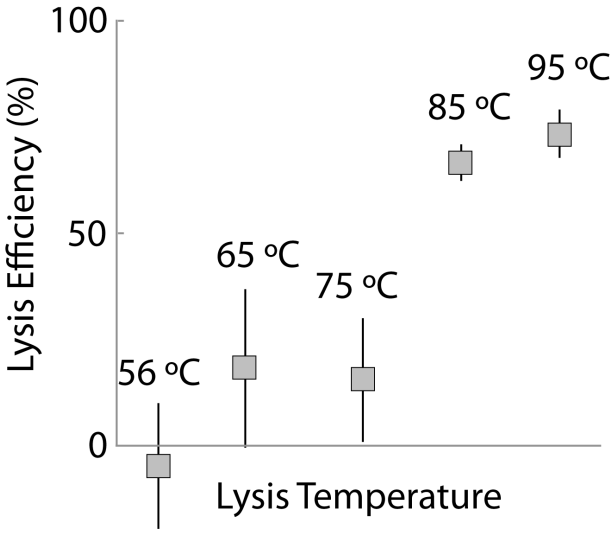

Figure 4-2. Lysis efficiency over maximum lysis temperatures between 56 °C and 95 °C. We compared pre-lysis and post-lysis parasite density by manual cell counting on disposable Cell-Vu hemocytometers. Parasite cells were visualized using SYBR Gold. Error bars indicate propagated 90% confidence interval based on Student t-distribution (N = 14 to 18 at each temperature).

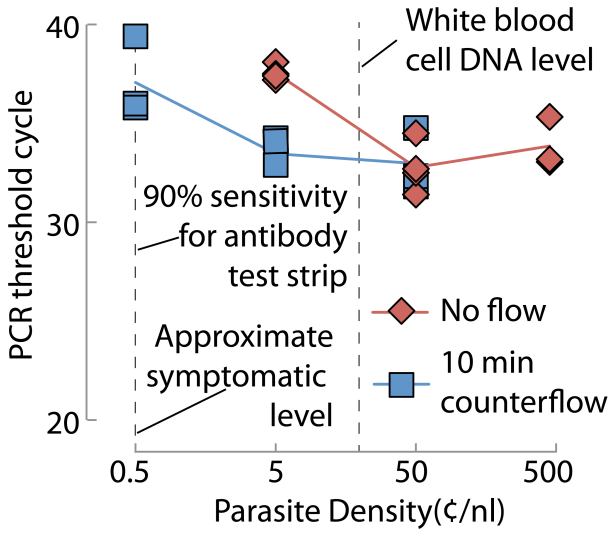

Figure 4-3. PCR threshold cycles from DNA extracted from malaria-infected erythrocytes using isotachophoresis (with and without counterflow to improve sensitivity). PCR primers targeted the circumsporozite gene in P. falciparum. Extending focusing time to 10 min (squares) using pressure-driven counterflow allowed us to detect parasite infection at the approximate clinical symptomatic threshold level of 0.5 parasites per nanoliter.[14]

Detection Limits

Manual microscopy of thick blood films can detect malaria infection at 0.05 parasites per nanoliter. However, microscopy is time-consuming and requires a highly trained operator. Commercial antibody test strip kits commonly achieve >90% sensitivity above 0.5 parasites per nanoliter, and 50% sensitivity at 0.05 parasites per nanoliter.[19,14] We detected *P. falciparum* parasites in human erythrocytes to a parasite density of 0.5 parasites per nanoliter, comparable to antibody test strips. Clinical parasite concentrations can range from 0.005-50 parasites per nanoliter in blood. Most symptomatic cases are above 0.5 parasites per nanoliter.[14] For example, a study of a Honduran population with endemic infections of *P. falciparum* and *P. vivax* measured an average concentration of 0.59 parasites per nanoliter in infected patients, including both symptomatic and non-symptomatic patients.[20]

Conclusion

We demonstrated extraction of DNA from the malaria-causing parasite *Plasmodium falciparum* in human erythrocytes using ITP with just a few manual steps. These malaria parasites are difficult to lyse compared to the host blood cells. We improved our nucleic acid yield by choosing a high lysis temperature, and increasing our extraction time using pressure-driven counterflow. We showed that the extracted DNA was purified of PCR inhibitors found in red blood cells and compatible with PCR, and achieved a clinically relevant qPCR detection limit of 0.5 parasites per nanoliter.

The pressure-driven counterflow technique we use here may be not compatible with some on-chip analysis systems. However, counterflow was used only to increase DNA yield by increasing the ITP focusing time. Other methods of increasing yield may include increasing channel length and cross-sectional area, increasing applied current, and/or simultaneously extracting into multiple channels. We are currently exploring methods to increase throughput without counterflow.

This demonstration of extraction of pathogenic DNA from parasites inside human erythrocytes by ITP represents a widening of the scope of applications of ITP as a microfluidic DNA sample preparation method. Such studies are a step toward producing clinical devices for diagnosis of infection on microfluidic platforms.

Acknowledgement

We thank Prof. Mark Levenston for use of his qPCR thermocycler. We thank Prof. Niaz Banaei and Ellen Yeh for providing *P. falciparum* samples. This work was supported in part by the Defense Advanced Research Projects Agency (DARPA) N/MEMS S&T Fundamentals Program under grant no. N66001-1-4003 issued by the Space and Naval Warfare Systems Center Pacific (SPAWAR) to the Micro/Nano Fluidics Fundamentals Focus (MF3) Center. We gratefully acknowledge funding from DARPA under grant number N660001-09-C-2082. We also gratefully acknowledge funding from the Gates Foundation under contract number OPP1007350 GCE.

Chapter 5 Integrated Devices for ITP Purification

Some of the contents of this chapter have been printed as an article in *Analytical Chemistry* by Lewis A. Marshall, Liang L. Wu, Sarkis Babakian, Mark Bachman, and Juan G. Santiago. They are adapted here with permission from Marshall, Wu, Babakian, Bachman, and Santiago (2012) Integrated Printed Circuit Board Device for Cell Lysis and Nucleic Acid Extraction, *Analytical Chemistry 84*, 9640-9645. Copyright 2012 American Chemical Society.

Introduction

Despite the advent of a wide range of on-chip assays, sample preparation remains a "weak link" in microfluidics.(1) When working with real biological or clinical samples, a microfluidic diagnostic device may have to overcome high concentrations of interfering species (e.g., proteins) to collect a relatively low concentration of target biomacromolecules, including target nucleic acids. Achieving rapid, robust sample preparation on microfluidic devices is a continuing challenge and a necessary component in developing fully integrated and useful microfluidic diagnostic devices.

To achieve nucleic acid extraction from cell samples, a microfluidic device needs to perform cell lysis (to make nucleic acids accessible) and nucleic acid extraction (to purify the nucleic acids from other cell components.) The most common way to integrate these two functions on a microchip is to use chaotropic agents for chemical cell lysis, followed by solid phase extraction.(2) As two examples, Chen et al. and Bienvenue et al. each applied guanidinium salts (strong chaotropic agents) to lyse cells on-chip and then used solid phase extraction (SPE) and multiple buffer exchanges and washes to extract DNA from the lysate.(3, 4) The disadvantage of the common approach of chaotropic agents and SPE is that it requires pressure-driven flow to perform the necessary buffer exchanges. This pressure-driven flow of multiple reactants often requires off-chip pumping and valve actuation or repeated manual reloading of solutions between the wash and elution steps. This leads to more design complexity and larger package size in on-chip SPE systems. We here present a microfluidic device that integrates mixing, thermal lysis of whole blood, and nucleic acid extraction in a compact chip with no moving parts. The system uses isotachophoresis (ITP) for nucleic acid extraction and so requires no off-

chip actuation except for electrical control with a voltage source. We use a fabrication method that leverages printed circuit board (PCB) technology to realize a low-cost, reconfigurable system.

Several systems have implemented and integrated heating with microfluidic devices. For example, Liu et al. used an off-chip Peltier heater coupled to a microfluidic system to perform on-chip lysis of captured *Escherichia coli* cells, followed by polymerase chain reaction (PCR).(5)Lee et al. developed a poly(dimethylsiloxane) (PDMS) device on a glass substrate with platinum surface deposited resistive heaters.(6) The latter device performed thermal lysis, microfluidic mixing, and PCR. However, neither device performed nucleic acid purification. Kim et al. demonstrated convective mixing and PCR in a microfluidic heating chamber but did not implement cell lysis.(7) We know of no previous microfluidic devices that integrate on-chip mixing, thermal lysis, and nucleic acid extraction.

Nucleic acid purification is critical when processing complex samples such as whole blood. Blood has relatively high ionic strength (order 100 mM)(8) and contains species inhibitory to DNA hybridization, protein–ligand binding, and amplification. For example, PCR is inhibited by hemoproteins, lactoferrin, immunoglobulin G, and, at sufficient ionic strength, mono- and divalent ions.(9)

ITP has been demonstrated as a purification technique for nucleic acids from blood,(10, 11)urine,(12) and cell culture.(13) To extract nucleic acids using ITP, a complex sample mixture is introduced into a two-buffer system. The leading electrolyte (LE) buffer contains an anionic species with electrophoretic mobility higher than that of DNA. The trailing electrolyte (TE) buffer is designed to contain an anionic species with an electrophoretic mobility lower than DNA but faster than anionic impurities (cationic impurities never exit the sample reservoir). When an electric field is applied across the two buffers, an electric field gradient forms between the TE and LE, and nucleic acids quickly move to and focus at the interface. ITP is robust,(14) is rapid,(12) and can be extremely selective.(15, 16) ITP does not rely on surface chemistry for species capture and is insensitive to substrate material and geometry. It is capable of preconcentrating small molecules by 10^6-fold(17) and can routinely extract and preconcentrate nucleic acids by more than 10^3-fold in about 1 min.(10) However, previous efforts to use ITP for

nucleic acid extraction have required at least one off-chip sample preparation step such as mixing with lysis buffer, heating, and/or incubation with a reagent such as proteinase K.

Our PCB microfluidic device performs rapid mixing and lysis on-chip using integrated resistive heaters, and the microfluidic components allow us to perform ITP separation of nucleic acids, with results comparable to a protocol using standard off-chip lysis and a glass capillary for ITP.(11) The results show that ITP and PCB microfluidic devices have potential to decouple microfluidic analysis from benchtop preparation techniques.

Experimental Methods

Device Fabrication

We first designed and fabricated a custom heating package for use on the PCB device. For the current work, we chose to integrate four 3.9 Ω resistive heaters (32R9407 thick film resistor, Panasonic, Secaucus, NJ) with a thermistor (LM 94023 IC temperature sensor, National Semiconductor, Santa Clara, CA). The components were soldered onto a 0.2 mm × 3.2 mm × 3.2 mm PCB board. The package was then encapsulated using thermal epoxy (50-3100 epoxy resin, Epoxies Etc., Cranston, RI). This yielded the final size for the heating package of 1 mm × 3.2 mm × 3.2 mm.

Our devices consist of two sections: the printed circuit board layer with surface-mount components and the microfluidic layer with reagent reservoirs attached. The trace layout for the PCB layer was designed using EagleCad software (CadSoft Computer GmbH, Delray Beach, FL). Metal traces are fabricated onto the epoxy-resin (FR-4) PCB through a standard foundry service (Sierra Circuits, Inc., Sunnyvale, CA). Surface mount components were then soldered onto the board.

Polyurethane casting and stamping procedures were used to create the microfluidic layer. The PCB layer was first inserted into a frame to hold polyurethane during pouring. The device was then planarized by pouring a thin layer of mixed polyurethane monomer and curing agent (Crystal Clear 202, viscosity of 600 cps, Smooth-On Inc., Easton, PA). We placed 1 mm glass beads in this layer as spacers to define the polymer thickness. The polyurethane was allowed to cure at room temperature for 2 h. After planarization, a second polyurethane layer was fabricated separately in

another container to create the fluidics. A PDMS mold was used to stamp the desired microfluidic pattern onto the fluidic layer. For the current work, the pattern was a simple, straight channel with a depth and width of 70 μm × 300 μm and length of 3.7 cm connecting the two 15 μL reservoirs. Before the microfluidic layer became fully cured, the PDMS mold was removed and both layers of polyurethane were sealed together and released from the frames. In addition, a thin layer of polyurethane-laminated poly(methyl methacrylate) (PMMA) with 4 mm access ports for the reservoirs was attached to the fluidics layer as a rigid support. Lastly, electrical connection pins were soldered in through access vias on the PCB board. The finished device is shown in Figure 1a. Detailed descriptions and characterization of the manufacturing process will be the focus of a future publication.

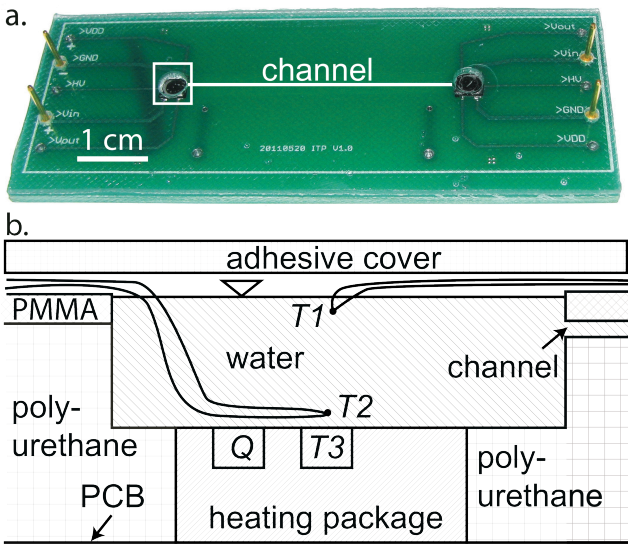

Figure 5-1. Hybrid PCB microfluidic device. (a) (Green) PCB substrate with surface-mounted components and (clear) polymer microfluidic layers. The channel location is highlighted using a white line for clarity. Each end-channel reservoir is integrated with a thermistor temperature sensor and heater. (b) Schematic of the cross section of the heated reservoir (outlined by the small white rectangle in part a). The thermistor (T3) and heaters lie within a 1 mm layer of thermal epoxy in the heating package. These are embedded in the 1 mm polyurethane planarization layer on the PCB substrate, above which is the polyurethane fluidic layer. The top layer of the device is 0.2 mm of stiff PMMA. Heat was applied at the embedded heater (Q). For temperature characterization, we instrumented the reservoirs with thermocouples T1 and T2, which measured temperature near the top and bottom of the liquid in the reservoir as shown.

Temperature Measurement

As shown in Figure 1b, each heater was embedded beneath the end-channel sample reservoirs in the microfluidics layer. It was activated by applying up to 200 mA to the resistive heating pins using a 1 kV maximum voltage sourcemeter (model 2410, Keithley, Cleveland, OH). The temperature was measured by supplying 3.3 V to the supply pin of the thermistor and measuring the voltage between the ground pin and the sensing pin of the thermistor. We used the voltage transfer function given by the thermistor manufacturer (see operation manual for LM 94023 IC) to calculate the thermistor temperature.

We investigated temperatures throughout the sample reservoir during heating using both the on-chip thermistor and the two free-standing 0.125 mm K-type thermocouples (Omega Inc. CHAL-005, Stamford, CT). We manually inserted the thermocouples into the reservoir, near the top and bottom surfaces, as shown schematically in Figure 1b. We recorded the thermocouple reading at 0.5 Hz using a dual thermocouple reader and its companion software (Omega Inc., Stamford, CT).

We also recorded temperature readings from the on-chip thermistor. The on-chip thermistor and the resistive heater are separated by about 1 mm and packaged within thermal epoxy. The thermistor temperature is therefore more strongly coupled to the resistive heater than to the liquid in the reservoir. However, the reservoir structure and its contents have a significant thermal mass. To take advantage of this, we developed and implemented a pulse-modulated heating and continuous sensing method to accurately estimate the temperature in the liquid. To this end, we operated the heater using 1.4 s rectangular pulses at 8 V separated by 5.6 s at 0 V (20% duty cycle), with measured maximum currents of approximately 500 mA (about 0.8 W time-averaged power). When the heater is on, the temperature in the heater quickly and significantly exceeds the liquid temperature. When the heater is off, the temperature in the heater and the liquid quickly converge. We accurately estimate the temperature of the liquid by measuring the temperature to which the thermistor converges. We collected data from the on-chip thermistor using a U12 DAQ (LabJack, Lakewood, CO) and its companion software.

Convection

Our heater provided a localized high-temperature region at the bottom of the sample reservoir (see the rectangles in Figure 4a). We characterized the thermal convective mixing caused by this localized heating using micro particle image velocimetry (micro-PIV). We filled the reservoirs with 15 μL of water seeded with 4 μm polystyrene particles doped with a proprietary red fluorescent dye with maximum excitation at 580 nm and maximum emission at 605 nm (Sigma-Aldrich, St. Louis, MO). Particles were illuminated using a mercury lamp in a BX60 epifluorescent microscope (Olympus, Center Valley, PA) using a 4× objective (numerical aperture 0.1) and a filter cube optimized for use with Cy3 (Omega Optics, Brattleboro, VT). Current between 0 and 180 mA was applied to the resistive heater, and images of the reservoir were captured using an intensified CCD camera (PI-MAX: 512, Princeton Instruments, Trenton, NJ) at a 200 ms exposure time. We used custom micro-PIV software to analyze the images. We used the standard (iterative) super-resolution approach(18) with 30 pixel square (final) interrogation regions and 200 ms time-between-frames.

Lysis and Separation

We demonstrated the efficacy of our devices using a series of heating, lysis, and ITP-based extraction experiments, with chemistry similar to that described by Marshall et al.(11) As with that previous work, we here were interested in sample preparation of pathogen nucleic acids from malaria parasites spiked into whole blood samples (malaria parasites require more aggressive lysing than host leukocytes). The protocol we used for on-chip lysis and ITP extraction is shown in Figure 2. We modified our protocol from the previous work by reducing the ionic strength of the buffers and changing the surfactant to Tween 20. Blood was mixed directly into a single mixture which served as both lysis buffer and trailing electrolyte buffer (instead of using separate lysis and ITP steps).

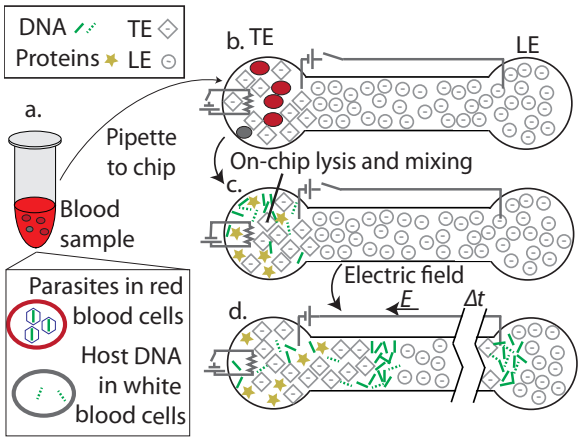

Figure 5-2. Schematic of malaria extraction protocol. (a) Malaria parasites were spiked into whole blood to provide a realistic sample. (b) The blood was pipetted directly into the on-chip reservoir, which was filled with the combined lysis and TE buffer. (c) This reservoir was sealed and heat was applied using the on-chip resistive heater. (d) After lysis, the heating was turned off and the electric field was applied between the two reservoirs. Nucleic acids were extracted and purified into the LE reservoir, where they were collected for off-chip analysis.

Briefly, we filled the channel and one reservoir with an aqueous leading electrolyte (LE) containing 50 mM Tris titrated with HCl to pH 8.2 with 0.1% Tween 20 and 10 μM SYTO 60 fluorescent dye (excitation at 652 nm, emission at 678 nm). We then emptied the opposite reservoir with vacuum and refilled it with 13 μL of an aqueous trailing electrolyte (TE) buffer containing 50 mM Tris titrated with 50 mM HEPES and 1 μL of proteinase K (Invitrogen, Carlsbad, CA). We pipetted 1 μL of whole blood spiked with *Plasmodium falciparum* parasites cultured in human erythrocytes. We then sealed both reservoirs with 5 mm × 5 mm squares of PCR-plate adhesive film (Bio-Rad, Hercules, CA) and applied 180 mA to both resistive heaters for 3 min. After this, the reservoirs were allowed to cool for 1 min (to approximately 40 °C), after which the adhesive seals were removed. We inserted platinum electrodes into both reservoirs and applied +500 V in the LE versus the ground electrode in the TE to initiate ITP. We monitored ITP by measuring current and by visualizing SYTO 60 fluorescence using the epifluorescent microscope and a filter cube optimized for Cy5 dye (Semrock, Lake Forest, IL). When the ITP interface reached the LE reservoir, we deactivated the voltage and then mixed and collected the contents of the LE reservoir for later, off-chip analysis. The PCB device had negligible autofluorescence in the SYTO 60 emission spectrum of

about 650–700 nm. At shorter wavelengths (e.g., the emission spectrum of SYBR Green DNA-specific fluorescent dye), the PCB substrate exhibited strong background fluorescence.

To verify that cells were being lysed during the on-chip heating, we performed manual cell counting of samples before and after cell lysis using disposable hemocytometers (Cell-Vu, New York, NY). We fluorescently labeled the malaria parasites using DNA-specific SYBR Gold dye. This allowed easy differentiation between DNA-free erythrocytes and DNA-containing malaria parasites.(19) We used the cell counts before and after the lysis protocol to calculate the lysis efficiency, defined as

$$\text{lysis efficiency} = 1 - \frac{\text{lysed cell count}}{\text{unlysed cell count}}$$

Polymerase Chain Reaction

We validated the purity and efficiency of our integrated and automated on-chip lysis and extraction using off-chip quantitative polymerase chain reaction (qPCR). These experiments confirmed the presence of the target nucleic acids and successful extraction from PCR-inhibiting chemical species in blood. For these experiments, we added 4 μL of DNA extracted with our PCB microfluidic device directly into a PCR tube containing 10 μL of Fast SYBR Green PCR master mix (Applied Biosystems, Carlsbad, CA), 6 μL of DNase free water, and 150 nM each of forward and reverse primers. We also performed positive control experiments in which the template was DNA extracted from the same malaria parasites using a commercial solid phase extraction kit (Qiagen, Valencia, CA). We used validated primers for the circumsporozite protein gene in *Plasmodium falciparum*(20) (PFCS79, 5′-GGAAGTCGTCAAACACAAG-3′, and PFCS233, 5′-CCATCATCATTTTCTCCAAG-3′). Analysis was performed in a miniOpticon qPCR thermocycler (Bio-Rad, Hercules, CA) with the following thermal profile: 20 s initial hold at 95 °C and 40 cycles composed of 3 s denaturation at 95 °C and 30 s annealing and extension at 60 °C. We obtained post-PCR dissociation curves using the same instrument.

Results and Discussion

Reservoir Temperature

We measured both transient and steady-state temperatures in the reservoir upon application of current to the resistive heater, as summarized in Figure 3. The device approaches steady state temperature within 3 min and can achieve temperatures ranging from room temperature to 90 °C (T1), depending on applied current. The resistive heater can sustain currents up to 200 mA; higher currents damage the device. The steady-state reservoir temperature is proportional to the square of the applied current, as shown by the quadratic fit lines in Figure 3b. This is consistent with a steady-state model in which power is supplied to the reservoir by Joule heating in the resistor and dissipated to the environment at a rate proportional to the temperature difference between the liquid and the environment. A simple model for this process is as follows: $Q_{in} = Q_{out}$ $Q_{in} = IV = I^2RQ_{out} = hA(T - T_o)$ Here, Q_{in} and Q_{out} are the power input and output, I is the applied current, V is the voltage drop across the resistive heaters, and R is the resistance. h is an effective heat transfer coefficient of heat rejection to the environment, A is the surface area of the reservoir, and $T - T_o$ is the difference between the (approximately uniform) reservoir temperature and room temperature. These equations can be combined and rearranged as follows: $(T - T_o) = I^2\frac{R}{hA}$ This simple analysis shows that reservoir temperature should be approximately proportional to the square of applied current.

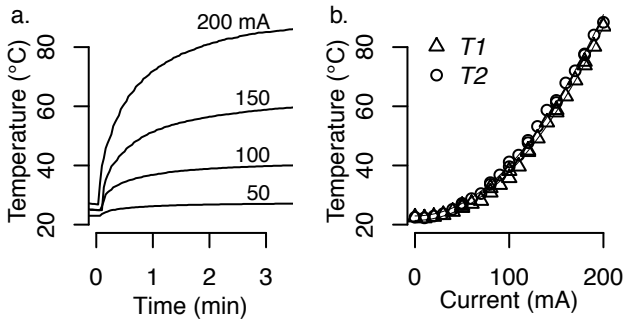

Figure 5-3. Measurements of on-chip heating temperatures. (a) Transient temperature profiles in the reservoir (T1) at various applied currents. Temperature approaches steady state within about 3 min. (b) Steady state temperatures as a function of applied current. Temperature was quantified using thermocouples T1 and T2 simultaneously. We here defined steady state as the temperature at which the reservoir was changing less than 0.5 °C/s. The difference between the T1 and T2 measured temperatures was less than about 5 °C, indicating vigorous mixing by thermal convection. Quadratic trend lines are plotted to show the relation between applied power and steady state temperature.

We demonstrated the efficacy of using our embedded thermistor and pulsed heating method to measure the temperature of the liquid in the reservoir. We obtained simultaneous measurements of the thermocouple T1 and the embedded thermistor. The temperature measured by the thermistor equilibrated to within about 5 °C of the measured water temperature at the end of each 5.6 s deactivated current interval. The on-chip thermistor was therefore able to fairly accurately measure the reservoir temperature.

Thermal Convection

We used micro-PIV(21, 22) to quantify the thermal convection-generated velocity fields in the reservoir. We placed the focal plane of our 0.4× objective (numerical aperture 0.1) 0.1 mm from the top surface of the 1.2 mm deep volume of liquid in the sample reservoir. A representative flow field is shown in Figure 4a. We quantified flow fields at a variety of applied currents. At a heating power of 0.58 W (180 mA applied current), we recorded in-plane flow velocities of up to 600 μm/s (as shown in Figure 4b). The flow velocities were steady and showed a clear pattern with heated liquid rising from the off-center heater at the bottom of the reservoir and circulating away and then downward near the far edges of the reservoir (see Figure 4). Although not shown here, we observed the complementary flow toward the heater when we analyzed flow velocities near the bottom of the reservoir. Repeated experiments show that the flow patterns were repeatable and the process ergodic. The flow velocities therefore imply

that, during the 3 min lysis step, fluid particles traversed the reservoir approximately 20 times, allowing for efficient mixing with the lysis buffer. We estimate the Rayleigh numbers (*Ra*), defined as $(g\beta\Delta TL^3)/(\nu\alpha)$, where g is the gravitational acceleration, β is the thermal expansion coefficient of water, L is the height of the reservoir, ν is the kinematic viscosity of water, α is the thermal diffusivity, and ΔT is the measured temperature differences between the top and bottom of the reservoir. These *Ra* values vary between 12 and 1200 for reservoir temperature differences (T2 – T1) ranging from 0.1 to 4.5 °C. These *Ra* are below the theoretical critical threshold value of 1710 for convection between two uniform-temperature flat plates.(23) We hypothesize that the strongly asymmetric and localized heating provided by our off-center heater design promoted strong circulation at lower *Ra*. We recommend that the study of geometries for achieving strong on-chip thermal convection and mixing at low temperature differences and in small geometries would be a good contribution to the microfluidics field.

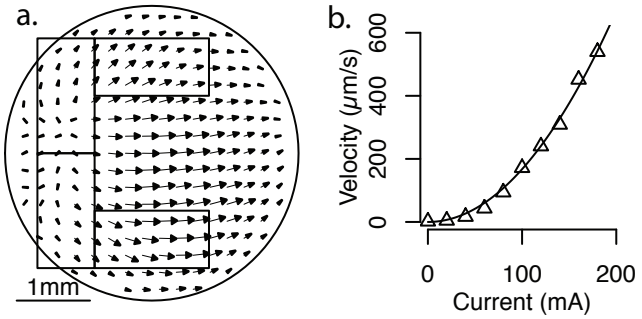

Figure 5-4. Convective mixing data. (a) Micro particle image velocimetry measurements of convective flow inside the reservoir during heating. Flow was visualized by seeding with 1 μm fluorescent beads and placing the focal plane 0.1 mm from the top of the 1.2 mm deep liquid level in the reservoir. Images were analyzed using custom micro-PIV software. Rectangles show the locations of the four embedded resistive heaters. (b) Maximum (in-plane) convective mixing velocity as a function of current applied to the on-chip heater. We show a quadratic fit line with the data.

Temperature-Induced Pressure Driven Flow

As described earlier, our protocol used an adhesive seal to cover the reservoir during heating. We observed that heating a single, covered reservoir connected to a channel caused a finite amount of pressure-driven flow out from that reservoir. This flow is likely caused by the increased vapor pressure in the reservoirs at elevated temperature. We developed a simple model for this flow based on thermodynamic equilibrium estimates of the partial pressures in the gas layer at the top of the sealed reservoir. The

analysis shows that pressure driven flow is minimized when both the inlet and outlet reservoirs are heated simultaneously such that the temperature in both reservoirs is equal and when the initial gas space is as small as possible. To reduce heat-induced pressure-driven flow in our experiments, we applied equal currents to both reservoir heaters and filled the reservoirs equally to within 1 μL of their capacities.

Lysis and Separation

We quantified the lysis efficiency of our system and compared it to off-chip lysis methods. Figure 5 summarizes our lysis results. Our on-chip lysis approach achieves up to 90% lysis efficiency at 180 mA applied current. We chose to operate our heater at 180 mA for the current extraction experiments.

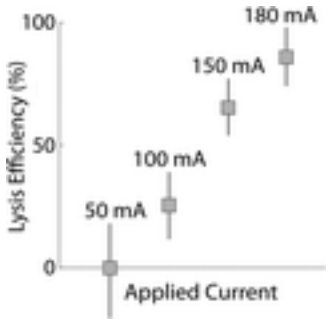

Figure 5-5. Measurements of lysis efficiency of malaria parasites in human blood. Cells were lysed at four applied currents in the on-chip heating system integrated within our PCB microfluidic device. Each measurement was repeated N = 14–18 times. Uncertainty bars indicate 95% confidence intervals on the means.

We visualized the focused and purified nucleic acids zone during ITP extraction using SYTO 60 red DNA-specific dye. A representative image of the extracted total nucleic acids in the microfluidic channel as they exit into the downstream reservoir is shown in Figure 6.

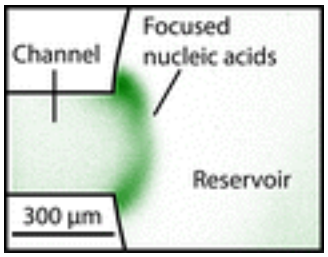

Figure 5-6. Example image of ITP zone of extracted DNA as it exits the channel and enters the downstream (leading electrolyte) reservoir of our PCB microfluidic device. Nucleic acids were labeled with SYTO 60. The ITP zone curved outward as shown when the current lines fringed outward.

Polymerase Chain Reaction

The results of our off-chip qPCR validation of the purity and amount of extracted nucleic acids are summarized in Figure 7. Our qPCR experiments show amplification down to 500 parasites per microliter. In Figure 7a, we compare our qPCR threshold cycles to those of Marshall et al.,(11) who used a similar ITP extraction method in a free-standing borosilicate glass capillary. The resulting trends are in close agreement, although they should not be quantitatively compared because they were performed on different qPCR machines. We constructed a calibration curve for DNA concentration as a function of the qPCR threshold cycle to estimate the extraction efficiency of our device.

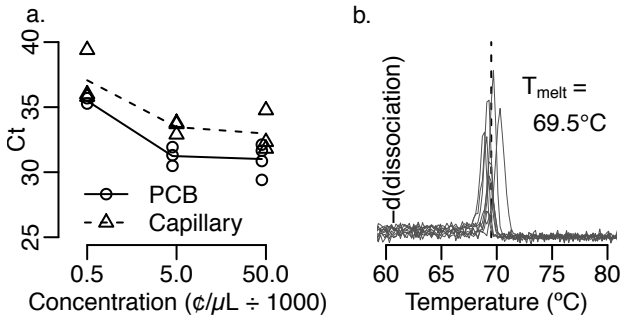

Figure 5-7. Off-chip qPCR measurements to show the purity, quantity, and PCR-compatibility of the nucleic acid extracted using our integrated device. (a) qPCR threshold cycles of the extracted nucleic acids as a function of parasite concentration in the original infected blood sample dispensed into the chip. PCR primers targeted the circumsporozite gene in P. falciparum. We observed no amplification in negative control reactions that contained unprocessed infected blood samples and nuclease-free water as template. Data from our PCB-device extractions (circles, solid line) is compared to similar data gathered using the same ITP chemistry and ITP process but with off-chip lysis and separation in a glass capillary (triangles, dotted line). Adapted from ref 11. Copyright 2011 American Chemical Society. Line segments connect mean threshold cycles. (b) Nine dissociation curves of the amplified PCR product of the extracted DNA. Dissociation temperatures cluster closely around the theoretical melting temperature for the target amplicon, shown as a vertical dotted line. This melting temperature matches positive controls using template DNA extracted from infected blood samples by a commercial solid phase extraction system (Qiagen, Valencia, CA).

Figure 7b shows dissociation data for the PCR product from nine samples. The product dissociates near the theoretical melting temperature, 69.5 °C, for our target sequence, consistent with our conclusion that we amplified the correct PCR product. The nine amplicon samples showed a standard deviation of 0.4 °C from the mean melting

temperature of 69.4 °C. The 69.5 °C theoretical value was predicted using mfold thermodynamic simulation software (RNA Institute, University of Albany).(24)

Conclusions

We demonstrated the operation of a PCB microfluidic device where we directly dispense 1 μL of unprocessed whole blood into a chip and automatically mix, lyse, and extract PCR-compatible nucleic acid into a downstream reservoir. The chip uses integrated heaters and temperature sensors to achieve controlled temperatures of up to 90 °C in a 15 μL reservoir. We achieved lysis using a combined lysis and trailing electrolyte ITP buffer and localized heating. Localized heating causes rapid thermal-convection-driven mixing and promotes lysis. After lysis, the heater is deactivated and ITP is used to automatically extract and purify PCR-compatible nucleic acids into a downstream reservoir. The chip can operate with no manual steps after dispensing blood, and the system has no moving parts. The device also uses no off-chip pumps, valves, or pressure sources.

The integration of electronics and microfluidics in PCB devices demonstrates that it is possible to break the heavy and nearly ubiquitous dependence of microfluidics on off-chip, benchtop-scale sample preparation methods for complex biological samples. By bringing more operations on-chip, we can begin to create robust, practical lab-on-chip devices for medical care.

Acknowledgements

We thank Prof. Niaz Banaei and Dr. Ellen Yeh for providing *P. falciparum* samples. This work was supported in part by the Defense Advanced Research Projects Agency (DARPA) N/MEMS S&T Fundamentals Program under Grant Number N66001-1-4003 issued by the Space and Naval Warfare Systems Center Pacific (SPAWAR) to the Micro/Nano Fluidics Fundamentals Focus (MF3) Center. J.G.S. and L.A.M. also gratefully acknowledge funding from DARPA under Grant Number HR0011-12-C-0080 as well as funding from the Gates Foundation under Contract Number OPP1007350 GCE.

References

Chapter 6 Conclusion

Contributions

- Literature review of the field of nucleic acid purification via ITP, and of the design and sizing of systems for analytical ITP, with an effort to adapt these ideas to ITP purification.
- Design of a microfluidic device for rapid, highly efficient extraction of nucleic acids using ITP.
- Demonstration of purification of nucleic acids from malaria-infected human blood samples.
- Demonstration of on-chip cell lysis and nucleic acid preparation from malaria-infected blood samples on an integrated microfluidic device with on-chip heaters and fluidic channels. (Device designed by the group of Mark Bachman at UC Irvine.)
- Development of a theory for the design principles for ITP as a purification process.

Recommendations

- Further research into continuous purification of nucleic acids from biological samples using free-flow ITP setups. Previously, continuous flow ITP has posed a significant challenge due to the instability of free-flow electrophoresis systems. However, recent advances in the art, particularly by the Bowser group at the University of Minnesota, have made this avenue more feasible. Furthermore, device throughput has been the most challenging aspect of designing devices for ITP purification of nucleic acids. A continuous flow device would help to ameliorate that issue.
- Further characterization of the mobilities and pKas of important PCR inhibitors. Currently, the most challenging portion of designing an ITP chemistry for purification of nucleic acids is the inability to exactly predict which inhibiting species will be effectively separated. Typically these species are not easy to track because they are mixed together and not inherently fluorescent, so their position in the channel can only be estimated based on the little available mobility evidence.

- Further analysis of the role of gels in ITP of nucleic acids. Right now, introducing a gel typically makes predicting the outcome of an experiment more difficult. However, gels have significant utility both in separating DNA by size and in selectively preventing flow in channels without significantly reducing the mobility of small molecules.
- Multilayer design for ITP purification. Introducing thicker channels improves the throughput of devices, but at the cost of increasing susceptibility to pressure-driven flow and increasing temperature due to larger characteristic distances for heat transfer. One way of solving this would be to build multilayer chips, perhaps out of glass, allowing high thermal conductivity and short length scales while still having a high cross-section for flow.
- Further literature review and analysis of the limits of current at electrodes. Currently, improvements in design, and specifically larger channel cross-sections have allowed operation of devices for ITP purification to overcome their previous throughput limits, which were imposed by Joule heating. However, this has caused the process to hit a new limit, imposed by the electrodes. High electrolysis rates cause rapid bubble formation. At sufficiently high rate, these bubbles can cling to the electrodes, causing poor electrical contact. This problem is exacerbated by the use of gel in the electrode reservoirs, because bubbles remain trapped in the gel, rather than rising to the surface due to buoyancy. These effects typically limit the current to the device to 250 μA. These limitations could likely be overcome by adjusting the geometry of the electrodes, but currently this problem has not been addressed for ITP purification.

Bibliography

Chapter 1

(1) Hiatt, J.; Turner, E.; Patwardhan, R.; Lee, C.; Shendure, J. *J Invest Med* **2009**, *57*, 114-114; Shendure, J.; Ji, H. L. *Nat Biotechnol* **2008**, *26*, 1135-1145.

(2) Ginzinger, D. G. *Exp Hematol* **2002**, *30*, 503-512.

(3) Heller, M. J. *Annu Rev Biomed Eng* **2002**, *4*, 129-153.

(4) Crick, F. *Nature* **1970**, *227*, 561-&.

(5) Mattick, J. S. *Bioessays* **2003**, *25*, 930-939.

(6) Espy, M. J.; Uhl, J. R.; Sloan, L. M.; Buckwalter, S. P.; Jones, M. F.; Vetter, E. A.; Yao, J. D. C.; Wengenack, N. L.; Rosenblatt, J. E.; Cockerill, F. R.; Smith, T. F. *Clin Microbiol Rev* **2006**, *19*, 165-+; Lazcka, O.; Del Campo, F. J.; Munoz, F. X. *Biosens Bioelectron* **2007**, *22*, 1205-1217.

(7) Orr, H. T.; Zoghbi, H. Y. *Annu Rev Neurosci* **2007**, *30*, 575-621; Hassold, T.; Hunt, P. *Nat Rev Genet* **2001**, *2*, 280-291; Tsang, J. H.; Lo, Y. M. D. **2010**, - *25*.

(8) King, M. C.; Marks, J. H.; Mandell, J. B.; Grp, N. Y. B. C. S. *Science* **2003**, *302*, 643-646.

(9) Gebauer, P.; Mala, Z.; Bocek, P. *Electrophoresis* **2007**, *28*, 26-32; Gebauer, P.; Mala, Z.; Bocek, P. *Electrophoresis* **2009**, *30*, 29-35; Gebauer, P.; Malá, Z.; Boček, P. **2011**, - *32*, - 89.

(10) Probstein, R. F. *Physicochemical Hydrodynamics: An Introduction*; Wiley Interscience: Hoboken, NJ, 2003.

(11) Gas, B. *Electrophoresis* **2009**, *30*, S7-S15.

(12) Hruska, V.; Gas, B. *Electrophoresis* **2007**, *28*, 3-14.

(13) Garcia-Schwarz, G.; Rogacs, A.; Bahga, S. S.; Santiago, J. G. *J Vis Exp* **2012**, e3890.

(14) Acharya, S. *Some Aspects of Physicochemical Properties of DNA and RNA*. Uppsala University, Uppsala, Sweden, 2006.

(15) Khurana, T. K.; Santiago, J. G. *Anal Chem* **2008**, *80*, 6300-6307.

(16) Dolnik, V.; Deml, M.; Bocek, P. *J Chromatogr* **1985**, *320*, 89-97.

(17) Rogacs, A.; Santiago, J. G. *Anal Chem* **2013**.

(18) Shackman, J. G.; Ross, D. *Anal Chem* **2007**, *79*, 6641-6649.

(19) Turgeon, R. T.; Bowser, M. T. *Anal Bioanal Chem* **2009**, *394*, 187-198.
(20) Doherty, E. A. S.; Meagher, R. J.; Albarghouthi, M. N.; Barron, A. E. *Electrophoresis* **2003**, *24*, 34-54.
(21) Stellwagen, N. C.; Gelfi, C.; Righetti, P. G. *Biopolymers* **1997**, *42*, 687-703.
(22) Bahga, S. S.; Han, C. M.; Santiago, J. G. *Analyst* **2013**, *138*, 87-90.
(23) Eid, C.; Garcia-Schwarz, G.; Santiago, J. G. *Analyst* **2013**, *138*, 3117-3120.
(24) Persat, A.; Chivukula, R. R.; Mendell, J. T.; Santiago, J. G. *Anal Chem* **2010**, *82*, 9631-9635; Persat, A.; Santiago, J. G. *Anal Chem* **2011**, *83*, 2310-2316.
(25) Schoch, R. B.; Ronaghi, M.; Santiago, J. G. *Lab on a Chip* **2009**, *9*, 2145-2152.
(26) Bessetti, J. *Profiles in DNA* **2007**.
(27) Gold, L.; Ayers, D.; Bertino, J.; Bock, C.; Bock, A.; Brody, E. N.; Carter, J.; Dalby, A. B.; Eaton, B. E.; Fitzwater, T.; Flather, D.; Forbes, A.; Foreman, T.; Fowler, C.; Gawande, B.; Goss, M.; Gunn, M.; Gupta, S.; Halladay, D.; Heil, J.; Heilig, J.; Hicke, B.; Husar, G.; Janjic, J.; Jarvis, T.; Jennings, S.; Katilius, E.; Keeney, T. R.; Kim, N.; Koch, T. H.; Kraemer, S.; Kroiss, L.; Le, N.; Levine, D.; Lindsey, W.; Lollo, B.; Mayfield, W.; Mehan, M.; Mehler, R.; Nelson, S. K.; Nelson, M.; Nieuwlandt, D.; Nikrad, M.; Ochsner, U.; Ostroff, R. M.; Otis, M.; Parker, T.; Pietrasiewicz, S.; Resnicow, D. I.; Rohloff, J.; Sanders, G.; Sattin, S.; Schneider, D.; Singer, B.; Stanton, M.; Sterkel, A.; Stewart, A.; Stratford, S.; Vaught, J. D.; Vrkljan, M.; Walker, J. J.; Watrobka, M.; Waugh, S.; Weiss, A.; Wilcox, S. K.; Wolfson, A.; Wolk, S. K.; Zhang, C.; Zichi, D. *Plos One* **2010**, *5*.
(28) Bjellqvist, B.; Hughes, G. J.; Pasquali, C.; Paquet, N.; Ravier, F.; Sanchez, J. C.; Frutiger, S.; Hochstrasser, D. *Electrophoresis* **1993**, *14*, 1023-1031; Fischer, H.; Polikarpov, I.; Craievich, A. F. *Protein Sci* **2004**, *13*, 2825-2828.
(29) Costanzo, L. S. *Physiology*, 4th ed.; Saunders/Elsevier: Philadelphia, PA, 2010.
(30) Opel, K. L.; Chung, D.; McCord, B. R. *J Forensic Sci* **2010**, *55*, 25-33.
(31) Highberger, J. H. **1939**, - *61*, - 2303.
(32) Stevenson, F. J. *Humus Chemistry: Genesis, Composition, Reactions*; Wiley: New York, NY, 1994.
(33) Magarelli, M.; Passamonti, P.; Renieri, C. *Revista CES Medicina Veterinaria y Zootecnia* **2010**, *5*, 18-28; Aghajanyan, A. E.; Hambardzumyan, A. A.; Hovsepyan, A. S.; Asaturian, R. A.; Vardanyan, A. A.; Saghiyan, A. A. **2005**, - *18*, - 135.

(35) Jaros, M.; Hruska, V.; Stedry, M.; Zuskova, I.; Gas, B. *Electrophoresis* **2004**, *25*, 3080-3085.
(36) Rauter, C.; Mueller, M.; Diterich, I.; Zeller, S.; Hassler, D.; Meergans, T.; Hartung, T. *Clin Diagn Lab Immun* **2005**, *12*, 910-917.
(37) Bull, H. B.; Breese, K.; Ferguson, G. L.; Swenson, C. A. **1964**, - *104*, - 304.
(38) Koepke, J. A.; Thoma, J. F.; Schmidt, R. M. *Clin Chem* **1975**, *21*, 1953-1955.
(39) Moguilevsky, N.; Retegui, L. A.; Masson, P. L. *Biochem J* **1985**, *229*, 353-359.
(40) Waldrep, J. C.; Noe, R. L.; Stulting, R. D. *Invest Ophth Vis Sci* **1988**, *29*, 1538-1543.
(41) Vuorema, A. *Reduction and Analysis Methods of Indigo*. University of Turku, Turku, Finland, 2008.
(42) Bocek, P.; Deml, M.; Kaplanova, B.; Janak, J. *J Chromatogr* **1978**, *160*, 1-9.
(43) Kondratova, V. N.; Botezatu, I. V.; Shelepov, V. P.; Lichtenstein, A. V. *Anal Biochem* **2011**, *408*, 304-308.
(44) Marshall, L. A.; Rogacs, A.; Meinhart, C.; Santiago, J. G. *In preparation.* **2013**.
(45) Kondratova, V. N.; Botezatu, I. V.; Shelepov, V. P.; Lichtenstein, A. V. *Biochemistry-Moscow+* **2009**, *74*, 1285-1288.
(46) Kondratova, V. N.; Serd'uk, O. I.; Shelepov, V. P.; Lichtenstein, A. *Biotechniques* **2005**, *39*, 695-699; Kondratova, V. N.; Serdyuk, O. I.; Shelepov, V. P.; Potapova, G. I.; Likhtenshtein, A. V. *Dokl Biochem Biophys* **2005**, *402*, 200-203.
(47) Persat, A.; Marshall, L. A.; Santiago, J. G. *Anal Chem* **2009**, *81*, 9507-9511.
(48) Marshall, L. A.; Han, C. M.; Santiago, J. G. *Anal Chem* **2011**, *83*, 9715-9718.
(49) Marshall, L. A.; Wu, L. L.; Babikian, S.; Bachman, M.; Santiago, J. G. *Anal Chem* **2012**, *84*, 9640-9645.
(50) Marshall, L. A.; Qu, Y.; Santiago, J. G. In *Microscale Bioseparations*: Charlottesvile 2013.

Chapter 2

(1) Everaerts, F. M.; Beckers, J. L.; Verheggen, T. P. E. M. *Isotachophoresis: Theory, Instrumentation and Applications*; Elsevier, 1976.

(2) Gebauer, P.; Mala, Z.; Bocek, P. *Electrophoresis* **2009**, *30*, 29-35; Gebauer, P.; Mala, Z.; Bocek, P. *Electrophoresis* **2007**, *28*, 26-32.

(3) Garcia-Schwarz, G.; Rogacs, A.; Bahga, S. S.; Santiago, J. G. *J Vis Exp* **2012**, e3890.

(4) Dolnik, V.; Deml, M.; Bocek, P. *J Chromatogr* **1985**, *320*, 89-97.

(5) Hirokawa, T.; Nakahara, K.; Kiso, Y. *J Chromatogr* **1989**, *463*, 39-49.

(6) Jung, B.; Bharadwaj, R.; Santiago, J. G. *Anal Chem* **2006**, *78*, 2319-2327; Kaigala, G. V.; Bercovici, M.; Behnam, M.; Elliott, D.; Santiago, J. G.; Backhouse, C. J. *Lab Chip* **2010**, *10*, 2242-2250; Bercovici, M.; Kaigala, G. V.; Santiago, J. G. *Anal Chem* **2010**, *82*, 2134-2138; Bercovici, M.; Kaigala, G. V.; Backhouse, C. J.; Santiago, J. G. *Anal Chem* **2010**, *82*, 1858-1866.

(7) Kondratova, V. N.; Botezatu, I. V.; Shelepov, V. P.; Lichtenstein, A. V. *Biochemistry-Moscow+* **2009**, *74*, 1285-1288; Kondratova, V. N.; Botezatu, I. V.; Shelepov, V. P.; Lichtenstein, A. V. *Anal Biochem* **2011**, *408*, 304-308; Kondratova, V. N.; Serdyuk, O. I.; Shelepov, V. P.; Potapova, G. I.; Likhtenshtein, A. V. *Dokl Biochem Biophys* **2005**, *402*, 200-203.

(8) Schoch, R. B.; Ronaghi, M.; Santiago, J. G. *Lab Chip* **2009**, *9*, 2145-2152.

(9) Persat, A.; Marshall, L. A.; Santiago, J. G. *Anal Chem* **2009**, *81*, 9507-9511.

(10) Marshall, L. A.; Wu, L. L.; Babikian, S.; Bachman, M.; Santiago, J. G. *Anal Chem* **2012**, *84*, 9640-9645.

(11) Bercovici, M.; Kaigala, G. V.; Mach, K. E.; Han, C. M.; Liao, J. C.; Santiago, J. G. *Anal Chem* **2011**, *83*, 4110-4117.

(12) Qu, Y.; Marshall, L. A.; Santiago, J. G. In *2013 AIChE Annual Meeting*: San Francisco, CA, 2013.

(13) Bocek, P.; Deml, M.; Kaplanova, B.; Janak, J. *J Chromatogr* **1978**, *160*, 1-9.

(14) Brouwer, G.; Postema, G. A. *J Electrochem Soc* **1970**, *117*, 874-&.

(15) Turgeon, R.; Bowser, M. *Anal Bioanal Chem* **2009**, *394*, 187-198.

(16) Khurana, T. K.; Santiago, J. G. *Anal Chem* **2008**, *80*, 6300-6307.

(17) Garcia-Schwarz, G.; Bercovici, M.; Marshall, L. A.; Santiago, J. G. *J Fluid Mech* **2011**, *679*, 455-475.

(18) Bharadwaj, R.; Santiago, J. G.; Mohammadi, B. *Electrophoresis* **2002**, *23*, 2729-2744.

(19) Thormann, W. *Separ Sci Technol* **1984**, *19*, 455-467.

(20) Bercovici, M.; Lele, S. K.; Santiago, J. G. *J Chromatogr A* **2009**, *1216*, 1008-1018.

(21) Persat, A.; Suss, M. E.; Santiago, J. G. *Lab Chip* **2009**, *9*, 2454-2469.

(22) Gebauer, P.; Bocek, P. *J Chromatogr* **1985**, *320*, 49-65.

(23) Bier, M. *Electrophoresis: Theory, Methods, and Applications*; Academic Press Inc., 1959.

(24) Swinney, K.; Bornhop, D. J. *Electrophoresis* **2002**, *23*, 613-620; Evenhuis, C. J.; Haddad, P. R. *Electrophoresis* **2009**, *30*, 897-909.

(25) Cifuentes, A.; Poppe, H. *Chromatographia* **1994**, *39*, 391-404.

(26) Rogacs, A.; Santiago, J. G. *Anal Chem* **2013**, *85*, 5103-5113.

(27) Molho, J. I.; Herr, A. E.; Mosier, B. P.; Santiago, J. G.; Kenny, T. W.; Brennen, R. A.; Gordon, G. B.; Mohammadi, B. *Anal Chem* **2001**, *73*, 1350-1360.

(28) Persat, A.; Chambers, R. D.; Santiago, J. G. *Lab Chip* **2009**, *9*, 2437-2453.

(29) Gabrielli, C.; Huet, F.; Keddam, M.; Macias, A.; Sahar, A. *J Appl Electrochem* **1989**, *19*, 617-629.

(30) Bird, R. B.; Stewart, W. E.; Lightfoot, E. N. *Transport Phenomena*; Wiley, 2007.

(31) Good, N. E.; Winget, G. D.; Winter, W.; Connolly, T. N.; Izawa, S.; Singh, R. M. M. *Biochemistry* **1966**, *5*, 467-477.

(32) Bahga, S. S.; Bercovici, M.; Santiago, J. G. *Electrophoresis* **2010**.

(33) Milanova, D.; Chambers, R. D.; Bahga, S. S.; Santiago, J. G. *Electrophoresis* **2011**, *32*, 3286-3294.

Chapter 3

(1) Marshall, L. A.; Han, C. M.; Santiago, J. G. *Anal Chem* **2011**, *83*, 9715-9718.

(2) Marshall, L. A.; Wu, L. L.; Babikian, S.; Bachman, M.; Santiago, J. G. *Anal Chem* **2012**, *84*, 9640-9645.

(3) Persat, A.; Marshall, L. A.; Santiago, J. G. *Anal Chem* **2009**, *81*, 9507-9511.

(4) Kondratova, V. N.; Botezatu, I. V.; Shelepov, V. P.; Lichtenstein, A. V. *Biochemistry-Moscow+* **2009**, *74*, 1285-1288; Kondratova, V. N.; Botezatu, I. V.; Shelepov, V. P.; Lichtenstein, A. V. *Anal Biochem* **2011**, *408*, 304-308; Kondratova, V. N.; Serdyuk, O. I.; Shelepov, V. P.; Potapova, G. I.; Likhtenshtein, A. V. *Dokl Biochem Biophys* **2005**, *402*, 200-203.

(5) Kondratova, V. N.; Serd'uk, O. I.; Shelepov, V. P.; Lichtenstein, A. *Biotechniques* **2005**, *39*, 695-699.

(6) Schoch, R. B.; Ronaghi, M.; Santiago, J. G. *Lab Chip* **2009**, *9*, 2145-2152.

(7) Bercovici, M.; Kaigala, G. V.; Mach, K. E.; Han, C. M.; Liao, J. C.; Santiago, J. G. *Anal Chem* **2011**, *83*, 4110-4117.

(8) Rogacs, A.; Qu, Y. T.; Santiago, J. G. *Anal Chem* **2012**, *84*, 5858-5863.

(9) Marshall, L. A.; Santiago, J. G. *In preparation.* **2013**.

(10) Johansson, B. L.; Larsson, A.; Ocklind, A.; Ohrlund, A. *J Appl Polym Sci* **2002**, *86*, 2618-2625.

(11) Molho, J. I.; Herr, A. E.; Mosier, B. P.; Santiago, J. G.; Kenny, T. W.; Brennen, R. A.; Gordon, G. B.; Mohammadi, B. *Anal Chem* **2001**, *73*, 1350-1360.

(12) Persat, A.; Suss, M. E.; Santiago, J. G. *Lab Chip* **2009**, *9*, 2454-2469; Persat, A.; Chambers, R. D.; Santiago, J. G. *Lab Chip* **2009**, *9*, 2437-2453.

(13) Vulto, P.; Medoro, G.; Altomare, L.; Urban, G. A.; Tartagni, M.; Guerrieri, R.; Manaresi, N. *J Micromech Microeng* **2006**, *16*, 1847-1853; Vulto, P.; Podszun, S.; Meyer, P.; Hermann, C.; Manz, A.; Urban, G. A. *Lab Chip* **2011**, *11*, 1596-1602.

(14) Gliere, A.; Delattre, C. *Sensor Actuat a-Phys* **2006**, *130*, 601-608; Furuberg, L.; Mielnik, M.; Gulliksen, A.; Solli, L.; Johansen, I. R.; Voitel, J.; Baier, T.; Riegger, L.; Karlsen, F. *Microsyst Technol* **2008**, *14*, 673-681; Leu, T. S.; Chang, P. Y. *Sensor Actuat a-Phys* **2004**, *115*, 508-515.

(15) Milanova, D.; Chambers, R. D.; Bahga, S. S.; Santiago, J. G. *Electrophoresis* **2011**, *32*, 3286-3294.

(16) Bocek, P.; Deml, M.; Kaplanova, B.; Janak, J. *J Chromatogr* **1978**, *160*, 1-9.

(17) Promega, 2003 http://www.promega.com/techserv/tools/biomath/calc11.htm.

Chapter 4

(1) Mariella, R., *Biomed. Microdevices* **2008,** *10*, 777-784.

(2) Toner, M.; Irimia, D., *Annu. Rev. Biomed. Eng.* **2005,** *7*, 77-103.

(3) Abu al-Soud, W.; Radstrom, P., *J. Clin. Microbiol.* **2001,** *39*, 485-493.

(4) Wen, J.; Legendre, L. A.; Bienvenue, J. M.; Landers, J. P., *Anal. Chem.* **2008,** *80*, 6472-6479.

(5) Auroux, P.-A.; Koc, Y.; deMello, A.; Manz, A.; Day, P. J. R., *Lab Chip* **2004,** *4*, 534-546.

(6) Bocek, P., *Top. Curr. Chem.* **1981,** *95*, 131-177.

(7) Bercovici, M.; Kaigala, G. V.; Mach, K. E.; Han, C. M.; Liao, J. C.; Santiago, J. G., *Anal. Chem.* **2011,** *83*, 4110-4117.

(8) Persat, A.; Santiago, J. G., *Anal. Chem.* **2011,** *83*, 2310-2316.

(9) Persat, A.; Chivukula, R. R.; Mendell, J. T.; Santiago, J. G., *Anal. Chem.* **2010,** *82*, 9631-9635.

(10) Jung, B.; Bharadwaj, R.; Santiago, J. G., *Anal. Chem.* **2006,** *78*, 2319-2327.

(11) Schoch, R. B.; Ronaghi, M.; Santiago, J. G., *Lab Chip* **2009,** *9*, 2145-2152.

(12) Persat, A.; Marshall, L. A.; Santiago, J. G., *Anal. Chem.* **2009,** *81*, 9507-9511.

(13) Trager, W.; Jensen, J., *J. Parasitol.* **2005,** *91*, 484-486.

(14) Moody, A., *Clin. Microbiol. Rev.* **2002,** *15*, 66-78.

(15) Wooden, J.; Kyes, S.; Sibley, C., *Parasitol. Today* **1993,** *9*, 303-305.

(16) Chomczynski, P.; Sacchi, N., *Nat. Protoc.* **2006,** *1*, 581-585.

(17) Smilkstein, M.; Sriwilaijaroen, N; Kelley, J. X.; Wilairat, P.; Riscoe, M., *Antimicrob. Agents Chemother.* **2004,** *48*, 1803-1806.

(18) Meyer, S. L., *Data analysis for scientists and engineers*. Wiley: New York, 1975; p 513.

(19) Murray, C. K.; Gasser, R. A.; Magill, A. J.; Miller, R. S.;, *Clin. Microbiol. Rev.* **2008,** *21*, 97-110.

(20) Quintana, M.; Piper, R.; Boling, H.-L., Makler, M.; Sherman, C.; Gill, E.; Fernandez, E.; Martin, S., *Am. J. Trop. Med. Hyg.* **1998,** *59*, 868-871.

Chapter 5

(1) Mariella, R. *Biomed. Microdevices* **2008**, 10, 777– 784

(2)Wen, J.; Legendre, L. A.; Bienvenue, J. M.; Landers, J. P. *Anal. Chem.* **2008**, 80, 6472–6479

(3) Chen, X.; Cui, D.; Liu, C.; Li, H.; Chen, J. *Anal. Chim. Acta* **2007**, 584, 237– 243

(4) Bienvenue, J. M.; Duncalf, N.; Marchiarullo, D.; Ferrance, J. P.; Landers, J. P. *J. Forensic Sci.* **2006**, 51, 266– 273

(5) Liu, R. H.; Yang, J.; Lenigk, R.; Bonanno, J.; Grodzinski, P. *Anal. Chem.* **2004**, 76, 1824–1831

(6) Lee, C.-Y.; Lee, G.-B.; Lin, J.-L.; Huang, F.-C.; Liao, C.-S. *J. Micromech. Microeng.* **2005**,15, 1215– 1223

(7) Kim, S. J.; Wang, F.; Burns, M. A.; Kurabayashi, K. *Anal. Chem.* **2009**, 81, 4510– 4516

(8) Allport-Settle, M.Investigations Operations Manual: FDA Field Inspection and Investigation Policy and Procedure Concise Reference; PharmaLogika, **2010**.

(9) Bessetti, J.An Introduction to PCR Inhibitors. In Promega Corporation Profiles in DNA,**2007**, 10(1), 9– 10. http://www.promega.com/resources/articles/profiles-in-dna/2007/an-introduction-to-pcr-inhibitors/. Accessed October 2012.

(10) Persat, A.; Marshall, L. A.; Santiago, J. *Anal. Chem.* **2009**, 81, 9507– 9511

(11) Marshall, L. A.; Han, C. M.; Santiago, J. G. *Anal. Chem.* **2011**, 83, 9715– 9718

(12) Bercovici, M.; Kaigala, G.; Mach, K.; Han, C.; Liao, J.; Santiago, J. *Anal. Chem.* **2011**, 83,4110– 4117

(13) Schoch, R. B.; Ronaghi, M.; Santiago, J. G. *Lab Chip* **2009**, 9, 2145

(14) Boček, P. *Analytical Isotachophoresis*; VCH: Weinheim, Germany, **1988**.

(15) Persat, A.; Chivukula, R. R.; Mendell, J. T.; Santiago, J. G. *Anal. Chem.* **2010**, 82, 9631–9635

(16) Persat, A.; Santiago, J. G. *Anal. Chem.* **2011**, 83, 2310– 2316

(17) Jung, B.; Bharadwaj, R.; Santiago, J. G. *Anal. Chem.* **2006**, 78, 2319– 2327

(18) Keane, R. D.; Adrian, R. J.; Zhang, Y. *Meas. Sci. Technol.* **1995**, 6, 754– 768

(19) Smilkstein, M.; Sriwilaijaroen, N.; Kelly, J.; Wilairat, P.; Riscoe, M. *Antimicrob. Agents Chemother.* **2004**, 48, 1803– 1806

(20) Wooden, J.; Kyes, S.; Sibley, C. *Parasitol. Today* **1993**, 9, 303– 305

(21) Santiago, J.; Wereley, S.; Meinhart, C.; Beebe, D.; Adrian, R. J. *Exp. Fluids* **1998**, 25, 316–319

(22) Wereley, S. T.; Meinhart, C. D. *Annu. Rev. Fluid Mech.* **2010**, 42, 557– 576

(23) Akiyama, M.; Hwang, G.; Cheng, K. *J. Heat Transfer* **1971**, 93, 335– 341

(24) Zuker, M. *Nucleic Acids Res.* **2003**, 31, 3406– 3415